

FINAL REPORT

Hydrothermal Technologies for On-Site Destruction of Site
Investigation Wastes Contaminated with Per- and Polyfluoroalkyl
Substances (PFAS)

Phase I

SERDP Project ER18-1501

SEPTEMBER 2020

Timothy J. Strathmann
Christopher Higgins
Colorado School of Mines

Dr. Rula Deeb
Geosyntec Consultants

Distribution Statement A

This document has been cleared for public release



Page Intentionally Left Blank

This report was prepared under contract to the Department of Defense Strategic Environmental Research and Development Program (SERDP). The publication of this report does not indicate endorsement by the Department of Defense, nor should the contents be construed as reflecting the official policy or position of the Department of Defense. Reference herein to any specific commercial product, process, or service by trade name, trademark, manufacturer, or otherwise, does not necessarily constitute or imply its endorsement, recommendation, or favoring by the Department of Defense.

Page Intentionally Left Blank

REPORT DOCUMENTATION PAGEForm Approved
OMB No. 0704-0188

Public reporting burden for this collection of information is estimated to average 1 hour per response, including the time for reviewing instructions, searching existing data sources, gathering and maintaining the data needed, and completing and reviewing this collection of information. Send comments regarding this burden estimate or any other aspect of this collection of information, including suggestions for reducing this burden to Department of Defense, Washington Headquarters Services, Directorate for Information Operations and Reports (0704-0188), 1215 Jefferson Davis Highway, Suite 1204, Arlington, VA 22202-4302. Respondents should be aware that notwithstanding any other provision of law, no person shall be subject to any penalty for failing to comply with a collection of information if it does not display a currently valid OMB control number. **PLEASE DO NOT RETURN YOUR FORM TO THE ABOVE ADDRESS.**

1. REPORT DATE (DD-MM-YYYY) 7-09-2020		2. REPORT TYPE SERDP Final Report		3. DATES COVERED (From - To) Sept 2018 - May 2020	
4. TITLE AND SUBTITLE Hydrothermal Technologies for On-Site Destruction of Site Investigation Wastes Contaminate with Per- and Polyfluoroalkyl Substances (PFASs)				5a. CONTRACT NUMBER	
				5b. GRANT NUMBER	
				5c. PROGRAM ELEMENT NUMBER	
6. AUTHOR(S) Strathmann, Timothy, J (Project Investigator), Higgins, Christopher P. (Co-Project Investigator), Deeb, Rula (Co-Project Investigator), Hao, Shilai (Graduate Student), Wu, Boran (Graduate Student Student), Younjeong Choi (Postdoctoral Associate)				5d. PROJECT NUMBER ER18-1501	
				5e. TASK NUMBER	
				5f. WORK UNIT NUMBER	
7. PERFORMING ORGANIZATION NAME(S) AND ADDRESS(ES) Colorado School of Mines, 1500 Illinois St., Golden, Geosyntec Consultants, 1111 Broadway Street 6th floor, Oakland, CA 94607				8. PERFORMING ORGANIZATION REPORT ER18-1501	
9. SPONSORING / MONITORING AGENCY NAME(S) AND ADDRESS(ES) Strategic Environmental Research and Development Program (SERDP), 4800 Mark Center Drive, Suite 16F16, Alexandria, VA 22350-3605				10. SPONSOR/MONITOR'S ACRONYM(S) SERDP	
				11. SPONSOR/MONITOR'S REPORT NUMBER(S) ER18-1501	
12. DISTRIBUTION / AVAILABILITY STATEMENT DISTRIBUTION STATEMENT A. Approved for public release: distribution unlimited.					
13. SUPPLEMENTARY NOTES					
14. ABSTRACT This SERDP limited scope project evaluated the effectiveness of applying nascent hydrothermal conversion technologies to destroy PFASs and co-contaminants present in liquid and soil wastes. Specifically, the research identified reaction conditions (e.g., temperature, time) and low-cost amendments that promote rapid degradation and defluorination of per- and polyfluoroalkyl substances (PFASs) associated with aqueous film-forming foam (AFFF), assessed the reaction kinetics and mechanisms, and applied the process to treat PFAS-contaminated water and soil samples, including investigation-derive waste (IDW). Results demonstrate that hydrothermal treatment can be an effective alternative to off-site incineration.					
15. SUBJECT TERMS PFAS, aqueous film-forming foam, remediation, site investigation					
16. SECURITY CLASSIFICATION OF:			17. LIMITATION OF ABSTRACT	18. NUMBER OF PAGES	19a. NAME OF RESPONSIBLE PERSON Timothy Strathmann
a. REPORT UNCLASS	b. ABSTRACT UNCLASS	c. THIS PAGE UNCLASS			SAR

Standard Form 298 (Rev. 8-98)
Prescribed by ANSI Std. Z39.18

Page Intentionally Left Blank

TABLE OF CONTENTS

ER18-1501	i
TABLE OF CONTENTS.....	ii
LIST OF FIGURES	iii
LIST OF TABLES.....	iv
LIST OF ACRONYMS	v
Abstract.....	1
Executive Summary	2
1.0 Objectives	9
2.0 Background.....	10
2.1 PFASs at DoD Facilities	10
2.2 Investigation-Derived Wastes.....	10
2.3 PFAS Chemistry and Properties	10
2.4 Need for PFAS Destruction Technologies.....	11
3.0 Materials and Methods.....	14
3.1 Overall Study Approach	14
3.2 Chemicals and Reagents	15
3.3 Investigation-Derived Wastes (IDW) and PFAS-Contaminated Soils.....	15
3.4 Hydrothermal Reactions	17
3.5 Analysis.....	19
4.0 Results and Discussion	28
4.1 Screening of Hydrothermal Reaction Amendments	28
4.2 Alkaline Hydrothermal Destruction of PFOS.....	32
4.3 Alkaline Hydrothermal Reactions of PFASs Contained in AFFF	37
4.4 Reactivity of AFFF Co-Solvents and Co-Contaminants	49
4.6 Tentative Mechanism for Hydrothermal Transformation and Mineralization of PFASs...	54
4.7 Assessment of Energy Requirements for Alkaline Hydrothermal PFAS Treatment.....	55
5.0 Conclusions and Implications for Future Research/Implementation.....	61
5.1 Summary and Conclusions of Present Study.....	61
5.2 Implications for Technology Development and Implementation	62
5.3 Potential Next Steps and Proposed Follow-On Research.....	64
6.0 Literature Cited.....	68
APPENDIX A: Supporting Data	73
APPENDIX B: LIST OF PUBLICATIONS	77

LIST OF FIGURES

Figure 2.1. Phase diagram of water	13
Figure 3.1 Experimental approach and tasks.....	14
Figure 3.4.1 Mini-tube batch reactors used for hydrothermal treatment experiments.....	17
Figure 3.5.1 Accuracy evaluation of electrode measurement of F ⁻ concentration.....	20
Figure 4.1.1 Screening of amendments for hydrothermal defluorination of PFOS.....	28
Figure 4.1.2 PFOS removal measured in reaction solutions amended with different reagents.....	29
Figure 4.1.3 Extent of PFOS defluorination observed with different amendments as a function of the measured pH after reaction.....	30
Figure 4.1.4 Effect of NaOH concentration and the pH of solutions amended with other reagents on hydrothermal defluorination of PFOS.....	31
Figure 4.1.5 Effect of preheating (and re-cooling) solutions amended with NaBH ₄ or K ₂ FeO ₄ before introducing PFOS and re-heating	31
Figure 4.2.1 Kinetic analysis on alkaline-based hydrothermal destruction of PFOS.....	33
Figure 4.2.2 Effect of reaction temperature on the extent of PFOS degradation and defluorination in solutions amended with NaOH.....	34
Figure 4.2.3 Intermediate products observed during treatment of PFOS and PFOA.....	35
Figure 4.2.4 ¹⁹ F-NMR spectra of PFOS solutions before and after hydrothermal reactions.....	36
Figure 4.3.1 Sorting of effective amendments in the hydrothermal defluorination of PFASs present in AFFF #1.....	40
Figure 4.3.2 Extent of hydrothermal defluorination of AFFF #1 when the mixture was diluted to different extents before reaction.....	41
Figure 4.3.3 Defluorination observed during alkaline hydrothermal treatment of AFFF #1 solution with different reaction temperatures and concentrations of NaOH.....	42
Figure 4.3.4 Removal of targeted PFAS following alkaline hydrothermal treatment of AFFF...	44
Figure 4.3.5 Bubble plots summarizing PFAS removal in AFFF #1.....	45
Figure 4.3.6 Bubble plots summarizing removal of PFAS identified in AFFF #2.....	46
Figure 4.3.7 ¹⁹ F-NMR spectra of diluted AFFF before and after hydrothermal reaction.....	47
Figure 4.3.8 GC-TCD and GC-FID chromatograms of headspace following alkaline hydrothermal treatment of AFFF #1.....	48
Figure 4.3.9 GC-MS of reactor headspace after alkaline hydrothermal treatment of AFFF #1...	49
Figure 4.6.1 Proposed mechanism for OH ⁻ mediated decomposition of PFOS.....	54
Figure 4.6.2 Proposed mechanism for hydrothermal decomposition of PFOA.....	55
Figure 4.7.1 Schematic of a continuous-flow hydrothermal reactor.....	57
Figure 4.7.2 Schematic of a rotary kiln incinerator with afterburner.....	58
Figure 4.7.3 Schematic of an incinerator with circulating fluidized bed combustion chamber...	59
Figure 5.2.1 Illustration of potential applications of the hydrothermal treatment technology.....	63
Figure 5.2.2 Hybrid treatment strategy that integrates hydrothermal treatment processes.....	63

LIST OF TABLES

Table 2.1. Representative PFAS structures identified in AFFF-impacted groundwater.....	11
Table 3.2.1 Reagent list.....	16
Table 3.5.1 PFAS analytes names (acronyms), acquisition masses, parameters, internal standard used for LC-MS/MS analysis.....	21
Table 3.5.2 List of LC-QToF-MS targeted analytes for PFAS analysis.....	23
Table 4.2.1 Measured reaction kinetics for PFOS.....	32
Table 4.2.2 Predicted reaction times required to reduce PFOS concentrations to the USEPA lifetime Health Advisory Level (HAL).....	34
Table 4.3.1 Composition of target PFAS measured in AFFF mixtures.....	37
Table 4.3.2 Semiquantitative analysis of PFAS identified in the AFFF	38
Table 4.4.1 Results for hydrothermal reactivity of co-solvents and co-contaminants.....	50
Table 4.5.1 Measured PFAS composition in aqueous IDW samples before and after alkaline hydrothermal treatment.....	51
Table 4.5.2 Soils properties of PFAS-contaminated soils used in study.....	52
Table 4.5.3 Measured PFAS composition in PFAS-contaminated soil from Wurtsmith AFB before and after alkaline hydrothermal treatment.....	52
Table 4.5.4 Measured PFAS composition in PFAS-contaminated soil from Jacksonville NAS before and after alkaline hydrothermal treatment.....	53
Table 4.5.5 Measured PFAS composition in PFAS-contaminated soil from Peterson AFB before and after alkaline hydrothermal treatment.....	53
Table 4.7.1 Estimated heat input requirements for alkaline hydrothermal treatment and incineration of PFAS-contaminated water.....	56
Table 4.7.2 Isochoric specific heat values of liquid water ($C_{v,i}$) at different temperatures.....	58
Table 4.7.3 Isobaric specific heat values of water vapor ($C_{p,i}$) at different temperatures.....	60
Table A1 Semiquantitative analysis of PFASs compounds.....	73

LIST OF ACRONYMS

6:2 FTS – 6:2 fluorotelomer sulfonate
6:2 FTSi – 6:2 fluorotelomer sulfinate
6:2 FTThA – 6:2 fluorotelomer thia acetic acid
6:2 FTTh-PrAd-DiMeEtS – 6:2 fluorotelomer thia propanoamido dimethyl ethyl sulfonate
8:2 FTS – 8:2 fluorotelomer sulfonate
8:2 FTSi – 8:2 fluorotelomer sulfinate
AEC – anion exchange capacity
AFB – Air Force Base
AFCEC – Air Force Civil Engineering Center
AFFF – aqueous film-forming foam
AmPr-FHxSA – N-dimethyl ammonio propyl perfluorohexane sulfonamide
bgs – below ground surface
BTEX – benzene, toluene, ethylbenzene, and xylenes
CE – collision energy
CEC – cation exchange capacity
CSM – Colorado School of Mines
CXP – collision cell exit potential
DFT – density functional theory
DGBE - diethylene glycol monobutyl ether
DoD – Department of Defense
DOM – dissolved organic matter
DP – declustering potential
DPT – direct push technology
EP – entrance potential
EPA – Environmental Protection Agency
ESI – electrospray ionization
ESTCP – Environmental Security Technology Certification Program
FTA – fire training area
GAC – granular activated carbon
GC-FID – gas chromatography with flame ionization detection
GC-MS/MS – gas chromatography with tandem mass spectrometry detection
GC-TCD – gas chromatography with thermal conductivity detector
HAL – Health Advisory Level
HF – hydrofluoric acid
HPLC – high pressure liquid chromatography
HPLC-DAD – high pressure liquid chromatography with diode array detection
HRMS – high resolution mass spectrometry
HTG – hydrothermal gasification
HTL – hydrothermal liquefaction
IC – ion chromatography
IDW – investigation-derived waste
IS – internal standard
ISCO – in situ chemical oxidation
ISE – ion selective electrode

IX – ion exchange
JAX – Jacksonville Naval Air Station
 k_{obs} – pseudo-first-order rate constants
LCS – lab control sample
LC-MS/MS – liquid chromatography tandem mass spectrometry
LC-QToF-MS – liquid chromatography with quantitative time-of-flight mass spectrometry detection
LOQ – limit of quantitation
NAS – Naval Air Station
NF - nanofiltration
NMR – nuclear magnetic resonance spectroscopy
PAFB – Peterson Air Force Base
PCBs – polychlorinated biphenyls
PCE – tetrachloroethylene
PFAAs – perfluoroalkyl acids
PFASs – per- and polyfluoroalkyl substances
PFBA – perfluorobutanoic acid
PFBS – perfluorobutane sulfonate
PFCAs – perfluorocarboxylic acids
PFDoA – perfluorododecanoic acid
PFDS – perfluorodecane sulfonate
PFHpA – perfluoroheptanoic acid
PFHxA – perfluorohexanoic acid
PFHxS – perfluorohexane sulfonate
PFNA – perfluorononanoic acid
PFOA – perfluorooctanoic acid
PFOS – perfluorooctane sulfonate
PFOSA – perfluorooctane sulfonamide
PFPeA – perfluoropentanoic acid
PFSAs – perfluoroalkyl sulfonic acids
PFTeA – perfluorotetradecanoic acid
PFTrA – perfluorotridecanoic acid
PFUnA – perfluoroundecanoic acid
QC – quality control
RT – retention time
SERDP - Strategic Environmental Research and Development Program
SON – statement of need
SPE – solid phase extraction
TCE – trichloroethylene
TFA – trifluoroacetic acid
TOC – total organic carbon
USEPA –United States Environmental Protection Agency
UV – ultraviolet light
XIC – extracted ion chromatogram
ZVI – zerovalent iron

Abstract

Introduction and Objectives

The overall goal of the proposed work was to evaluate the effectiveness of applying nascent hydrothermal conversion technologies to destroy per- and polyfluoroalkyl substances (PFASs) and co-contaminants present in liquid and soil wastes. Specifically, the project aimed to identify reaction conditions (e.g., temperature, time) and low-cost amendments that promote rapid degradation and defluorination of PFASs associated with aqueous film-forming foam (AFFF), assess the reaction kinetics and mechanisms, and apply the process to treat PFAS-contaminated water and soil samples, including investigation-derive waste (IDW).

Technical Approach

A series of research tasks were performed to address the project objectives and test associated hypotheses. An initial screening experiment tested the effectiveness of several solution amendments, including acids, bases, salts, oxidants, reductants, and metal nanoparticles, in promoting degradation and defluorination of perfluorooctane sulfonate (PFOS) at subcritical hydrothermal conditions (350°C, 17 MPa).

Detailed studies were then conducted with the most promising amendments to evaluate reaction kinetics and assess the applicability for treatment of a wider diversity of PFASs identified in AFFF mixtures. Experiments were then undertaken to evaluate the stability and degradation of co-solvents (e.g., DGBE) and co-contaminants (e.g., hydrocarbon fuels) often associated with AFFF use. Finally, proof-of-concept experiments were performed to apply the optimal reaction conditions identified to treat PFAS-contaminated soil and water samples obtained from DoD sites, including IDW. These results were used to inform an analysis of the heat requirements for hydrothermal destruction of PFAS-contaminated water in comparison to incineration of the same materials.

Results

Results of screening experiments showed that amendments which raise pH conditions, including low-cost alkalis like NaOH, are effective in promoting rapid degradation and defluorination of PFOS. Reaction rates are proportional to the added NaOH concentration, and the observed kinetics and products support a reaction mechanism involving nucleophilic attack at the polar head group in the PFAS structure. The same reaction conditions were then found to be effective for degrading and defluorinating the full suite of PFASs detected by high resolution mass spectrometry methods in AFFF mixtures and AFFF-contaminated water and soil samples collected from DoD sites. Tests with multiple techniques show that alkaline hydrothermal treatment can achieve ~100% destruction and defluorination of PFASs present in aqueous and soil matrices.

Benefits

Analysis of process heat requirements indicate that hydrothermal processing of PFAS-contaminated water requires significantly less energy inputs than incineration of the same materials. Thus, findings from this limited scope project support further development of this technology pathway for use in managing PFAS-contamination at DoD facilities. Translation of the technology into mobile units that can be used on-site to treat IDW or heavily contaminated source zones is particularly promising. Additional research aimed at strengthening the underlying science, expanding the application space, and developing continuous processing reactors is recommended.

Executive Summary

Introduction

Extensive use of per- and polyfluoroalkyl substances (PFASs) in aqueous film-forming foams (AFFF) has led to significant environmental releases at Department of Defense (DoD) facilities. As a result, soil and groundwater underlying these sites now represent major source zones for PFAS contamination. To address concerns about PFAS contamination, identify source zones, and prepare for future cleanup efforts, DoD has initiated remedial site investigations nationwide. These activities generate significant liquid and solid waste materials, including soil drilling core materials, well purging water samples, and equipment washing residues. These “investigation-derived waste” materials (IDW) contain varying levels of contamination by PFAS and other site co-contaminants. Currently, IDW is shipped off site for disposal or incineration, but this is costly and does not completely eliminate liabilities. Incineration can lead to complete PFAS destruction, but this technology is expensive and requires large energy inputs for water samples and soil samples with high moisture content. Ideally, small-scale field-deployable technologies capable of completely destroying PFASs in wet samples would be available to manage these IDW on site.

The fluorinated backbone within PFASs imparts extreme recalcitrance and environmental persistence, and there is only limited evidence for slow biodegradation of these contaminants. As a result, monitored natural attenuation is not a viable remediation strategy for PFASs, and concentrations in groundwater are expected to remain well above action levels indefinitely without active interventions. There is considerable interest in technologies that can not only remove PFASs from environmental media, but also mineralize the chemicals so that they pose no future risk or liability. However, physical-chemical approaches that have been successful for other legacy contaminants, including in situ chemical oxidation (ISCO) and zerovalent iron (ZVI), have shown only limited success in destroying PFASs. Ensuring complete mineralization generally requires incineration or other high temperature thermal treatments. While this may be practical for PFAS-containing solid wastes, incineration of wet wastes and concentrate solutions is inefficient because of the high energy requirements for vaporizing water.

This limited scope project examined the feasibility of applying subcritical hydrothermal processing as an alternative technology for managing wet waste concentrates, including IDW. Hydrothermal technologies apply elevated temperatures and pressures (200-374°C, 2-22 MPa) to water in a sealed environment that prevents vaporization (**Figure ES-1**), leading to a uniquely reactive environment that has been shown to catalyze many chemical

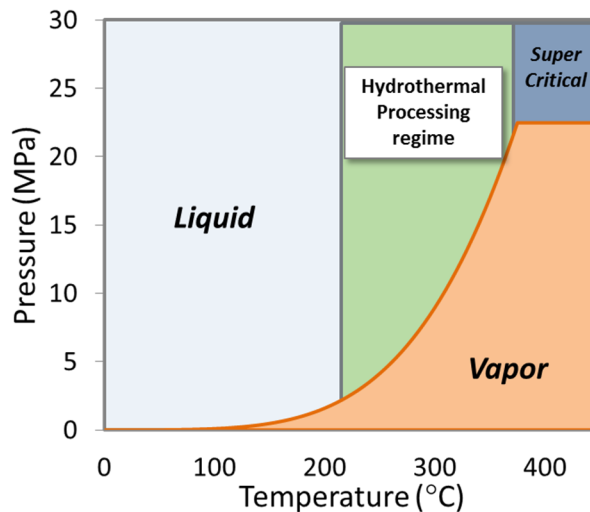


Figure ES-1. Phase diagram of water with conditions for subcritical hydrothermal reaction conditions highlighted.

transformations that do not occur at lower temperatures. While somewhat counterintuitive, heating compressed water to subcritical hydrothermal conditions consumes much less energy than evaporating water at lower temperatures. As a result, subcritical hydrothermal reactions are currently being heavily exploited for production of biorenewable fuels and chemicals. The same properties responsible for decomposition and transformation of biomass under hydrothermal conditions can potentially be exploited to degrade organic contaminants, including PFASs.

Objectives

The overall goal of the proposed work was to evaluate the effectiveness of applying hydrothermal conversion technologies to destroy PFASs and co-contaminants present in liquid and soil wastes. We tested a hypothesis that hydrothermal reaction conditions can be coupled with low-cost reactive amendments to effectively degrade and defluorinate the full range of PFAS structures identified at AFFF-impacted sites. High resolution mass spectrometry methods were applied to monitor the transformation of a wide range of PFAS structures, including the most commonly measured perfluoroalkyl acids (i.e., PFOS and PFOA) and their polyfluorinated precursors, during hydrothermal treatment applications. Experimental work addressed the following specific objectives:

Identify hydrothermal reactions conditions (e.g., temperature, reaction time) and reactive amendments (e.g., acids, bases, oxidants, reductants) that promote PFAS degradation and defluorination;

Track the fate and decomposition of diverse PFASs identified in AFFF formulations;

Evaluate fate and degradation of common co-solvents and co-contaminants (e.g., hydrocarbon fuel compounds, chlorinated solvents) associated with AFFF;

Assess treatment of PFAS-contaminated aqueous and soil samples, including IDW;

Identify transformation pathways and mechanisms leading to mineralization of PFASs;

Compare energy input requirements for hydrothermal treatment of PFAS-contaminated water with incineration.

Technical Approach

The overall study design included seven related tasks. Task 1 focused on screening a wide range of reaction amendments, including acids, bases, oxidants, reductants, and metallic nanoparticles, for their potential to enhance PFOS and PFOA degradation and defluorination under hydrothermal conditions. Task 2 applied high resolution mass spectrometry methods to evaluate degradation of the wider range of PFASs present in AFFF under conditions that were found to be optimal for PFOS degradation. Task 3 then evaluated the stability and degradation of representative AFFF co-solvents and co-contaminants, and Task 4 measured degradations of PFASs present in aqueous and solid IDW samples under the same reaction conditions. Task 5 combined the results of experiments and available literature to provide an initial assessment of the major pathways and mechanisms for hydrothermal decomposition of PFASs, and Task 6 provided an initial assessment of the heat requirements for hydrothermal treatment of wet waste materials in comparison with incineration. Finally, Task 7 included all reporting and technology transfer activities.

Experiments were conducted using commercial AFFF mixtures and PFAS-contaminated water and soil samples obtained from DoD sites throughout the country. Liquid chromatography quadrupole time-of-flight mass spectrometry (LC-QToF-MS) analysis of samples showed a wide diversity of PFASs, spanning the full range of structures identified at contaminated sites.

Hydrothermal reactions of PFASs were evaluated in laboratory batch reactor systems. PFAS-containing solutions and soil suspensions were added to reactors together with water and the appropriate reactive amendments before sealing and heating to the desired temperature. After completion of reactions, contents were collected for analysis of residual PFASs, fluoride, and other selected analytes. PFAS concentrations were measured by LC-QToF-MS and LC with tandem mass spectrometry (LC-MS/MS). Fluoride ion released upon degradation of PFASs was measured by ion selective electrode analysis. Gas chromatography methods were applied to evaluate gas-phase reaction products. Co-solvent and co-contaminant concentrations were measured by total organic carbon (TOC) and high pressure liquid chromatography with diode array detection (HPLC-DAD).

Results & Discussion

Degradation and Defluorination of PFOS: Initially, a series of amendments, including acids, bases, salts, oxidants, reductants, and metal nanoparticles, were screened for their potential to promote defluorination of perfluorooctane sulfonate (PFOS) under near-critical hydrothermal conditions (350°C, 16.5 MPa autogenous pressure). **Figure ES-2** shows that the extent of F⁻ release varied widely, ranging from near 0% (for the unamended control and roughly half the screened amendments) to 80% fluoride release.

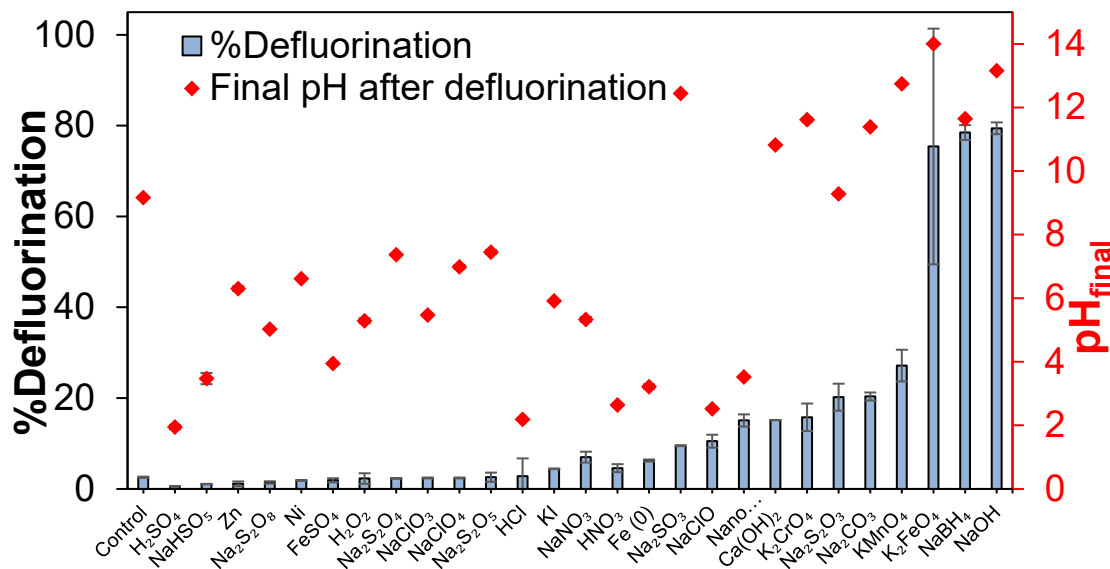


Figure ES-2 Screening of the potential of different reactive amendments for defluorination of PFOS under hydrothermal reaction conditions: 50 mg/L PFOS, 1 M reactive amendment, 350°C, 90 min reaction. Solution pH value after reaction shown on right axis.

The most effective reagents, yielding >70% defluorination, include sodium hydroxide (NaOH), sodium borohydride (NaBH₄), and potassium ferrate (K₂FeO₄). Although the most effective amendments belong to different classes of reagents, subsequent tests strongly suggest that their effectiveness was related to the increase in solution pH caused by their addition to solution. As a result, further investigation focused on hydrothermal reactions in solutions amended with NaOH, a low-cost alkali.

An analysis of PFOS degradation showed that reaction kinetics follow a generalized second-order rate law, where rates were proportional to both PFOS and hydroxide ion (OH⁻) concentrations. Tests also showed that reaction rates increase with increasing reaction temperature. Together, these findings provide for model predictions that can be applied to design reactor process conditions to ensure treatment goals are met. Analysis of reaction solutions confirms formation of some fluorinated organic intermediates, albeit at very low concentrations, indicating conversion of PFOS to shorter-chain carboxylate intermediates that rapidly degrade and release fluoride. Mineralization of PFOS and conversion of organic C-F bonds to fluoride ion were further confirmed by application of nuclear magnetic resonance spectroscopy (¹⁹F-NMR).

Degradation and Defluorination of AFFF: Experiments conducted with two AFFF mixtures (one dominated by perfluoroalkyl sulfonates and one dominated by fluorotelomer acids) demonstrated that the same alkali-inducing amendments that were effective for degrading PFOS also were efficient in promoting destruction and defluorination of the wider suite of PFASs identified in

AFFF mixtures. Through LC-QToF-MS targeted and suspect screening analysis as well as ¹⁹F-NMR analysis, degradation of the full suite of structures was confirmed. **Figure ES-3** shows “bubble plots” tracking the estimated concentrations of PFASs in one of the AFFF mixtures before and after hydrothermal reaction. In these plots, individual bubbles represent different PFAS structures detected in the AFFF arranged according to their chromatographic retention times (x-axis) and mass-to-charge ratio (m/z; y-axis), and the diameters of the individual bubbles are proportional to chromatographic peak area. More than 99% of the PFASs identified through suspect screening analysis of AFFF were degraded within 90 min.

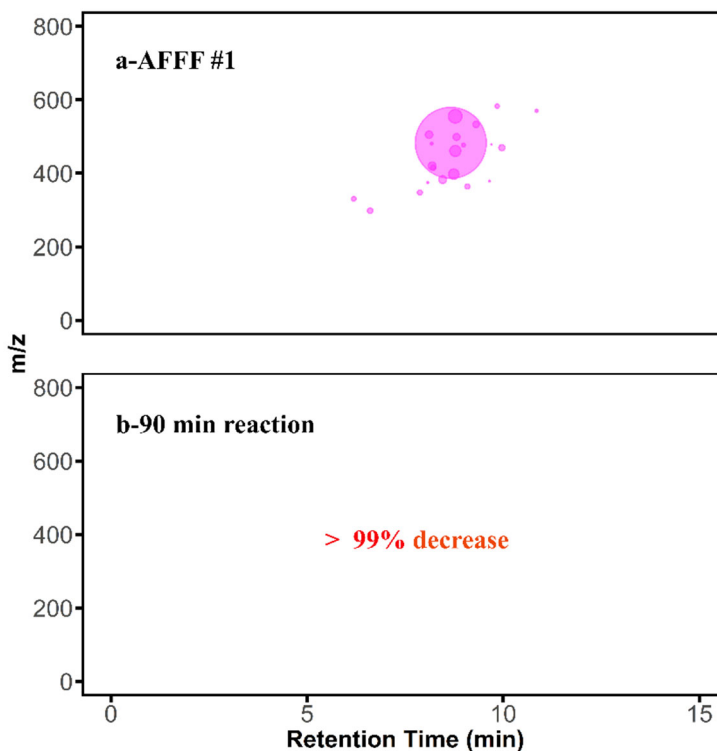


Figure ES-3 Bubble plots summarizing the removal of PFASs identified in AFFF by LC-QToF-MS analysis. Reaction conditions: AFFF diluted 1-to-1000, 350°C, 5 M NaOH.

Analysis of fluorine by ^{19}F -NMR and ion selective electrode analysis confirmed near-complete mineralization and release of fluoride ion from PFASs present in the AFFF. Furthermore, analysis of volatile products by gas chromatography methods showed principally carbon dioxide, with smaller amounts of hydrocarbon products (butene isomers, ethane); no organofluorine products were detected.

Results are consistent with a tentative mechanism for PFAS transformation wherein OH^- catalyzes a series of nucleophilic substitution and decarboxylation reactions that defluorinate PFOS/PFOA and perfluorocarboxylate intermediates. For PFOS, an initial OH^- substitution reaction with the sulfonate headgroup leads to a series of unstable intermediates that hydrolyze to form PFOA, and further decarboxylation then converts PFOA sequentially to increasingly short-chain perfluorocarboxylates, releasing 2F^- ions with each reaction.

Reactivity of AFFF co-solvents and co-contaminants: Tests showed that two co-solvents, DGBE and methanol, are minimally affected by exposure to alkaline hydrothermal conditions found to degrade PFASs, whereas several model co-contaminants, including TCE (a model chlorinated solvent) and aromatic hydrocarbon contaminants (benzene, toluene, ethylbenzene, and m-xylene) are completely degraded under the same conditions. Degradation of TCE suggests a common nucleophilic attack mechanisms that might be applicable to halogenated organic contaminants in general. The mechanisms for degradation of the aromatic hydrocarbons is unclear, but it is possible that the same reactive nucleophiles responsible for PFAS decomposition attack the electron-rich aromatic bonds in these structures. Nonetheless, findings suggest that this technology may be broadly applicable for many of the contaminants detected at these locations.

Reactivity of PFAS in AFFF-impacted water and soil: Tests of hydrothermal reactions were conducted with two PFAS-contaminated IDW aqueous samples and three PFAS-contaminated soil samples collected from DoD sites. These tests confirmed that PFASs in contaminated matrices can be destroyed by alkaline hydrothermal treatment. Greater than 99% removal of the PFASs detected in the original aqueous IDW samples was measured following hydrothermal treatment, and >90% removal was observed following treatment of the three PFAS-contaminated soil samples. Followup studies are recommended to characterize these treatments in greater detail and identify the influences of important soil and water conditions to reaction rates.

Assessment of energy input requirements: A preliminary analysis of energy input requirements for alkaline hydrothermal treatment indicate significant potential for energy savings compared to incineration processes for PFAS-contaminated water and sediment samples. Avoiding vaporization of water through hydrothermal reactions in compressed water at subcritical conditions yields expected energy requirements of $110\text{--}127 \text{ kWh m}^{-3}$ for hydrothermal treatment at $300\text{--}350^\circ\text{C}$ with integrated heat recovery, much lower than estimates for incineration of the same samples (534 kWh m^{-3} for incineration in a circulating fluidized bed combustion chamber at $1,100^\circ\text{C}$ with integrated heat recovery; $1,336 \text{ kWh m}^{-3}$ for incineration in a cement kiln with $1,100^\circ\text{C}$ afterburner and no heat recovery). While these estimates are necessarily rough, they support further development of alkaline hydrothermal treatment technologies.

Implications for Future Research and Benefits

Findings from this limited scope project demonstrate a promising new strategy for achieving complete destruction and defluorination of PFASs present in IDW as well as other concentrate streams. To our knowledge, this is the first effort demonstrating that subcritical hydrothermal reaction conditions can be combined with low-cost alkali amendments to achieve complete degradation and defluorination of PFASs, both individual solutes and complex mixtures of PFASs (e.g., AFFF). These findings indicate a very promising technology pathway for treatment of PFAS-contamination that can achieve complete destruction of the PFASs, thereby eliminating future liabilities associated with contamination at DoD facilities. The broad efficacy and lower heat requirements compared to conventional hazardous waste incineration is suggestive of an alternative technology for managing a variety of high moisture content PFAS wastes and concentrates, including:

- Aqueous and soil investigation-derived wastes
- Unused stockpiles of AFFF containing legacy PFASs requiring disposal
- PFAS-contaminated source zone soils, sediments, and concentrated solutions
- Waste ion exchange concentrate management, including PFAS-contaminated still bottoms and aqueous/co-solvent mixtures
- High pressure membrane reject streams with elevated PFAS concentrations
- Accident site wastes collected following application of AFFF
- PFAS-contaminated wastewater sludge and biosolids
- Rinse solutions from AFFF spray equipment
- Manufacturing wastewater with elevated PFAS concentrations where adsorption/membranes are not practical for direct treatment

For dilute contaminated water, it is recommended that alkaline hydrothermal treatment be combined into hybrid treatment systems where physical separation processes (e.g., ion exchange, nanofiltration) are applied to concentrate the PFASs in a low-volume secondary stream (e.g., waste ion exchange regenerant brine) that would then be subjected to hydrothermal treatment and destruction.

While incineration is a mature technology, public acceptance of incineration of PFAS-containing wastes is low, and some incinerators are reluctant to accept PFAS-containing wastes due to concerns about generation of corrosive hydrofluoric acid and impending regulations on PFAS-associated emissions. Transportation of PFAS-contaminated wastes off site to centralized incineration facilities also raises serious concerns about accidental releases. Hydrothermal destruction technologies are conducive to application of mobile treatment units for small scale treatment needs (e.g., treatment of IDW samples generated on site). Still, further research is needed to address a number of important issues related to the underlying mechanisms of hydrothermal destruction processes, application to important PFAS-contaminated matrices (including those listed above), translation of the technology to continuous-flow reactors systems, and scale-up and demonstration at DoD facilities.

Publications and Presentations

The project has resulted in two peer-reviewed publications to date, with two additional publications currently in preparation for submission. The work has also led to submission of a full patent application that is pending. Technology transfer has also been supported by eleven conference presentations, lectures and webinars to the broader community.

1.0 Objectives

This SERDP project was funded based on a proposal submitted in response to the FY 2018 Statement of Need (SON) seeking innovative approaches for treatment of per- and polyfluoroalkyl substance (PFASs) present in subsurface investigation-derived wastes (IDW). The proposed hydrothermal technology supports the SON's emphasis on destructive technologies that treat the IDW rather than rely on landfilling so as to avoid potential future environmental liability given that disposal requirements for PFASs are evolving.

The overall goal of the proposed work was to evaluate the effectiveness of applying nascent hydrothermal conversion technologies to destroy PFASs and co-contaminants present in liquid and soil wastes. Specifically, we proposed that hydrothermal reaction conditions can be coupled with low-cost reactive amendments to effectively degrade and defluorinate the full range of PFAS structures identified at AFFF-impacted sites. Application of high resolution LC-QToF-MS together with an extensive suspect target list (~1500 PFASs) enabled us to examine the fate and transformation of a wide range of PFAS structures, including the most commonly measured perfluoroalkyl acids and their polyfluorinated precursors, during hydrothermal treatment applications.

To attain the overall project goal, the following specific objectives were developed:

- (1) Identify hydrothermal reactions conditions (e.g., temperature, reaction time) and reactive amendments (e.g., acids, bases, oxidants, reductants) that promote PFAS degradation and defluorination;*
- (2) Track the fate and decomposition of diverse PFASs identified as components in different commercial AFFF formulations during hydrothermal reactions;*
- (3) Evaluate fate and degradation of common co-solvents and co-contaminants (e.g., hydrocarbon fuel compounds, chlorinated solvents) associated with AFFF contamination;*
- (4) Assess treatment of PFAS-contaminated aqueous and soil samples collected from DoD sites, including IDW;*
- (5) Identify transformation pathways and mechanisms leading to mineralization of PFASs;*
- (6) Estimated energy input requirements for hydrothermal treatment of PFAS-contaminated aqueous and soil samples, and compare with energy requirements for incineration.*

Project efforts included a series of tasks involving bench-scale batch experiments designed to meet these project objectives and provide valuable proof-of-concept data that will serve as the basis of future technology development work that will optimize and translate these processes into practical field-scale technologies.

2.0 Background

2.1 PFASs at DoD Facilities

Since their development in 1940s, poly- and perfluoroalkyl substances (PFASs) have been extensively used due to their distinctive surface-active properties and chemical stability (Moody and Field, 2000; Schultz et al., 2003). While widespread applications include use in the manufacture of nonstick coatings, stain-repellants, paper packaging, their use in aqueous film-forming foams (AFFF) has led to significant environmental releases at Department of Defense (DoD) facilities (Moody and Field, 2000; Schultz et al., 2003; Wang et al., 2017). AFFF use has been critical to protecting human life because of their superior properties in rapidly extinguishing fuel-based fires (e.g., aircraft accidents). Widespread release of AFFF has been traced to their use in fire training activities, and many DoD facilities have fire training areas where AFFF have been applied together with various co-contaminants (e.g., hydrocarbon fuel, halogenated solvents) to prepare personnel to handle potential accidents on the bases (Moody and Field, 2000). Many of these fire training areas did not contain adequate underlinings or systems for collection of liquid wastes. As a result, soil and groundwater underlying these sites now represent major source zones for PFAS contamination.

2.2 Investigation-Derived Wastes

To address concerns about PFAS contamination, identify source zones, and prepare for future cleanup efforts, DoD has initiated widespread remedial site investigations at facilities throughout the nation. These activities generate significant liquid and solid waste materials, including soil drilling core materials, well purging water samples, and equipment washing residues. These materials contain varying levels of contamination by PFASs and other site co-contaminants. Currently, these materials are shipped off site for disposal or incineration. Off-site disposal in hazardous waste landfills is costly and does not completely eliminate liabilities. Incineration can lead to complete PFAS destruction, but is costly and requires large energy inputs for water samples and soil samples with high moisture content. Ideally, a small-scale field-deployable technology capable of complete PFAS destruction in wet samples would be used for this purpose, providing for complete elimination of PFAS-associated liabilities resulting from secondary contamination from site investigation activities.

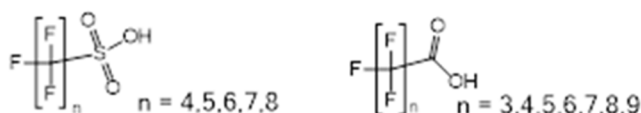
2.3 PFAS Chemistry and Properties

PFASs include a wide range of chemical structures that have been synthesized to have specific properties of interfacial and surface activity, hydrophilicity/hydrophobicity, and thermochemical stability. While most studies on PFAS occurrence and treatment have focused almost exclusively on a small number of PFAS structures, most notably PFOS and PFOA, these analytes represent only a small fraction of PFASs identified at AFFF-impacted sites (Hu et al., 2016; K. Barzen-Hanson et al., n.d.; Moody and Field, 1999). Recent application of high resolution mass spectrometry (e.g., LC-QToF-MS) has led to the identification of a much wider range of PFAS structures (**Table 2.1**) (Backe et al., 2013; Barzen-Hanson et al., 2017; Barzen-Hanson and Field, 2015). Structures are highly variable, including different polar headgroups (e.g., sulfonate vs. carboxylate vs. sulfonamide), fluoroalkyl chain lengths, extent of fluorination, and degree of branching. Perfluorinated structures refer to those with alkyl chains that are fully fluorinated, whereas polyfluorinated structures refer to structures with incomplete fluorination. Perfluoroalkyl

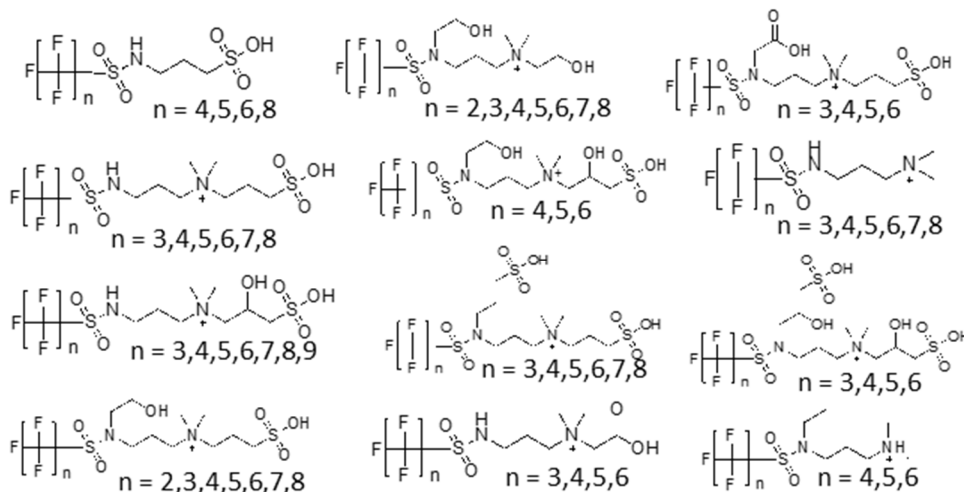
acids (PFAAs) refer to the most recalcitrant subgroup of PFASs where a perfluoroalkyl chain is terminated by either a sulfonic or carboxylic acid headgroup. This category includes PFOS and PFOA. PFAA precursors represent a broad group of structures containing additional structural features (e.g., sulfonamido acetic acid groups) that have been shown to transform over time into the more recalcitrant PFAAs. Although there is currently a lack of toxicity data on the majority of PFAS structures identified (Wang et al., 2017), their continued presence in waste materials raises concerns about potential future liabilities.

Table 2.1. Representative PFAS structures identified in AFFF-impacted groundwater, including novel structures identified by LC-QToF-MS in co-PI Higgins’s laboratory (Backe et al., 2013; Barzen-Hanson et al., 2017; Barzen-Hanson and Field, 2015)

Perfluoroalkyl sulfonic acids (PFSAs) and carboxylic acids (PFCAs)



Selected novel PFASs recently identified by LC-QToF-MS



2.4 Need for PFAS Destruction Technologies

The fluorinated backbone within PFASs imparts extreme recalcitrance and environmental persistence (Arvaniti and Stasinakis, 2015; Houtz et al., 2013; Parsons et al., 2008a; Schultz and Gundl, 2000). Many of the same remedial technologies used for other legacy contaminants (e.g., air stripping, bioremediation) are ineffective for PFASs (Merino et al., 2016; Remde and Debus, 1996; Parsons et al., 2008b; Houde et al., 2006; Prevedouros et al., 2006). There is only limited evidence of slow biodegradation of PFAAs like PFOS or PFOA under aerobic or anaerobic conditions (Houde et al., 2006; Huang and Jaffé, 2019; Parsons et al., 2008b; Prevedouros et al., 2006; Remde and Debus, 1996). Selected fluorotelomer alcohol and sulfonamide derivatives are slowly biotransformed to the corresponding PFAAs, but no further transformation is documented (Butt et al., 2014; Houtz et al., 2013). In addition, there is no evidence for natural attenuation by

abiotic reactions like oxidation or reduction by aquifer minerals. Thus, monitored natural attenuation is not a viable remediation strategy for PFASs, and their concentrations in groundwater are expected to remain well above action levels indefinitely without active interventions.

Due to the high chemical stability of PFASs, treatment contaminated water has been limited mostly to physical adsorption processes (e.g., activated carbon, ion exchange) that serve to transfer PFASs to a solid phase, which must be frequently replaced and disposed (Appleman et al., 2014; Merino et al., 2016). As a result, there is considerable interest in technologies that can, not only remove PFASs from environmental media, but also mineralize the chemicals so that they pose no future risk or liability. Conventional physical-chemical approaches to destroy PFASs in-situ have also been met with limited success. In situ chemical oxidation (ISCO) with activated persulfate has received considerable attention (Lee et al., 2011, 2009; Park et al., 2011; Tsitonaki et al., 2010; Yang et al., 2013), but while results to date show some success destroying PFOA and related perfluoroalkyl carboxylic acids (PFCAs), the more widely detected perfluoroalkyl sulfonic acids (PFSA) like PFOS remain resistant to treatment (Yang et al., 2013). Reactions with zerovalent iron (ZVI) at ambient environmental conditions, an effective option for treating chlorinated hydrocarbon contaminants (e.g., PCE, TCE) (Miehr et al., 2004; Su and Puls, 1999), is completely ineffective for treating fluorinated chemicals like PFASs due to the much stronger C-F bonds (Merino et al., 2016).

Recent studies have reported on PFAS transformations via electrochemical (Le et al., 2019), UV photochemical and photocatalytic (Gu et al., 2016; Sahu et al., 2018), sonochemical (Vecitis et al., 2010), plasma (Stratton et al., 2017), and mechanochemical (Zhang et al., 2013) technologies that can be applied in an ex-situ fashion. However, most of these reports indicate incomplete mineralization of PFASs and/or ineffectiveness for some PFASs, e.g., such as perfluorooctane sulfonate (PFOS) during activated persulfate treatment (Bruton and Sedlak, 2017). Furthermore, electrochemical and other treatment systems that rely on reactions of PFASs at solid surfaces (e.g., direct reactions at anodes) (Lin et al., 2012; Ochiai et al., 2011; Schaefer et al., 2015; Zhuo et al., 2016) can be expected to be of limited utility treating on-site waste samples containing a mixture of solids and water. Slow or incomplete PFAS transformation is often accompanied by detection of shorter-chain fluorinated compounds that may still pose environmental risks (Brendel et al., 2018; Ochoa-Herrera et al., 2008). Ensuring complete mineralization generally requires incineration or other high temperature thermal treatments (Wang et al., 2013; Watanabe et al., 2018). While this may be practical for PFAS-containing solid wastes, incineration of wet wastes and concentrate solutions is inefficient because of the high energy requirements for vaporizing water (González-Martínez et al., 2019).

2.5 Hydrothermal Processing of Organic Materials

Subcritical hydrothermal processing is an alternative technology uniquely suited to processing wet waste concentrates, including contaminated IDW. Hydrothermal technologies apply elevated temperatures and pressures (200-374°C, 2-22 MPa) to water in a sealed environment that prevents vaporization (**Figure 2.1**), leading to a uniquely reactive environment that has been shown to catalyze many chemical transformations that do not occur at lower temperatures (Peterson et al., 2008; Savage, 2009). For example, increasing the temperature of condensed phase water dramatically reduces the dielectric constant of water (making it more like a polar organic solvent)

while simultaneously increasing the acid self-dissociation constant by nearly two orders-of-magnitude (thereby increasing rates of acid- and base-catalyzed reactions) (Savage, 2009).

Subcritical hydrothermal reactions are currently being heavily exploited for production of biorenewable fuels and chemicals (Peterson et al., 2008; Savage, 2012; Vardon et al., 2011). While somewhat counterintuitive, heating compressed water to subcritical hydrothermal conditions consumes much less energy than evaporating water at lower temperatures. As a result, processing wet materials in their native state without drying eliminates parasitic energy losses present in dry thermal processing technologies (e.g., pyrolysis, gasification, incineration). Thus, hydrothermal technologies are leading contenders for processing a diverse stream of renewable wet organic waste materials (e.g., algal biomass, wastewater solid residuals), generating liquid biocrude products that can be upgraded to transportation-grade fuels (Biller et al., 2015; Elliott et al., 2014, 1990), and pilot-scale reactor systems are currently being demonstrated at several locations. (“Genifuel - Welcome,” n.d.)

The same properties responsible for decomposition and transformation of biomass under hydrothermal conditions can potentially be exploited to degrade recalcitrant organic contaminants, including PFASs. For example, scattered reports in literature show that halogenated organics, including polychlorinated biphenyls (PCBs) and haloacetic acids are effectively degraded under hydrothermal conditions (Yamasaki et al., 1980).

While PFASs are highly recalcitrant chemicals that are unreactive with common chemical reagents (e.g., oxidants, reductants) at ambient temperature (Merino et al., 2016), rapid reaction with the same reagents may occur under hydrothermal conditions

For example, Hori and co-workers reported promising results of experiments showing decomposition and defluorination of PFOS and perfluorohexane sulfonate (PFHxS) in subcritical hydrothermal solutions amended with zerovalent iron.^{26,27} Although the PFASs were transformed, reactions required elevated iron loadings (>50 g/L) and mineralization was incomplete. While these findings support the promise of hydrothermal processing for PFAS destruction, a more systematic screening of reactive amendments was needed to identify lower cost reagents that are more effective in catalyzing the mineralization of PFASs and identify the controlling reaction mechanisms.

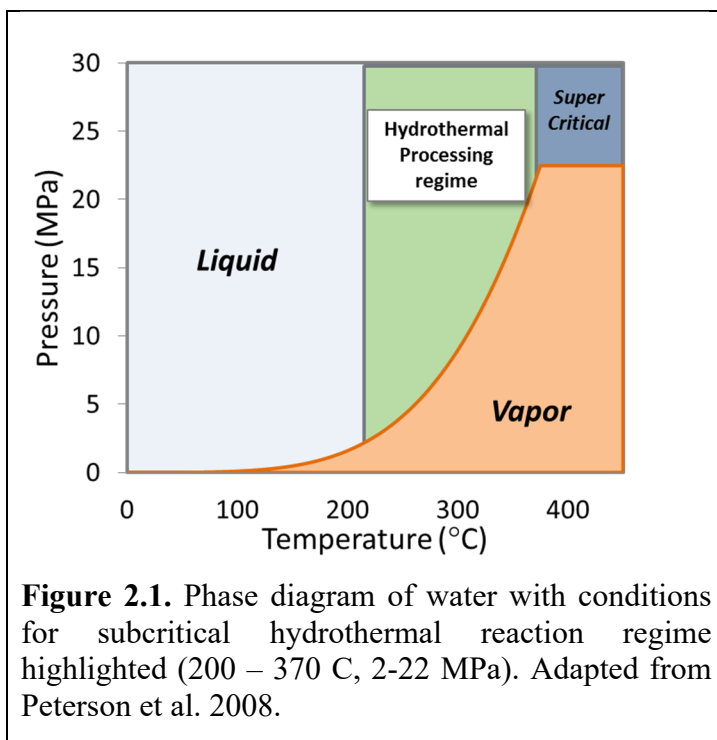


Figure 2.1. Phase diagram of water with conditions for subcritical hydrothermal reaction regime highlighted (200 – 370 C, 2-22 MPa). Adapted from Peterson et al. 2008.

3.0 Materials and Methods

3.1 Overall Study Approach

The overall study design included seven related tasks that are summarized in **Figure 3.1**. Task 1 focused on screening a wide range of reaction amendments, including acids, bases, oxidants, reductants, and metallic nanoparticles, for their potential to enhance PFOS and PFOA degradation and defluorination under hydrothermal conditions. As such, both the extent of fluoride ion release and residual PFOS concentration were measured following reactions. For the most reactive amendments, follow-up experiments were conducted to measure reaction kinetics and products in greater detail.

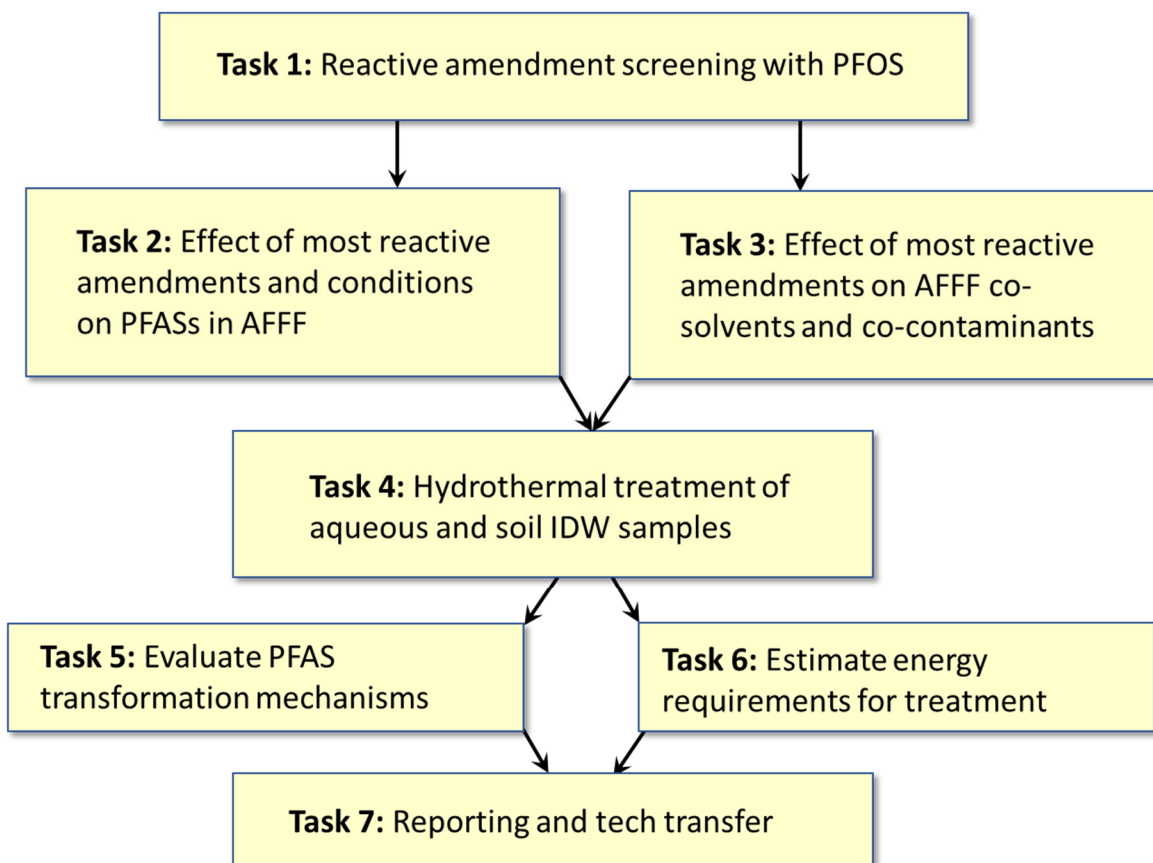


Figure 3.1 Experimental approach and tasks.

Task 2 then evaluated degradation of the wider range of PFASs present in AFFF under conditions that were found in Task 1 to be optimal for PFOS degradation. This effort benefitted from application of high resolution LC-QToF-MS analysis using both a target list of PFAS analytes as well as a larger suspect screening library of >1500 PFAS structures to track a wide diversity of PFASs identified in different AFFF formulations.

Task 3 then evaluated the stability and degradation of model AFFF co-solvents and co-contaminants, and Task 4 measured degradation of PFASs present in aqueous and solid IDW

samples under the same reaction conditions. Co-solvents included diethylene glycol monobutyl ether (DGBE), a common co-solvent used in AFFF and methanol. Representative co-contaminants considered included trichloroethylene as a model halogenated solvent and benzene, toluene, m-xylene, and ethylbenzene as model hydrocarbon fuel-derived contaminants. Aqueous and soil IDW samples were collected from an old fire training area (FTA) and an active fire station at Plattsburgh, respectively. PFAS concentrations measured in the soil IDW samples were very low, so three PFAS-contaminated soils collected previously from other DoD sites throughout the U.S. were utilized.

Task 5 combined the results of experiments and available literature to provide an initial assessment of the major pathways and mechanisms for hydrothermal decomposition of PFASs, and Task 6 provided an initial assessment of the energy requirements for hydrothermal treatment of wet waste materials in comparison with incineration. Finally, Task 7 included all reporting and technology transfer activities.

3.2 Chemicals and Reagents

Table 3.2.1 provides a complete list of the commercial chemical reagents used in experiments. All PFAS standards and internal standards were purchased from Wellington Laboratories, Ontario, Canada. In addition to these individual reagents, experiments were conducted using two aqueous film-forming foam (AFFF) stock solutions. Analysis of one AFFF (designated AFFF #1), used for most experiments, indicates it is derived from an electrochemical fluorination process that produces predominantly perfluoroalkyl sulfonic acids with even and odd numbers of perfluorocarbons. This AFFF was obtained from Peterson Air Force Base in Colorado. For comparison, selected experiments were also conducted with a second AFFF (designated AFFF #2) containing PFASs characteristic of synthesis through the telomerization process. The second AFFF was obtained from the University of Minnesota.

3.3 Investigation-Derived Wastes (IDW) and PFAS-Contaminated Soils

IDW collected for the project included two groundwater samples (MW-008 and MW-004) and two soils (PFFTA-MW-001 and PFFTA-MW-002). MW-008 and MW-004 were collected from an old FTA and an active fire station at Plattsburgh AFB (NY), respectively. PFFTA-MW-001 and PFFTA-MW-002 were collected from a sandy surficial aquifer during installation of a pair of Till and Bedrock wells located on the edge of the former FTA. The samples from each location represent a composite of subsamples collected from approximately 0-50 ft below ground surface (bgs). Our initial characterization of the soil IDW samples showed PFAS concentrations were very low, so three other PFAS-contaminated soils collected previously from other DoD sites throughout the U.S. (Wurtsmith soil, JAX soil, and PAFB soil) were used instead for testing hydrothermal reaction of PFAS-contaminated soil. Wurtsmith soil was collected from Wurtsmith AFB (MI) by hand shovel. JAX soil was sampled from 11.5-12.5 ft bgs increment of a soil core collected by applying direct push technology (DPT) methods at the Jacksonville Naval Air Station (NAS) (FL). PAFB soil was collected by hand shovel at the Peterson AFB (CO) fire station. All contaminated water and soil samples were refrigerated prior to use.

Table 3.2.1 Reagent list

Reagent	Purity grade	CAS#	Supplier
Bases and Acids			
NaOH	97%	1310-73-2	Merck, Germany
Ca(OH) ₂	95%	1305-62-0	Sigma-Aldrich, USA
Na ₂ CO ₃	99.5%	497-19-8	Sigma-Aldrich, USA
HCl	30 wt.% in water	7647-01-0	Sigma-Aldrich, USA
H ₂ SO ₄	98%	7664-93-9	Sigma-Aldrich, USA
HNO ₃	65 wt.% in water	7697-37-2	Sigma-Aldrich, USA
Oxidants			
K ₂ FeO ₄	97%	39469-86-8	Element 26 Technol, TX, USA
KMnO ₄	97%	7722-64-7	Sigma-Aldrich, USA
K ₂ CrO ₄	99%	9016-11-9	Sigma-Aldrich, USA
NaClO ₄	98%	7601-89-0	Sigma-Aldrich, USA
NaClO ₃	97%	7775-09-9	Sigma-Aldrich, USA
NaClO	Available chlorine: 5 wt. % in water	7681-52-9	Sigma-Aldrich, USA
H ₂ O ₂	30 wt.% in water	7722-84-1	Sigma-Aldrich, USA
Reductants			
NaBH ₄	98%	16940-66-2	Sigma-Aldrich, USA
Na ₂ SO ₃	98%	7757-83-7	Sigma-Aldrich, USA
Na ₂ S ₂ O ₃	99.5%	7772-98-7	Sigma-Aldrich, USA
Na ₂ S ₂ O ₄	82.5%	7775-14-6	Sigma-Aldrich, USA
Na ₂ S ₂ O ₅	98%	7681-57-4	Sigma-Aldrich, USA
Na ₂ S ₂ O ₈	98%	7775-27-1	Sigma-Aldrich, USA
NaHSO ₅	98%	28831-12-1	Sigma-Aldrich, USA
KI	99%	7681-11-0	Sigma-Aldrich, USA
FeSO ₄	99%	7782-63-0	Sigma-Aldrich, USA
Fe(0)	97%, 325 mesh	7439-89-6	Sigma-Aldrich, USA
AFFF Co-solvents			
Diethylene glycol monobutyl ether	≥98.0%	112-34-5	Sigma-Aldrich, USA
Methanol	Optima LC-MS grade	67-56-1	Fisher Scientific, USA
AFFF Co-contaminants			
Trichloroethylene	≥99.5%	79-01-6	Sigma-Aldrich, USA
Toluene	99.8%	108-88-3	Sigma-Aldrich, USA
Benzene	99.8%	71-43-2	Sigma-Aldrich, USA
m-Xylene	≥99%	108-38-3	Sigma-Aldrich, USA
Ethylbenzene	99.8%	100-41-4	Sigma-Aldrich, USA
Other			
NaNO ₃	99%	7631-99-4	Sigma-Aldrich, USA
FeCl ₃	97%	7705-08-0	Sigma-Aldrich, USA
NiCl ₂	98%	7718-54-9	Sigma-Aldrich, USA
ZnCl ₂	97%	7646-85-7	Sigma-Aldrich, USA
NaH ₂ PO ₄	99%	7558-80-7	Sigma-Aldrich, USA
Na ₂ HPO ₄	99%	7558-79-4	Sigma-Aldrich, USA
NaF	99%	7681-49-4	Sigma-Aldrich, USA
D ₂ O	99.96 atom % D	7789-20-0	Sigma-Aldrich, USA
Ammonium acetate	Optima LC-MS grade	631-61-8	Fisher Scientific, USA
Ammonium hydroxide	Optima grade	1336-21-6	Fisher Scientific, USA
Methanol	Optima LC-MS grade	67-56-1	Fisher Scientific, USA
Isopropanol	Optima LC-MS grade	67-63-0	Fisher Scientific, USA
Water (for LC-MS/MS)	Optima LC-MS grade	7732-18-5	Fisher Scientific, USA

3.4 Hydrothermal Reactions

Batch hydrothermal reactions were conducted in duplicate using stainless steel mini-tube reactors plugged with Swagelok® stainless steel-316 port connectors on both ends (1.27 cm outer diameter × 10 cm length, 0.12 cm wall thickness, , and 5.33 mL working volume) (**Figure 3.4.1a**). PFAS-containing solutions and soil suspensions were added to the reactors together with water and the appropriate reactive amendments before sealing. The reactor was then heated to the desired temperature by submersing in a temperature-controlled fluidized sand bath (TIPTEMP company, NJ, USA) that was preheated to the desired reaction temperature (200-350 °C). After the specified reaction time, the reaction was quenched by submersing the reactor in tap water. Separate tests with thermocouples inserted into the same reactors filled with water showed that the reactor temperature reached the target value within 4 min. Thermocouple readings also showed that reactor contents were cooled within 2 min. The reactor was then opened, and liquid and solid contents were collected for analysis. For selected reactions, experiments were carried out in modified reactors outfitted with a gas sampling port to analyze for potential volatile products (**Figure 3.4.1b**).

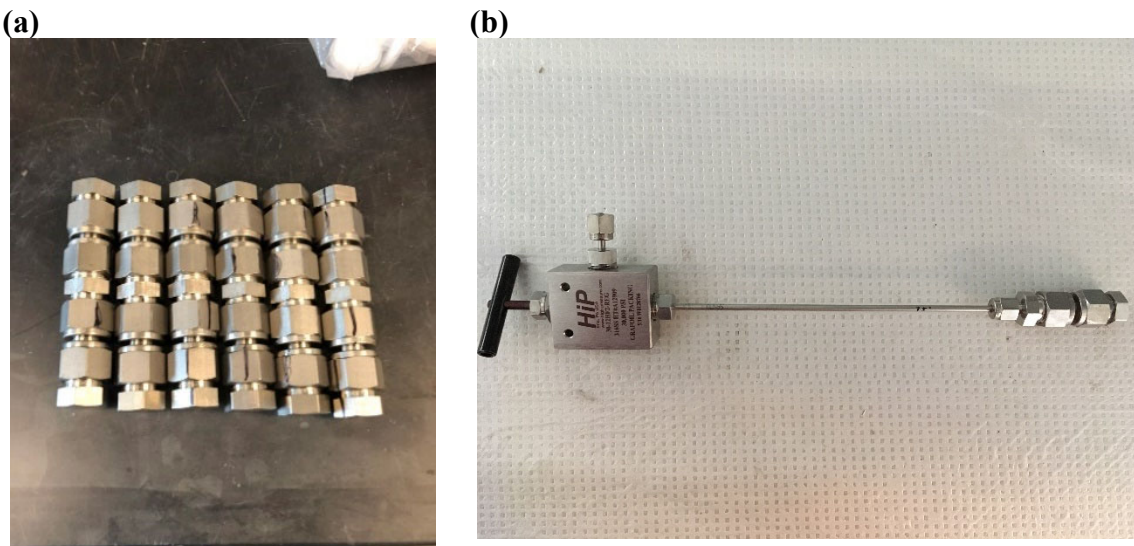


Figure 3.4.1 (a) Mini-tube batch reactors used for hydrothermal treatment experiments. (b) Reactors outfitted with specialized gas sampling valve.

3.4.1 Amendment screening experiments

Amendment screening experiments were first conducted to examine PFOS degradation and defluorination in the presence of a wide range of acids, bases, oxidants, and reductants. Hydrothermal conversion experiments focused on identifying amendments that promote degradation of PFOS because initial tests showed that it was much more recalcitrant than perfluorooctanoic acid (PFOA). Whereas test reactions without any added amendments showed >99% degradation of 50 mg/L PFOA (250°C, 30 min), <1% of PFOS degraded under the same conditions. Thus, an aqueous solution containing 50 mg/L PFOS (0.001 mol/L) was added to the reactor together with the desired amendment (typically 1 mol/L) before sealing and heating to 350

°C (and an estimated 16.5 MPa autogenous pressure developed inside the reactor) for a reaction time of 90 min. After cooling, liquid contents of the reactor were collected and analyzed for final pH, released F⁻ concentration, and residual PFOS concentration.

3.4.2 PFOS and PFOA reactions

Screening experiments indicated that optimal PFOS reactivity was observed in solutions amended with NaOH. Additional batch experiments were then conducted to evaluate the kinetics of PFOS degradation and defluorination in solutions amended with variable concentration of NaOH, batch experiments were conducted to evaluate the effect of reaction temperatures, and the effects of pre-heating/re-cooling reactive amendments before introducing PFOS. Furthermore, initial attempts were made to identify organic transformation products in reactions initiated with either PFOS or PFOA.

3.4.3 AFFF experiments

Building on results of experiments conducted with only PFOS or PFOA, hydrothermal reactions were conducted in water amended with AFFF mixtures. The experimental procedure and reactors were the same as those described in earlier sections. Screening experiments were first conducted in which the most effective amendments identified with PFOS were screened for hydrothermal defluorination of AFFF #1 (350°C, 1 mol/L amendment, 180 min reaction time). More detailed reaction studies with AFFF were then conducted using NaOH as the optimal amendment. A wide range of reaction conditions, including initial AFFF dilution ratio (diluted from 1-to-1000 in water to 1-to-2), AFFF composition (PFSA-dominant vs. fluorotelomer-dominant formulas), reaction temperature (200 – 350°C), and reaction time (15 – 360 min) were evaluated. Aqueous products from the reactor were collected and analyzed for PFASs (LC-QToF-MS - both targeted analysis and suspect screening analysis), release of fluoride (ISE), and average molecular fluorine speciation (¹⁹F-NMR spectroscopy). Selected experiments were also conducted in reactors outfitted with a gas collection port to allow for collection of headspace samples for analysis (**Figure 3.4.1**). Gas products were collected in gas sampling bags and analyzed by gas chromatography with flame-ionization detection (GC-FID), thermal conductivity detector (GC-TCD), and tandem mass spectrometry (GC-MS/MS).

3.4.4 Reactions of co-solvents and co-contaminants

Separate batch hydrothermal experiments were conducted to provide a preliminary assessment of the stability and reactivity of co-solvents and co-contaminants often associated with AFFF and AFFF FTA sites. Reactions were conducted in water amended with NaOH and two different co-solvents, diethylene glycol monobutyl ether (DGBE) and methanol, and five different co-contaminants, trichloroethylene (TCE), benzene, toluene, ethylbenzene, and m-xylene. The hydrothermal reactivities of these compounds were investigated individually under identical hydrothermal conditions (350°C, 1 mol/L NaOH, and 90 min reaction time). The initial concentrations of DGBE and methanol were set to 5000 mg/L and initial co-contaminant concentrations were set at 50 mg/L. After reaction, residual concentrations were measured to assess stability of the chemicals under conditions where destruction of PFASs was observed.

3.4.5 Experiments with IDW and PFAS-contaminated soils

Finally, experiments were conducted to evaluate destruction of PFASs present in aqueous IDW samples and PFAS-contaminated soil samples collected from DoD facilities. PFAS composition and concentrations in the aqueous and soil samples were analyzed before use in experiments using methods described below. Soil samples were subjected to an extraction and cleanup procedure before analysis. Approximately 0.5 g of soil was weighed into a 50 ml polypropylene centrifuge tube, and then 4 mL methanol was added to the tube, which was vortexed for 30 s, sonicated for 15 min at 30°C, and centrifuged at 2470 rcf for 20 min. Finally, the supernatant was decanted and the next extraction round was begun. After four extraction rounds, the supernatants were pooled and passed through ENVI-Carb (Sigma-Aldrich, 250 mg) solid-phase extraction (SPE) cartridges. The resultant pooled extract was evaporated to dryness under nitrogen (N₂) in a 30 °C water bath and reconstituted in 1.5 mL of 1% acetic acid in methanol. One method blank, containing only extraction solvents and PFAS internal standards, was prepared alongside each extraction batch.

Aqueous IDW and soil samples were subjected to hydrothermal reaction at 350°C, 5 mol/L NaOH, and a reaction time of 90 min. For PFAS-contaminated soils, 0.5 g of each soil were added to reactors together with 3 ml of the NaOH solution (20 wt% solid suspension) before sealing and subjecting to reaction conditions. After reaction, soil was subjected to the same extraction and cleanup procedure used to characterize the unreacted soils. Aqueous phase reaction solutions were also analyzed for fluoride ion before and after reaction.

3.5 Analysis

3.5.1 Fluoride ion release

Fluoride ion concentrations were measured by a fluorine ion selective electrode (Thermo Fisher, MA USA) after pH buffering of the samples to pH 5.0-5.5. NaF standard addition tests and ion chromatography (IC) analysis were conducted to verify the accuracy of fluoride ion measurement by electrode method. For the standard addition tests, known concentrations of fluoride were added into the reacted samples (50 mg·L⁻¹ PFOS, 1 mol·L⁻¹ NaOH; 350 °C, 90 min) as NaF, and the electrode-measured recovery rates of additional fluoride ion were 110-115% as shown in **Figure 3.5.1a**. The electrode-measured fluoride ion concentration of time-course samples (50 mg·L⁻¹ PFOS, 1 mol·L⁻¹ NaOH; 350 °C, 0-480 min) was also in accordance with that of ion chromatography (IC) analysis (**Figure 3.5.1b**).

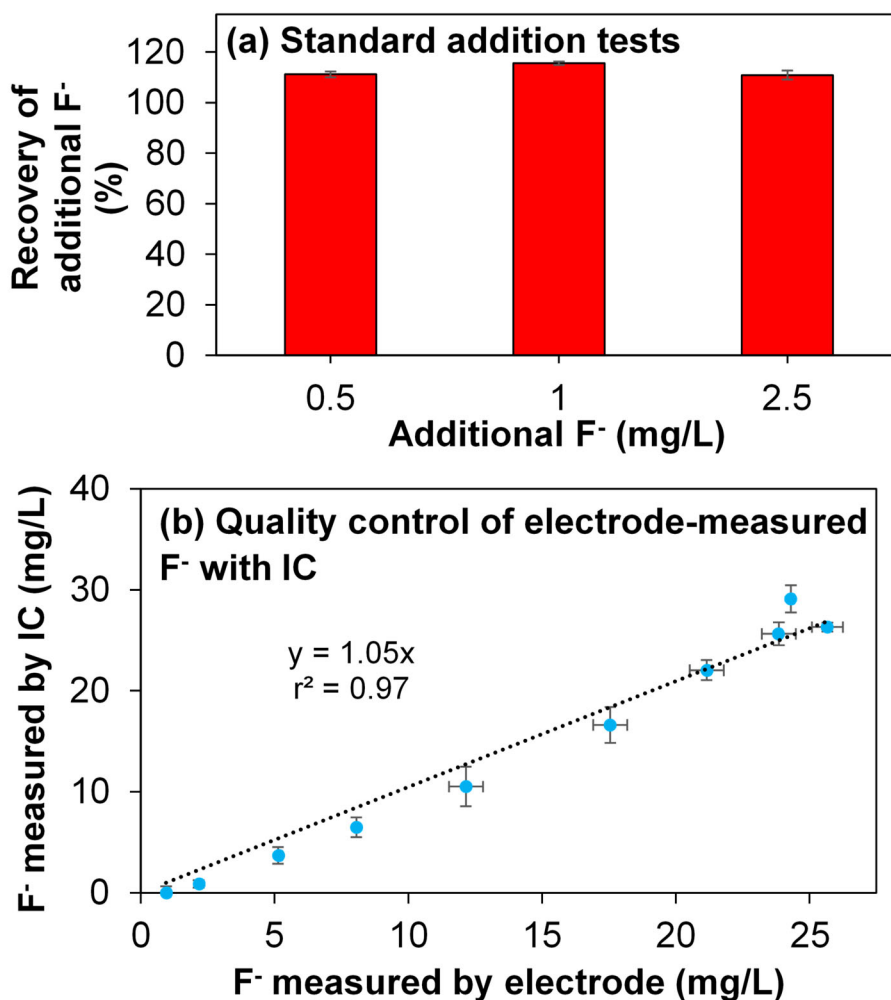


Figure 3.5.1 Accuracy evaluation of electrode measurement of fluoride ion concentration. (a) Electrode measured recovery rates of additional fluoride ions added to the reacted samples (50 mg·L⁻¹ PFOS, 1 mol·L⁻¹ NaOH; 350 °C, 90 min). (b) Comparison of IC- and ISE-measured fluoride ion concentrations of reacted PFOS samples for different reaction time periods. Each symbol represents one sample collected at a certain reaction time. The higher yield of fluoride ion was due to the longer reaction time. Reaction conditions: PFOS (50 mg/L), NaOH (1 mol/L), 350 °C, 0-480 min. Error bars represent min/max values observed for duplicate experiments (smaller than symbol if not visible).

3.5.2 PFAS analysis

A. LC-MS/MS. For experiments initiated with PFOS or PFOA alone, concentrations of the parent PFAS and selective perfluoroalkyl acid intermediate products were determined by liquid chromatography coupled with triple quadrupole mass spectrometry (LC-MS/MS; Agilent 1100 LC coupled to an Applied Biosystem API 3200 triple-quad mass spectrometer). Prior to analysis, samples were diluted 100,000-fold with a solution containing isotopically labeled internal standards, methanol, isopropanol, and dilute ammonium hydroxide. Chromatographic separations of the injected samples (1 mL) were performed using a Phenomenex (Torrance, CA, USA) Gemini

C18 (100 × 3 mm, 5 μm) analytical column, which was preceded by a Phenomenex Gemini C18 guard column (4 × 2 mm) and two Agilent (Santa Clara, CA, USA) Zorbax Diol guard columns (4.6 × 12.5 mm, 6 μm). Analytical and guard columns were maintained at 40 °C during analysis. Flow rate was 0.6 ml/min, and the gradient mobile phase consisted of 20 mM of ammonium acetate in water (A) and in methanol (B) starting at 10% B, increased to 50% B in the first 0.5 min, increased to 99% B at 8 min, and maintained for 5 min, decreased to 10% B in 0.5 min, and maintained at 10% B to 20 min. Samples were introduced into the mass spectrometer via electrospray ionization (negative mode) with an applied voltage of -4500 V. Source temperature was 550 °C, spectra accumulation time was 0.2 s, and scan time was 0.842 s. Detailed MS/MS analysis conditions are described in **Table 3.5.1**.

Table 3.5.1 PFAS analytes names (acronyms), acquisition masses, parameters, internal standard used for LC-MS/MS analysis. Number next to analytes name represents selected for quantification (1) or confirmation (2).

Name (Acronym)	Precursor > Product ion	DP	EP	CE	CXP	IS
PFBA(1)	212.83 > 168.9	-10	-4.5	-12	0	MPFBA(1)
PFPeA(1)	262.84 > 218.9	-10	-5	-12	0	M5PFPeA(1)
PFHxA(1)	312.906 > 269	-10	-6	-12	0	M2PFHxA(1)
PFHxA(2)	312.906 > 118.8	-10	-6	-30	-4	M2PFHxA(1)
PFHpA(1)	362.9 > 319.1	-10	-4	-12	-2	M4PFHpA(1)
PFHpA(2)	362.9 > 168.9	-10	-4	-26	0	M4PFHpA(2)
PFOA(1)	412.912 > 369	-10	-4.5	-14	-2	M4PFOA(1)
PFOA(2)	412.912 > 168.9	-10	-4.5	-24	-4	M4PFOA(1)
PFOS(1)	498.897 > 79.9	-70	-7.5	-86	-6	MPFOS(1)
PFOS(2)	498.897 > 98.9	-70	-7.5	-54	0	MPFOS(1)
MPFBA(1)	216.859 > 171.8	-10	-4.5	-16	0	
M5PFPeA(1)	267.852 > 222.9	-10	-4	-12	-2	
M2PFHxA(1)	314.98 > 269.98	-10	-6	-12	-2	
M2PFHxA(2)	314.98 > 120	-10	-6	-30	0	
M4PFHpA(1)	366.898 > 322	-15	-5.5	-12	-2	
M4PFHpA(2)	366.898 > 171.9	-15	-5.5	-24	0	
M4PFOA(1)	416.929 > 372.1	-10	-4	-14	0	
M4PFOA(2)	416.929 > 171.9	-10	-4	-28	-4	
MPFOS(1)	502.968 > 79.9	-70	-7	-74	-6	
MPFOS(2)	502.968 > 98.9	-70	-7	-66	0	

1. Selected for Quantification; (2), selected for confirmation; DP, declustering potential; CE, collision energy; EP, entrance potential; CXP, collision cell exit potential; IS, internal standard

B. LC-QToF-MS. For experiments with AFFF and IDW, target analysis (45 PFAS analytes with commercial standards), suspect screening analysis (1425 suspected PFAS compounds in a custom extracted ion chromatogram (XIC) list), and semiquantitative analysis were conducted by high

resolution LC-QToF-MS to determine the parent PFAS degradation and identify selected transformation products. Recent work by Nickerson et al. (Nickerson et al., 2020) reported this PFASs analytical method and more details are described below.

Each aqueous sample was diluted to maintain concentrations within the calibration range (0.07 - 7,400 ng·L⁻¹ PFAS concentrations) and adjusted to pH = 5 - 9. Aqueous ammonium hydroxide solution (0.01 % Optima® HPLC-grade ammonium hydroxide (Fisher Scientific, Fair Lawn, NJ) in Optima® HPLC-grade water (Fisher Scientific)), Optima® HPLC-grade isopropanol (Fisher Scientific), internal standards (labeled PFASs from Wellington Laboratories Inc), and Optima® HPLC-grade methanol (Fisher Scientific) were added into samples to make up a solution containing 64% of total volume of sample, 23% methanol, 3% ammonium hydroxide in water, 10% isopropanol, and 100 pg/1.35 mL IS. Each sample was then vortexed for 15 s and centrifuged at 4,000 rpm for 10 minutes. A 1.35 mL aliquot was then transferred to a 2 mL amber glass HPLC vials for analysis.

One mL of each sample was injected into a SCIEX Exion LC high-pressure liquid chromatography (HPLC) system with a Gemini C18 analytical column (3 mm x 100 mm x 5 µm; Phenomenex, Torrance, CA) with one SecurityGuard™ C18 Guard Cartridge (4 mm x 2 mm I.D.; Phenomenex) and two Zorbax DIOL guard columns (4.6 mm x 12.5 mm x 6 µm; Agilent, Santa Clara, CA). The column oven temperature was 40 °C. The aqueous mobile phase included two eluents: (A) 20 mM ammonium acetate (Fisher Scientific) in Optima® HPLC-grade water and (B) 100% Optima® HPLC-grade methanol. Eluent flow rate was held at 0.60 mL/min, and composition was ramped from 0 - 0.5 min (90% A and 10% B), 0.5 - 8 min (50% A and 50% B), from 8 - 13 min (1% A and 99% B), from 13 - 20 min (90% A and 10% B).

PFASs were measured on a SCIEX X500R QTOF-MS system (Framingham, MA) using electrospray ionization in negative mode (ESI-) with SWATH® Data-Independent Acquisition for both TOFMS and MS/MS mode. Precursor ion data was collected for m/z 100-1200 for 1283 cycles with a total scan time of 842 ms and accumulation time of 20 ms, with ion spray voltage set at -4500 V and temperature set to 550 °C. The ion source, curtain, and collision gas were set to 60 psi, 35 psi, and 10 psi, respectively. The collision energy was set to -5 V and the declustering potential to -20 V, both with no spread. Product ion (MS/MS) scanning was conducted for m/z 50-1200 Da. The accumulation time for each SWATH window was 50 ms and collision energy was -35 V with 30 V spread. The instrument was mass calibrated every 5 injections using SCIEX ESI Negative Calibration Solution.

Quality assurance samples were included during sample preparation. For each sample batch (a group of 20 samples or less) a method blank, laboratory control sample (LCS), and matrix spike were included. Method blanks (internal standard added) consist of HPLC-grade water prepared by the same procedure used for the real samples. The LCS was also prepared by spiking HPLC-grade water with a known concentration of standards with the same recipe used for the real samples. The final concentration of PFAS in the LCS was greater than the limit of quantification of all PFAS, but also falls below the midpoint of the calibration curve. The matrix spike was spiked in the same way with a randomly selected sample from the batch. The LCS and matrix spike were then treated as samples. All samples, including all QC, were spiked with internal standards. All concentrations in all samples were corrected for internal standard recoveries. Analytes with internal standard or injection standard recoveries outside of 50-150% were flagged and the whole batch was

reanalyzed. Method blanks were less than half the lower quantitation limit for compounds with reference standards: if this was not the case, the reporting limit (RL) was raised for those affected analytes (the RL will be set to 3 times the highest blank concentration). The LCS was used as a check that analytes were not lost during the preparation process, with calculated concentrations within 30% of expected concentrations. The same criteria applied to matrix spikes. Analytical replicates prepared in triplicate gives % Relative Standard Deviation \leq 30% (in case of duplicate, % Relative Percent Difference \leq 30%).

Quantitative data acquisition and processing were done using SCIEX OS Version 1.5.0 to quantify targeted analytes. Confirmation of targeted analytes with signal-to-noise ratio $>$ 10:1 was based on retention time and accurate mass (XIC window 0.02 Da) compared to analytical standards. Expected retention time for each analyte was set based on a calibration point near the middle of the calibration curve that ran at the beginning of the sequence. Initial integration parameters included defining 90% of lowest-intensity peaks as noise, using a baseline-subtract window of 2 minutes, a minimum peak intensity of 100, and a peak width of 10 points. Some peaks with peak intensity below the threshold were manually integrated where retention time, accurate mass, and isotope confidence were determined to be satisfactory. Confirmation of targeted analytes was based on retention time and accurate mass compared to analytical standards ($<$ 10 ppm). A list of target analytes and internal standards used for quantitation is provided in **Table 3.5.2**. Calibration range, limit of quantitation, and linear fit (r^2) of calibration curves for all analytes were recorded for each analytical run. If the blanks were all $<$ 1/2 LOQ, the RL was set as the LOQ. Otherwise, the RL was set to 3 times the highest blank concentration.

Table 3.5.2 List of targeted analytes for PFAS analysis.

Chemical Name	Acronym	Neutral Molecular Formula	Internal Standard
Perfluoroalkanoic acids			
Perfluoro-n-butanoic acid	PFBA	C ₄ HO ₂ F ₇	¹³ C ₄ -PFBA
Perfluoro-n-pentanoic acid	PFPeA	C ₅ HO ₂ F ₉	¹³ C ₅ -PFPeA
Perfluoro-n-hexanoic acid	PFHxA	C ₆ HO ₂ F ₁₁	¹³ C ₂ -PFHxA
Perfluoro-n-heptanoic acid	PFHpA	C ₇ HO ₂ F ₁₃	¹³ C ₄ -PFHpA
Perfluoro-n-octanoic acid	PFOA	C ₈ HO ₂ F ₁₅	¹³ C ₄ -PFOA
Perfluoro-n-nonanoic acid	PFNA	C ₉ HO ₂ F ₁₇	¹³ C ₅ -PFNA
Perfluoro-n-decanoic acid	PFDA	C ₁₀ HO ₂ F ₁₉	¹³ C ₂ -PFDA
Perfluoro-n-undecanoic acid	PFUdA	C ₁₁ HO ₂ F ₂₁	¹³ C ₂ -PFUdA
Perfluoro-n-dodecanoic acid	PFDoA	C ₁₂ HO ₂ F ₂₃	¹³ C ₂ -PFDoA
Perfluoro-n-tridecanoic acid	PFTTrDA	C ₁₃ HO ₂ F ₂₅	¹³ C ₂ -PFTTrDA
Perfluoro-n-tetradecanoic acid	PFTeDA	C ₁₄ HO ₂ F ₂₇	¹³ C ₂ -PFTeDA
Perfluoro-n-hexadecanoic acid	PFHxDA	C ₁₆ HO ₂ F ₃₁	¹³ C ₂ -PFHxDA
Perfluoro-n-octadecanoic acid	PFODA	C ₁₈ HO ₂ F ₃₅	¹³ C ₂ -PFHxDA
Perfluoroalkane Sulfonates			
Perfluoropropane sulfonate	PFPrS	C ₃ HO ₃ SF ₇	¹³ C ₃ -PFBS
Perfluorobutane sulfonate	PFBS	C ₄ HO ₃ SF ₉	¹³ C ₃ -PFBS
Perfluoropentane sulfonate	PFPeS	C ₅ HO ₃ SF ₁₁	¹³ C ₂ -PFOS
Perfluorohexane sulfonate	PFHxS	C ₆ HO ₃ SF ₁₃	¹⁸ O ₂ -PFHxS

Perfluoroheptane sulfonate	PFHpS	C ₇ HO ₃ SF ₁₅	¹⁸ O ₂ -PFHxS
Perfluorooctane sulfonate	PFOS	C ₈ HO ₃ SF ₁₇	¹³ C ₄ -PFOS
Perfluorononane sulfonate	PFNS	C ₉ HO ₃ SF ₁₉	¹³ C ₄ -PFOS
Perfluorodecane sulfonate	PFDS	C ₁₀ HO ₃ SF ₂₁	¹³ C ₄ -PFOS
Perfluoroundecane sulfonate	PFUDS	C ₁₁ HO ₃ SF ₂₃	¹³ C ₄ -PFOS
Perfluorododecane sulfonate	PFDoS	C ₁₂ HO ₃ SF ₂₅	¹³ C ₄ -PFOS
Chlorinated perfluoroalkane sulfonates and ether sulfonates			
8-chloro-perfluorooctane sulfonate	Cl-PFOS	C ₈ HO ₃ SClF ₁₆	¹³ C ₄ -PFOS
9-chloro-3-oxa-perfluorononane sulfonate	Cl-O-PFNS	C ₈ HO ₄ SClF ₁₆	¹³ C ₄ -PFOS
11-chloro-3-oxa-perfluoroundecane sulfonate	Cl-O-PFUDS	C ₁₀ HO ₄ SClF ₂₀	¹³ C ₄ -PFOS
Perfluoroalkane sulfonamides			
Perfluorooctane sulfonamide	FOSA	C ₈ H ₂ O ₂ SNF ₁₇	¹³ C ₈ -FOSA
N-methylperfluoro-1-octane sulfonamide	MeFOSA	C ₉ H ₄ O ₂ SNF ₁₇	d3-MeFOSA
N-ethylperfluoro-1-octane sulfonamide	EtFOSA	C ₁₀ H ₆ O ₂ SNF ₁₇	d5-EtFOSA
Perfluoroalkane sulfonamido acetic acids			
Perfluorooctane sulfonamido acetic acid	FOSAA	C ₁₀ H ₄ O ₄ SNF ₁₇	d3-MeFOSAA
N-methylperfluorooctane sulfonamido acetic acid	MeFOSAA	C ₁₁ H ₆ O ₄ SNF ₁₇	d3-MeFOSAA
N-ethylperfluorooctane sulfonamido acetic acid	EtFOSAA	C ₁₂ H ₈ O ₄ SNF ₁₇	d5-EtFOSAA
Fluorotelomer Sulfonates			
4:2 fluorotelomer sulfonate	4:2 FTS	C ₆ H ₅ O ₃ SF ₉	¹³ C ₂ -4:2 FTS
6:2 fluorotelomer sulfonate	6:2 FTS	C ₈ H ₅ O ₃ SF ₁₃	¹³ C ₂ -6:2 FTS
8:2 fluorotelomer sulfonate	8:2 FTS	C ₁₀ H ₅ O ₃ SF ₁₇	¹³ C ₂ -8:2 FTS
10:2 fluorotelomer sulfonate	10:2 FTS	C ₁₂ H ₅ O ₃ SF ₂₁	¹³ C ₂ -8:2 FTS
Fluorotelomer Alkanoic Acids			
3:3 fluorotelomer carboxylic acid	3:3 FTCA	C ₆ H ₅ O ₂ F ₇	¹³ C ₂ -6:2 FTCA
5:3 fluorotelomer carboxylic acid	5:3 FTCA	C ₈ H ₅ O ₂ F ₁₁	¹³ C ₂ -8:2 FTCA
7:3 fluorotelomer carboxylic acid	7:3 FTCA	C ₁₀ H ₅ O ₂ F ₁₅	¹³ C ₂ -10:2 FTCA
6:2 fluorotelomer carboxylic acid	6:2 FTCA	C ₈ H ₃ O ₂ F ₁₃	¹³ C ₂ -6:2 FTCA
8:2 fluorotelomer carboxylic acid	8:2 FTCA	C ₁₀ H ₃ O ₂ F ₁₇	¹³ C ₂ -8:2 FTCA
10:2 fluorotelomer carboxylic acid	10:2 FTCA	C ₁₂ H ₃ O ₂ F ₂₁	¹³ C ₂ -10:2 FTCA
2H-Perfluoro-2-octenoic acid (6:2)	6:2 UFTCA	C ₈ H ₂ O ₂ F ₁₂	¹³ C ₂ -6:2 UFTCA
2H-Perfluoro-2-decenoic acid (8:2)	8:2 UFTCA	C ₁₀ H ₂ O ₂ F ₁₆	¹³ C ₂ -8:2 UFTCA
2H-Perfluoro-2-dodecenoic acid (10:2)	10:2 UFTCA	C ₁₂ H ₂ O ₂ F ₂₀	¹³ C ₂ -10:2 UFTCA
Miscellaneous Emerging			
Dodecafluoro-3H-4,8-dioxanonanoate	ADONA	C ₇ H ₂ O ₄ F ₁₂	¹³ C ₄ -PFOA
Perfluoro-4-ethylcyclohexane sulfonate	PFEtCHxS	C ₈ HO ₃ SF ₁₅	¹³ C ₄ -PFOS
Tetrafluoro-2 (heptafluoropropoxy)propanoic acid	HFPO-DA	C ₆ HO ₃ F ₁₁	¹³ C ₃ -HFPO-DA

Qualitative suspect screening entailed the comparison of identified mass spectral features against an extracted ion chromatogram (XIC) list. To identify additional PFASs of interest beyond the target analyte list, high-resolution QTOF data collected via SWATH[®] Data-Independent Acquisition was screened using a custom spectral library containing spectra for >300 AFFF-associated PFASs and a custom XIC list containing molecular formulas and neutral masses for >

1,400 PFASs, including a wide variety of well-characterized PFASs, PFASs reported in literature, and theoretical homologs. Identification of unknown PFASs was based on accurate mass measurement for the molecular ion, isotopic pattern matching scores, and, for compounds present in the MS/MS library, the library purity score. Samples were screened by searching for the deprotonated molecular ion $[M-H]^-$ for ESI- analysis using an XIC window of 0.008 Da, a signal-to-noise threshold of 10:1, a minimum peak intensity 100, and baseline subtraction over 2 minutes. In cases where there are multiple possible hits for one peak, the largest peak found was reported unless other lines of evidence, such as retention times of homologous compounds, supported the identification of a smaller peak. The HRMS MS/MS library was screened for matches using a mass error threshold of 0.1 Da for the precursor ion and 0.4 Da for the product ion, and an intensity threshold of 5% of the highest peak in the MS/MS spectrum. Library purity score was calculated by an algorithm in SCIEX OS software based on the quality of match between the library and experimental MS/MS spectrum (both presence/absence of expected fragments and relative fragment abundance). Data were exported from SCIEX OS and parsed using an R script (R v 3.4.3) to identify MS/MS library and XIC list matches. Only matches with purity score > 70%, mass error < 10 ppm, and isotopic pattern error < 20% were considered library matches. For features with library scores < 70%, or no match located in the library, the peak was considered as an XIC list match only for mass error < 5 ppm and isotopic pattern error < 10%. Features for which there was more than one possible identification based on mass and isotope pattern were flagged as isomers. After processing, the list of hits was evaluated manually to ensure that all matches were well-defined peaks and retention times were consistent for homologue series, and a confidence level was assigned to each identification based on the Schymanski scale (Schymanski et al., 2014). Suspect screening results were typically reported in terms of area counts with associated confidence levels.

Semiquantitative analysis followed a protocol recently reported by Nickerson and co-workers (Nickerson et al., 2020). Based on suspect screening results, the concentration of compounds identified from XIC list was estimated with a target calibrant and internal standard in the target analyte list. The target calibrant and internal standard were selected by ionizable functional group and perfluorinated chain length shared commonly with each XIC list associated compound. The target calibrant and internal standard pairs matched with each suspect compound are provided in **Table A1** in the report's appendix. The concentrations of suspect hit compounds were estimated using Eq 3.5.1,

$$"mass"_{suspect} = (RF_{target-IS}) * \frac{molar\ mass_{suspect}}{molar\ mass_{target}} * \frac{area_{suspect}}{area_{IS}} * nominal\ mass_{IS} \quad (3.5.1)$$

where $RF_{target-IS}$ is the response factor for the selected internal standard. Concentrations were estimated as a function of response factor of the associated target calibrant/internal standard pair (the slope of the calibration curve), the molar mass of the target calibrant, the molar mass of the suspect compound, the observed peak area of the suspect compound-matched peak, the observed peak area of the internal standard, and the nominal spiked mass of the internal standard.

To assess the effects of fluorine substitution on hydrothermal reactivity, an experiment was conducted with octanoic acid, the un-fluorinated analogue of PFOA. This chemical was analyzed before and after reaction using by high pressure liquid chromatography (HPLC; Agilent 1200 HPLC coupled to differential refraction index (RID) detector). The chromatographic separations

of the injected samples (50 μL) were performed using a Spherisorb ODS2 Column (80 \AA , 5 μm , 4.6 mm \times 250 mm, 1/pkg). The flow rate was 1 mL/min, and the mobile phase consisted of H_2SO_4 in HPLC water (pH 2.4, 2 mL 1N H_2SO_4 in 500 mL HPLC water) (A, 40%) and acetonitrile (B, 60%). The elution time for octanoic acid was 20 min.

3.5.3 Co-solvent and co-contaminant analysis

Co-solvent (DGBE, methanol) concentrations were tracked by total organic carbon (TOC) analysis using a Shimadzu TOCV-TNM-LCSH analyzer (Shimadzu Corporation, Japan). The concentrations of co-contaminants (TCE, BTEX compounds) were measured by a HPLC-DAD (Agilent 1200 HPLC coupled to DAD detector). The chromatographic separations of the injected samples (50 μL) were performed using a Spherisorb ODS2 Column (80 \AA , 5 μm , 4.6 mm \times 250 mm, 1/pkg). The flow rate was 1 mL/min, and the mobile phase consisted of HPLC water (A, 40%) and methanol (B, 60%). Individual reagents were quantified by monitoring at 210 nm and comparison against external standards.

3.5.4 ^{19}F -NMR spectroscopy

^{19}F NMR analysis of reacted and unreacted PFOS and AFFF solutions was used to verify the defluorination performance and to identify the chemical form of possible residual organic fluorine. To enhance the signal intensity, NMR analysis was performed on reactions initiated with an elevated initial concentration of PFOS or AFFF-derived PFASs. For experiments conducted with PFOS, reaction conditions were as follows: PFOS (5 mM, total fluorine = 85 mM), NaOH (1 mol/L), 350 $^\circ\text{C}$, 0-600 min. All the samples were diluted 50:50 in D_2O before collecting spectra. ^{19}F spectra were recorded at 500 MHz on a JEOL ECA-500 spectrometer. A total of 128 scans were obtained in 13107 data points over a spectral window from -200 ppm to 200 ppm (0.544 s acquisition time) using a 30 $^\circ$ flip-angle pulse with ^1H decoupling. The ^{19}F 90 $^\circ$ pulse width was 8.5 μs . A 10 s relaxation delay was employed. The free induction decays (FIDs) were processed using exponential multiplication (line-broadening 1 Hz) before Fourier transformation. Fluorine concentrations were quantified by peak area comparison against the spectrum of trifluoroacetate (0.015 mol/L).

3.5.5 Analysis of volatile reaction products

Volatile products were collected and analyzed for selected reactions using GC-TCD, GC-FID, and tandem GC-MS/MS analysis. For GC-TCD, the separation was carried out on a Supelco Carboxen 1010 column (30 m length \times 0.53 mm inter diameter \times 30 μm thickness) with He as carrier gas at flow rate of 3 mL \cdot min $^{-1}$. Other settings included setting the split ratio to 2, the injector temperature to 100 $^\circ\text{C}$, the detector temperature to 250 $^\circ\text{C}$, and the filament temperature to 300 $^\circ\text{C}$. Oven temperature was initially set at 35 $^\circ\text{C}$ for 6 min, then ramped at a rate of 25 $^\circ\text{C}/\text{min}$ to 220 $^\circ\text{C}$ and held for 6.4 min.

For GC-FID, the injection volume was 20 μL , the carrier gas was He, the column flow was kept at a constant column pressure of 4.3 psi, the split flow rate was 80 mL \cdot min $^{-1}$, the purge flow was 5 mL \cdot min $^{-1}$, the injector temperature was 130 $^\circ\text{C}$, the detector temperature was 200 $^\circ\text{C}$, the oven temperature was 135 $^\circ\text{C}$, and the run time was 8 min. A refinery gas standard #2 (Restek

Corporation, PA, USA) was run as a reference standard to compare with gas products observed in the headspace of reactors following hydrothermal reaction of AFFF #1.

GC-MS/MS analysis was performed on a Thermo Scientific Trace Ultra GC interfaced with a Thermo Scientific ITQ 1100 mass spectrometer fitted with a Rxi-5Sil MS column (Restek Corporation, U.S.) (30 m × 0.25 mm; 0.25 μm film thickness). The initial temperature of the column was set at 60°C for 3 min and was heated at a rate of 15 °C /min until the temperature reached 320°C. The injector temperature was 230°C, and the injection volume 0.1 μL, with a split ratio of 1:50. MS were taken at 70 eV with a mass range of m/z 40-450. The chemical compounds were identified by MSD ChemStation E.02 with a NIST library.

3.5.6 Geochemical characterization of IDW and PFAS-contaminated soils

Common properties of three PFAS-contaminated soils including the content of sand, silt, and clay, cation exchange capacity (CEC), anion exchange capacity (AEC), organic content, and pH were characterized by Agvise Laboratories (Northwood, ND).

4.0 Results and Discussion

4.1 Screening of Hydrothermal Reaction Amendments

Initially, a series of amendments were screened for their potential to promote PFOS defluorination under near-critical hydrothermal conditions (350°C, 16.5 MPa autogenous pressure). **Figure 4.1.1** shows the extent of fluoride ion release measured after 90 min, varying from near 0% (for the unamended control and roughly half the screened amendments) to 80%. The most effective reagents, yielding >70% defluorination, include sodium hydroxide (NaOH), sodium borohydride (NaBH₄), and potassium ferrate (K₂FeO₄). Potassium permanganate (KMnO₄), sodium carbonate (Na₂CO₃), and sodium thiosulfate (Na₂S₂O₃) also led to >20% defluorination. Importantly, sodium persulfate, a oxidizing agent being developed to remediate PFASs (Bruton and Sedlak, 2017), had little effect on PFOS concentration or F⁻ release during hydrothermal reactions. This agrees with a recent report documenting a lack of reactivity for perfluoroalkyl sulfonates like PFOS during heat-activated persulfate treatment (Bruton and Sedlak, 2017), despite previous reports showing reactivity with PFOA and related perfluoroalkyl carboxylates and their precursors (Lee et al., 2009).

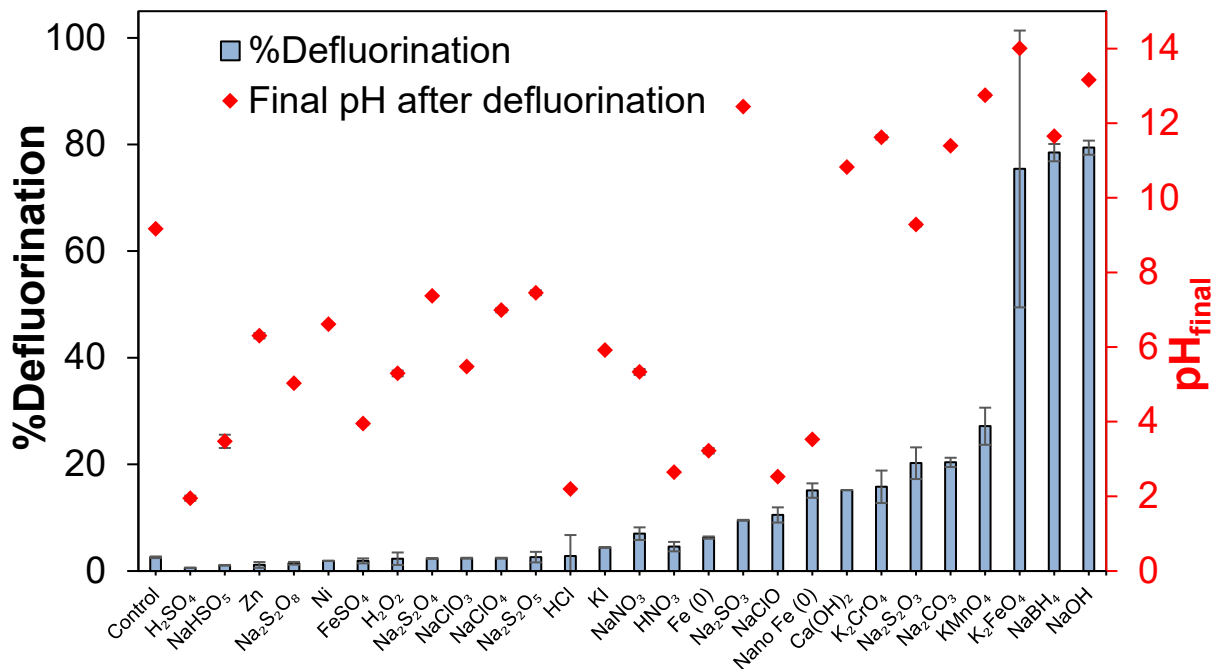


Figure 4.1.1 Sorting of effective amendments in the hydrothermal destruction of PFOS. Symbols show the measured pH of the solution following reaction. Reaction conditions: PFOS (50 mg/L) and amendment (1 mol/L) in water at 350 °C for 90 min. Control: only PFOS (50 mg/L) in water at 350 °C for 90 min. Error bars represent min/max values observed for duplicate experiments (smaller than symbol if not shown).

The only previous report of subcritical hydrothermal PFOS defluorination (Hori et al., 2006) showed 51% defluorination upon addition of >50 g/L Fe(0) to a reaction at 350°C for 300 min. Powdered Fe(0) exhibited much less reactivity here, leading to only 6.3% defluorination. Nano Fe(0) (i.e., nZVI) was more effective, but still yielded less defluorination (15.1%) than the other

amendments.

LC-MS/MS analysis of residual PFOS concentrations in the screening samples confirms the reactivity trends observed from F^- measurements (**Figures 4.1.2**). Little PFOS degradation was observed for amendments where minimal F^- release was detected (**Figure 4.1.2a**), whereas $>50\%$ PFOS loss was observed for all amendments yielding $>15\%$ defluorination, and $>80\%$ PFOS degradation was measured in NaOH-, NaBH₄- and K₂FeO₄-amended samples (**Figure 4.1.2b**). The greater extents to which parent PFOS loss was observed as compared to the F^- released indicates that the initial reaction step converts PFOS into one or more fluorinated organic intermediates.

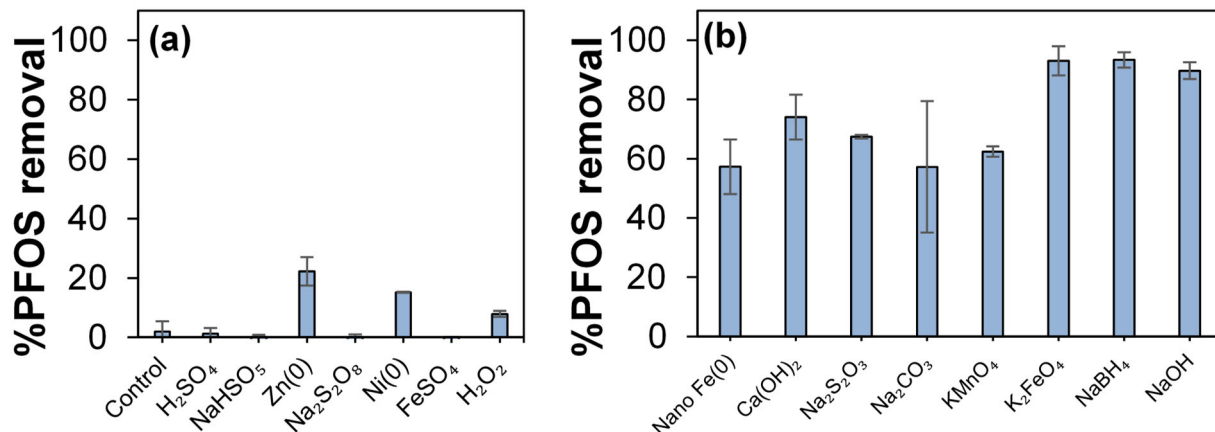
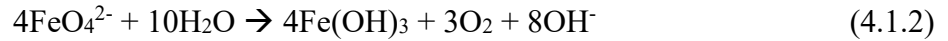


Figure 4.1.2 PFOS removal measured in reaction solutions amended with (a) seven reagents that yielded the lowest extent of defluorination, (b) eight reagents that yielded the greatest degree of defluorination (as shown in Figure 4.1.1). Error bars represent min/max values observed for duplicate experiments.

Although the most effective reagents include bases (NaOH, Na₂CO₃, Ca(OH)₂), oxidants (K₂FeO₄, KMnO₄), and reductants (NaBH₄, Na₂S₂O₃), they all share the common feature that their addition to solution causes a dramatic increase in pH. Furthermore, **Figure 4.1.3** highlights the fact that the amendments that caused the greatest defluorination also tended to increase the final pH the most. This suggests a common OH⁻ catalyzed mechanism, and that the reactivity observed for oxidants and reductants is an indirect result of their effect on solution pH.

The importance of alkaline pH conditions was further supported by results observed in a series of control experiments. First, the extent of defluorination increased with increasing concentration of NaOH added to solution (**Figure 4.1.4a**). Second, the extent of PFOS defluorination in NaBH₄- and K₂FeO₄-amended solutions decreased dramatically when solutions were buffered at lower pH conditions before hydrothermal reaction (**Figure 4.1.4b**). Additionally, ferrate is a stronger oxidant under acidic conditions (FeO₄²⁻/Fe³⁺, E⁰=2.20 V) than alkaline conditions (FeO₄²⁻/Fe(OH)₃, E⁰=0.72 V) (Sharma, 2002), so decreased reactivity at lower pH conditions is counter to expectations if PFOS oxidation was the operative mechanism.

Finally, NaBH₄ and K₂FeO₄ are both unstable in water and rapidly decay under thermal conditions,



losing their reactive properties while simultaneously releasing OH^- ions that increase pH. Separate tests showed that pre-heating NaBH_4 and K_2FeO_4 solutions to drive eqs 4.1.1 and 4.1.2 to completion before introducing PFOS had only a small effect on the resulting extent of defluorination (**Figure 4.1.5**).

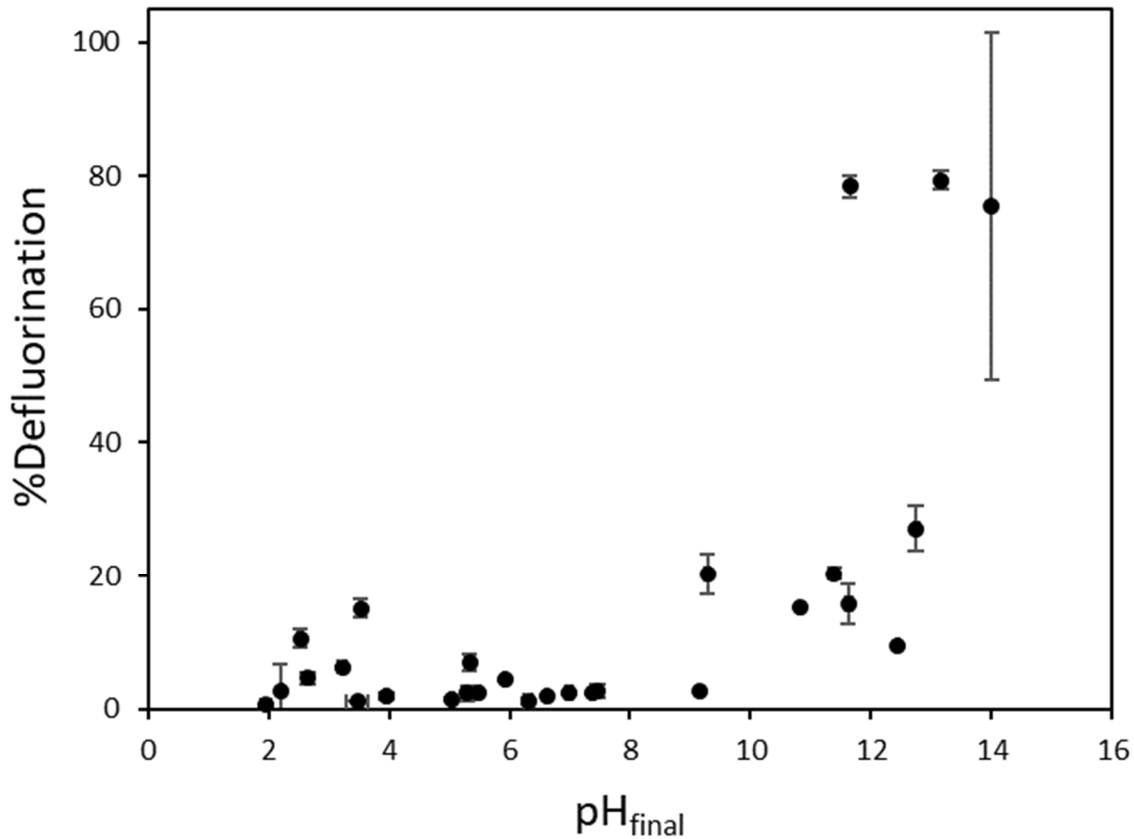


Figure 4.1.3 Plot showing the percent defluorination observed with different reaction amendments as a function of the measured final pH in the solution following hydrothermal reaction at 350 °C for 90 min. Data from Figure 4.1.1.

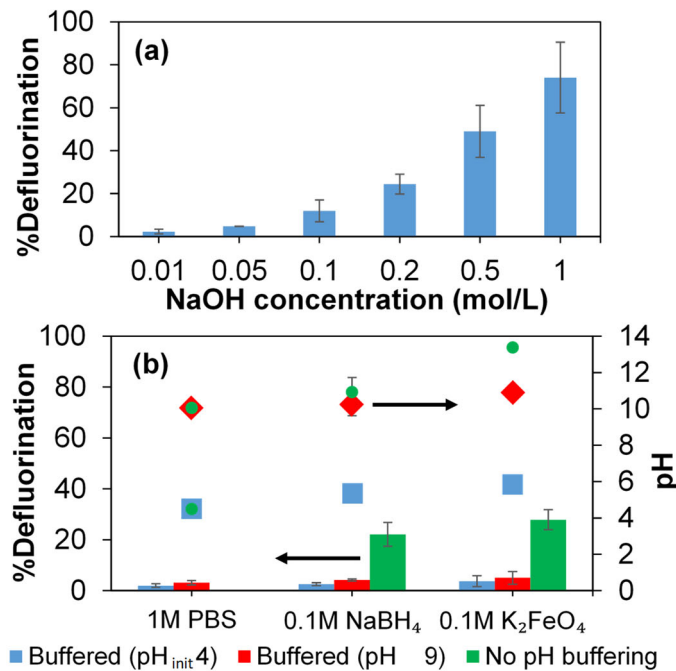


Figure 4.1.4 Effect of NaOH concentration and the pH of solutions amended with other reagents on hydrothermal defluorination of PFOS. (a) Extent of PFOS defluorination observed following 90 min reaction (350 °C) in water amended with varying NaOH concentrations. (b) Extent of PFOS defluorination following 90 min reaction in water amended with either a strong reductant (NaBH₄) or strong oxidant (K₂FeO₄) where solutions are either unbuffered or buffered at pH 9 or 4 using phosphate (PBS, 1 mol/L). Bars indicate the extent of defluorination (left axis) and symbols represent the pH values measured after quenching the reactions. Error bars represent min/max values observed for duplicate experiments (smaller than symbol if not visible).

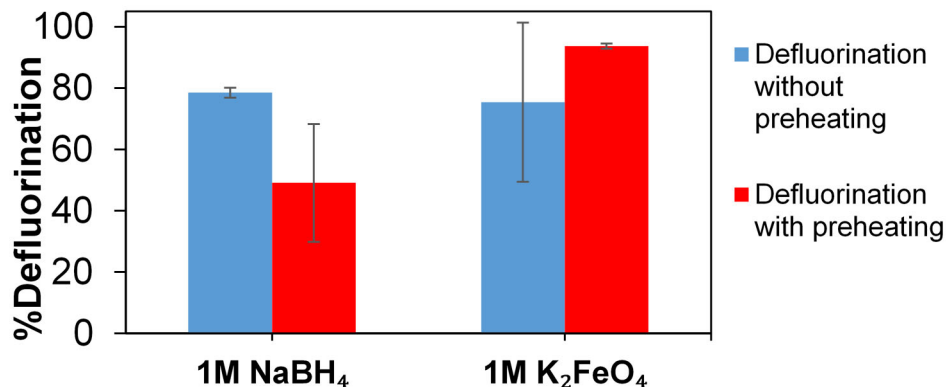


Figure 4.1.5 Effect of preheating (and re-cooling) solutions amended with NaBH₄ or K₂FeO₄ before introducing PFOS and re-heating on the extent of PFOS defluorination. Reaction conditions: 50 mg/L PFOS; Solutions pre-heated to 350°C for 90 min before re-cooling and introducing 50 mg/L PFOS and reacting at 350°C for another 90 min. Error bars represent min/max values observed for duplicate experiments.

4.2 Alkaline Hydrothermal Destruction of PFOS

4.2.1 Kinetics of PFOS degradation and defluorination

Since the hydrothermal defluorination appeared to be closely linked to the alkaline conditions, a more in-depth examination of reactions in NaOH-amended solutions was undertaken. **Table 4.2.1** and **Figure 4.2.1** show the effects of varying NaOH concentration on PFOS degradation and defluorination kinetics. Degradation of PFOS observed in individual batch reactors followed pseudo-first-order kinetics (**Figure 4.2.1a**), and the resulting pseudo-first-order rate constants (k_{obs} , min^{-1}) were linearly dependent on NaOH concentration (**Figure 4.2.1b**). It follows that PFOS removal can be described by a general second-order law:

$$\frac{d[\text{PFOS}]}{dt} = -k_{\text{obs}}[\text{PFOS}] = -k_2[\text{OH}^-][\text{PFOS}] \quad (4.2.1)$$

where $[\text{PFOS}]$ and $[\text{OH}^-]$ are the molar concentrations of PFOS and OH^- , respectively, t is time (min), and k_2 is the second-order rate constant ($\text{M}^{-1} \text{min}^{-1}$). Fit of the data yields a k_2 value of $0.052 \pm 0.004 \text{ M}^{-1} \text{min}^{-1}$ for 350°C (**Table 4.2.1**), and model-predicted reaction times listed in **Table 4.2.2** to PFOS concentration from different initial values down to the USEPA's drinking water health advisory level (70 ng/L). As expected, the rate of PFOS decomposition also varies with reaction temperature (**Figure 4.2.2**).

Figure 4.2.1c compares the incremental extent of defluorination with PFOS loss during experiments. While data for treatment with 2.5 M NaOH showed close agreement between %PFOS degradation and %defluorination, %defluorination initially lags behind %PFOS degradation for the other two concentrations. This finding is consistent with the general observation for the most effective amendments screened, where %defluorination lagged behind the %PFOS degradation. For NaOH, the lag in defluorination becomes less pronounced at higher temperatures (**Figure 4.2.2**). This is consistent with an initial formation of organic-fluorine intermediates.

Table 4.2.1 Measured reaction kinetics for PFOS

PFOS (mg/L)	NaOH (mol/L)	k_{obs} (min^{-1})	r^2	$k_{2,350^\circ\text{C}}$ ($\text{M}^{-1} \cdot \text{min}^{-1}$)
	1	0.015 ± 0.001	0.95	
50	2.5	0.10 ± 0.01	0.95	0.052 ± 0.004
	5	0.28 ± 0.02	0.96	

^aReaction conditions: PFOS (50 mg/L) and NaOH amendment (1, 2.5 and 5 mol/L) in deionized water at 350°C for 0-480 min. Uncertainties in k_{obs} values represent min/max values determined in duplicate experiments. Uncertainties in $k_{2,350^\circ\text{C}}$ values represent the min/max values obtained by plotting k_{obs} values and NaOH concentrations.

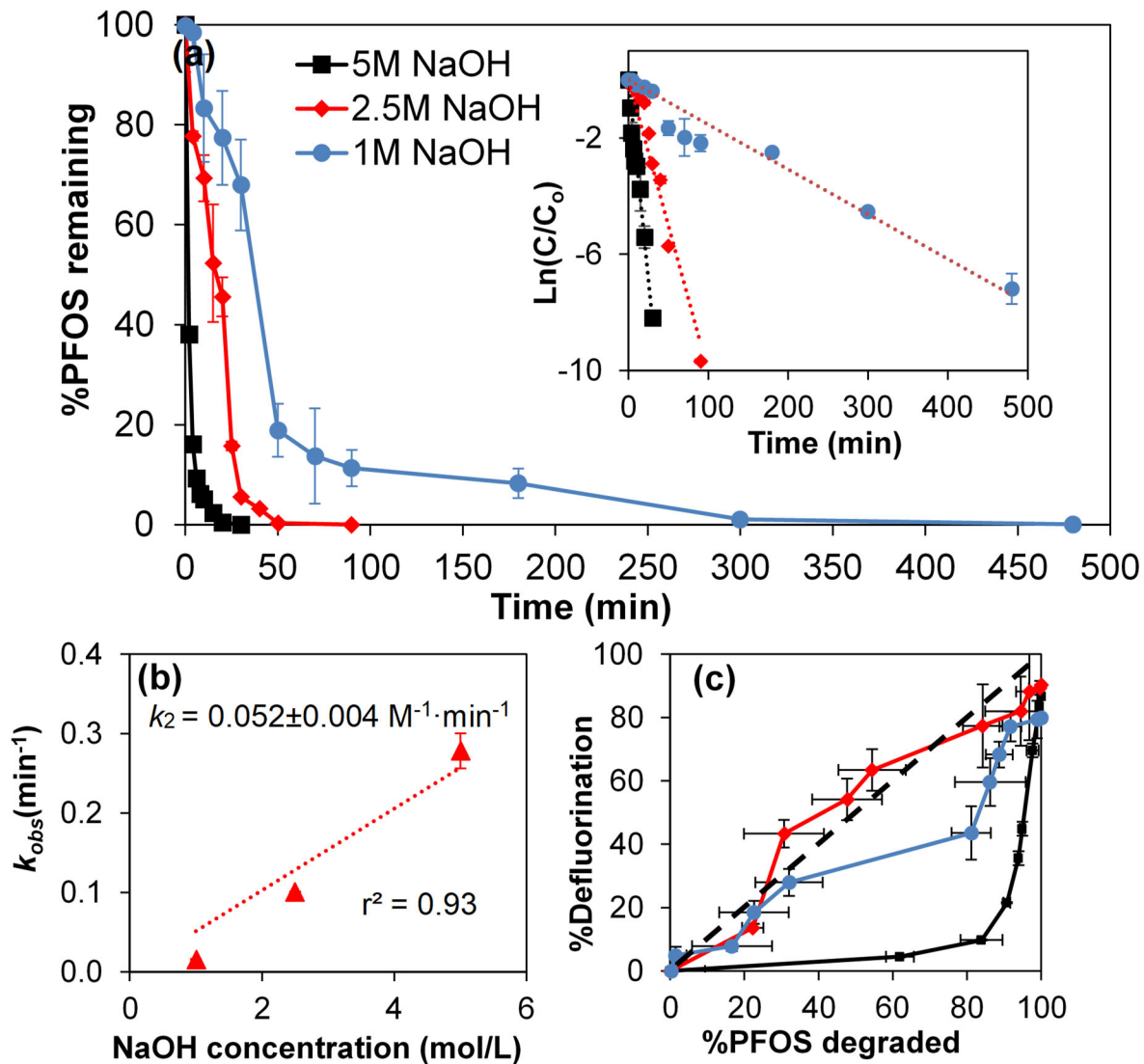


Figure 4.2.1 Kinetic analysis on alkaline-based hydrothermal destruction of PFOS. Reaction conditions: PFOS (50 mg/L) and NaOH amendment (1, 2.5, and 5 mol/L) in water at 350 °C for 0–480 min. (a) PFOS decay, (b) linear relationship between k_{obs} vs NaOH concentration, and (c) extent of defluorination vs extent of PFOS degraded. Error bars represent min/max values observed for duplicate experiments (smaller than symbol if not shown). The inset in panel a shows linearized first-order model fits.

Table 4.2.2 Predicted reaction times required to reduce PFOS concentrations from different input feed concentrations to the USEPA lifetime Health Advisory Level (HAL) of 70 ng/L

[PFOS] _{init}	Reaction time to reach 70 ng/L (min)	
	1 M NaOH	5 M NaOH
50 mg/L	260	52
10 mg/L	230	45
1 mg/L	180	37
100 µg/L	140	28
10 µg/L	95	19
10 µg/L	51	10

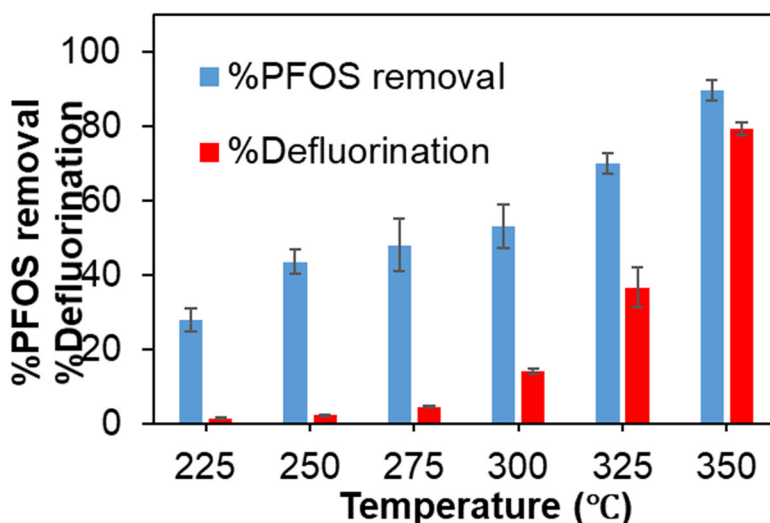


Figure 4.2.2 Effect of reaction temperature on the extent of PFOS degradation and defluorination in solutions amended with NaOH. Reaction conditions: PFOS (50 mg/L), NaOH (1 M), 350°C, 90 min. Error bars represent min/max values observed for duplicate experiments.

4.2.2 Reaction intermediates and products

LC-MS/MS analysis confirms formation of fluorinated organic intermediates, albeit at very low concentrations (**Figure 4.2.3**). Analysis of samples from PFOS reaction in 1 M NaOH revealed formation of perfluorohexanoic acid (PFHxA) and perfluoropentanoic acid (PFPeA), but concentrations only reached 0.062% and 1.1% (mol/mol), respectively, of the initial PFOS concentration. Still, these observations indicate conversion of the sulfonate to shorter chain perfluoroalkyl carboxylates. Separate tests showed that perfluoroalkyl carboxylates are much less stable in hydrothermal media than PFOS (e.g., >99% PFOA degraded within 30 min at 250°C without amendments). Further experiments initiated with PFOA at lower temperature (200°C) and

NaOH concentration (0.001 M) showed 94% degradation within 30 min (**Figure 4.2.3b**), with maximum concentrations of shorter-chain analogues reaching $1.4 \pm 0.1\%$ of the initial PFOA concentration (**Figure 4.2.3c**). Furthermore, temporal trends show that the C7 perfluoroheptanoic acid (PFHpA) peaks in concentration before concentrations of shorter-chain homologues increase, consistent with sequential decarboxylation.

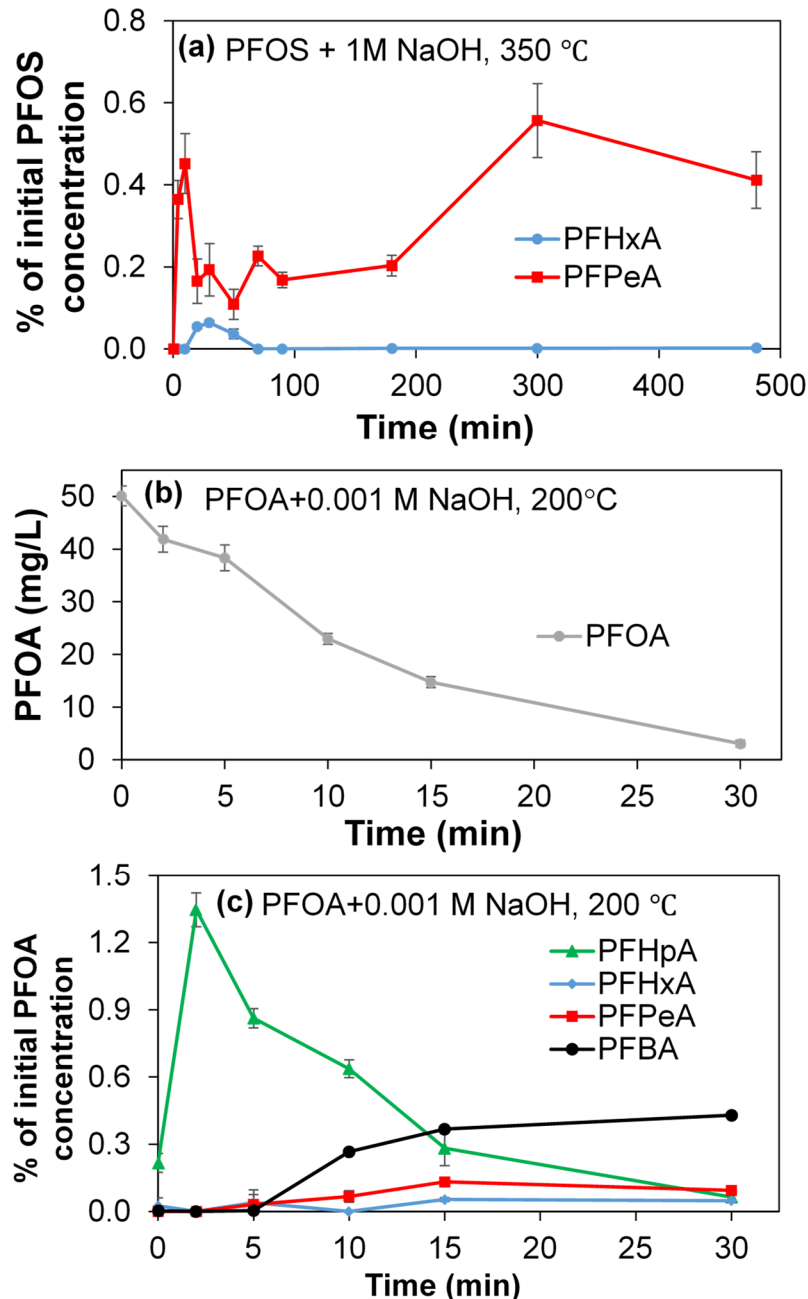


Figure 4.2.3 Intermediate products observed during hydrothermal treatment of (a) 50 mg/L PFOS with 1 M NaOH at 350 °C, (b, c) 50 mg/L PFOA with 0.001 M NaOH at 200 °C. Error bars represent min/max values observed for duplicate experiments (smaller than symbol if not visible).

4.2.3 ^{19}F -NMR spectroscopy

^{19}F -NMR measurements collected during reactions are consistent with the small difference between the extents of PFOS degradation and defluorination as well as the very small concentration of detected organic intermediates. **Figure 4.2.4** shows complex spectral features associated with different C-F bonds in PFOS (time = 0 min) are replaced by a single dominant peak matching F^- after only 10 min of reaction, and spectral features associated with organic fluorine are completely absent after 40 min.

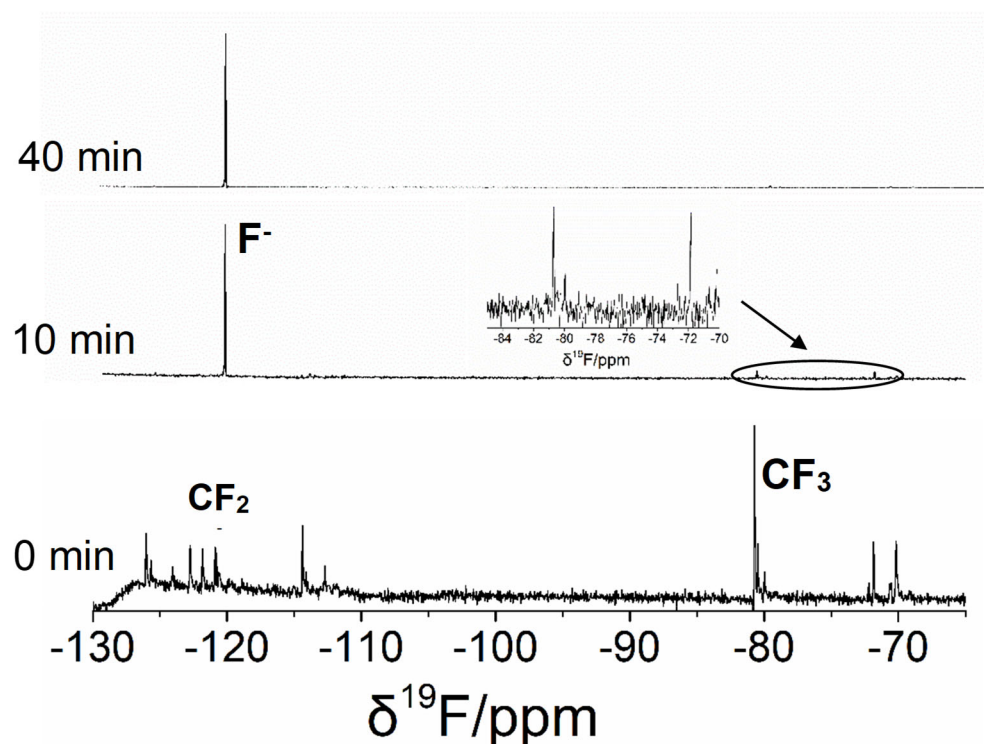


Figure 4.2.4 ^{19}F -NMR spectra of PFOS solutions collected before and after hydrothermal reactions for different time periods. Reaction conditions: PFOS (5 mM, total fluorine = 85 mM), NaOH (1 mol/L), 350 °C, 0–40 min. The ^{19}F chemical shift ranges of CF_3 and CF_2 are from -86 to -74 ppm and from -127 to -121 ppm, respectively; the chemical shift of F^- is -120.7 ppm.

4.3 Alkaline Hydrothermal Reactions of PFASs Contained in AFFF

4.3.1 AFFF composition

Experiments were conducted with two AFFF mixtures (AFFF #1 and AFFF #2). The concentrations of PFASs included in the target analysis lists of these two mixtures are provided in **Table 4.3.1**, and semi-quantitative analysis of PFASs identified through suspect screening analysis is provided in **Table 4.3.2**. For AFFF #1, targeted analysis showed many PFAAs, including PFCAs and PFSAs, as the dominant species. PFCAs with chain lengths of $n = 4$ through 8 were measured in the undiluted mixture at concentrations ranging from 21.7 ± 2.70 mg/L (PFBA) to 244 ± 20.9 mg/L (PFOA), and PFSAs with chain lengths of $n = 3$ through 10 were found at concentrations ranging from 5.05 ± 2.09 mg/L (PFDS) to 6580 ± 100 mg/L (PFOS). Targeted analysis of AFFF #2 showed that two fluorotelomer sulfonates, 6:2 fluorotelomer sulfonate (6:2 FTS) and 8:2 fluorotelomer sulfonate (8:2 FTS), were present at concentrations of 28.6 ± 0.79 mg/L and 18.5 ± 1.21 mg/L, respectively. PFHxA was also found in AFFF #2 at a concentration of 12.7 ± 1.38 mg/L. Otherwise, PFASs present in the AFFF #2 were not structures included in the target analysis group.

Table 4.3.1 Composition of targeted PFAS measured in AFFF mixtures

PFASs Name	Neutral Molecular Formula	AFFF #1 (mg/L)	AFFF #2 (mg/L)
Perfluoro-n-butanoic acid (PFBA)	$C_4HO_2F_7$	21.7 ± 2.70	n.d.*
Perfluoro-n-pentanoic acid (PFPeA)	$C_5HO_2F_9$	69.3 ± 5.40	n.d.
Perfluoro-n-hexanoic acid (PFHxA)	$C_6HO_2F_{11}$	178 ± 17.4	12.7 ± 1.38
Perfluoro-n-heptanoic acid (PFHpA)	$C_7HO_2F_{13}$	59.2 ± 10.9	n.d.
Perfluoro-n-octanoic acid (PFOA)	$C_8HO_2F_{15}$	244 ± 20.9	n.d.
Perfluoropropane sulfonate (PFPrS)	$C_3HO_3SF_7$	121 ± 11.0	n.d.
Perfluorobutane sulfonate (PFBS)	$C_4HO_3SF_9$	237 ± 22.2	n.d.
Perfluoropentane sulfonate (PFPeS)	$C_5HO_3SF_{11}$	226 ± 25.5	n.d.
Perfluorohexane sulfonate (PFHxS)	$C_6HO_3SF_{13}$	996 ± 9.74	n.d.
Perfluoroheptane sulfonate (PFHpS)	$C_7HO_3SF_{15}$	146 ± 21.9	n.d.
Perfluorooctane sulfonate (PFOS)	$C_8HO_3SF_{17}$	6580 ± 100	n.d.
Perfluorononane sulfonate (PFNS)	$C_9HO_3SF_{19}$	6.83 ± 0.67	n.d.
Perfluorodecane sulfonate (PFDS)	$C_{10}HO_3SF_{21}$	5.05 ± 2.09	n.d.
8-chloro-perfluorooctane sulfonate (Cl-PFOS)	$C_8HO_3SClF_{16}$	95.6 ± 1.72	n.d.
6:2 fluorotelomer sulfonate (6:2 FTS)	$C_8H_5F_{13}SO_3$	n.d.	28.6 ± 0.79
8:2 fluorotelomer sulfonate (8:2 FTS)	$C_{10}H_5O_3SF_{17}$	n.d.	18.5 ± 1.21
Perfluoro-4-ethylcyclohexane sulfonate (PFEtCHxS)	$C_8HO_3SF_{15}$	28.7 ± 12.3	n.d.

*n.d., not detected.

Table 4.3.2 Semiquantitative analysis of PFAS identified in the AFFF by LC-QToF-MS suspect screening analysis

PFASs Name	Neutral Molecular Formula	AFFF #1 (mg/L)	AFFF #2 (mg/L)
N-dimethyl ammonio propyl perfluoroheptane sulfonamide (AmPr-FHpSA)	C ₁₂ H ₁₃ O ₂ SN ₂ F ₁₅	22.3	n.d.*
N-dimethyl ammonio propyl perfluorohexane sulfonamide (AmPr-FHxSA)	C ₁₁ H ₁₃ O ₂ SN ₂ F ₁₃	2620	n.d.
N-dimethyl ammonio propyl perfluorohexane sulfonamido propanoic acid (AmPr-FHxSA-PrA)	C ₁₄ H ₁₇ O ₄ SN ₂ F ₁₃	626	n.d.
N-dimethyl ammonio propyl perfluorooctane sulfonamide (AmPr-FOSA)	C ₁₃ H ₁₃ O ₂ SN ₂ F ₁₇	13.2	n.d.
N-dimethyl ammonio propyl perfluoropentane sulfonamido propanoic acid (AmPr-FPeSA-PrA)	C ₁₃ H ₁₇ O ₄ SN ₂ F ₁₁	172	n.d.
Chloro-perfluorohexane sulfonate (Cl-PFHxS)	C ₆ HO ₃ SClF ₁₂	5.69	n.d.
Perfluorobutane sulfonamide (FBSA)	C ₄ H ₂ O ₂ SNF ₉	15.9	n.d.
Perfluorohexane sulfonamide (FHxSA)	C ₆ H ₂ O ₂ SNF ₁₃	28.7	n.d.
Perfluoropentane sulfonamide (FPeSA)	C ₅ H ₂ O ₂ SNF ₁₁	13.2	n.d.
Hydrido-perfluorooctane sulfonate (H-PFOS)	C ₈ H ₂ O ₃ SF ₁₆	5.19	n.d.
Hydrido-perfluoropentane sulfonate (H-PFPeS)	C ₅ H ₂ O ₃ SF ₁₀	3.11	n.d.
Perfluorodecane unsaturated ether/alcohol (-1F, +1H) (H-UPFD-O/OH)	C ₁₀ H ₂ OF ₁₈	7.75	n.d.
Keto-perfluorooctane sulfonate (K-PFOS)	C ₈ HO ₄ SF ₁₅	4.30	n.d.
N-methylperfluoropentane sulfonamido acetic acid (MeFPeSAA)	C ₈ H ₆ O ₄ SNF ₁₁	71.8	n.d.
N-oxidedimethylammonio propyl-perfluorohexanesulfonamide (OAmPr-FHxSA)	C ₁₁ H ₁₃ O ₃ SN ₂ F ₁₃	23.4	n.d.
Perfluoro cyclohexane sulfonate (PFCHxS)	C ₆ HO ₃ SF ₁₁	2.01	n.d.
Perfluoro ethyl cyclopentane carboxylic acid (PFEtCPeCA)	C ₈ HO ₂ F ₁₃	3.10	n.d.
perfluorohexane sulfinatate (PFHxSi)	C ₆ HO ₂ SF ₁₃	10.4	n.d.
Unsaturated perfluorooctane sulfonate (UPFOS)	C ₈ HO ₃ SF ₁₅	26.2	n.d.
6:2 fluorotelomer thia acetic acid (6:2 FTThA)	C ₁₀ H ₇ O ₂ SF ₁₃	n.d.	96.0
6:2 fluorotelomer sulfinatate (6:2 FTSi)	C ₈ H ₅ O ₂ SF ₁₃	n.d.	87.8
8:2 fluorotelomer sulfinatate (8:2 FTSi)	C ₁₀ H ₅ O ₂ SF ₁₇	n.d.	123
6:2 fluorotelomer thia propanoamido dimethyl ethyl sulfonate (6:2 FTTh-PrAd-DiMeEtS)	C ₁₅ H ₁₈ O ₄ S ₂ NF ₁₃	n.d.	280

*n.d., not detected

Several classes of PFASs without an in-house standard were identified through suspect screening analysis of the AFFF #1 (see Table 4.3.2). These classes include sulfonamide, sulfonamide precursors, fluorotelomer sulfonamides, fluorotelomer acids, halogenated, ether, and H-substituted sulfonates, cyclic carboxylic acids, keto-substituted sulfonate, unsaturated sulfonate, and PFSA derivatives. Their concentrations, estimated by semiquantitative analysis, varied from trace levels up to 2620 mg/L (AmPr-FHxSA).

For AFFF #2, fluorotelomers were the major class of PFASs identified through suspect screening analysis. 6:2 fluorotelomer thia acetic acid (6:2 FTThA, 96.0 mg/L), 6:2 fluorotelomer sulfinate (6:2 FTSi, 87.8 mg/L), 8:2 fluorotelomer sulfinate (8:2 FTSi, 123 mg/L), and 6:2 fluorotelomer thia propanoamido dimethyl ethyl sulfonate (6:2 FTTh-PrAd-DiMeEtS, 280 mg/L) were detected in AFFF #2.

Total fluorine content of the undiluted AFFF mixtures was quantified by ^{19}F NMR spectroscopy. Due to the low sensitivity of ^{19}F NMR, NMR analysis was performed on AFFF at a less diluted ratio before and after hydrothermal reaction. Trifluoroacetic acid (TFA) was used as internal standard (IS) for quantification since there is no overlap of fluorine signal between TFA and all samples. D_2O was added to the samples to lock the field of NMR. The total fluorine content of the AFFF mixtures was calculated according to

$$\text{Total F in AFFF} = \frac{\text{The total integrated area of F signal from AFFF}}{\text{The integrated area of F signal from IS}} \times \text{F concentration of IS} \quad (4.3.1)$$

which yielded total organic F values in the AFFF #1 and AFFF #2 of $0.71 \pm 0.02 \text{ M}$ and $0.24 \pm 0.03 \text{ M}$, respectively.

4.3.2 Defluorination of AFFF mixtures

Results of the screening experiments conducted with PFOS, described above, showed that a few reagents, including sodium hydroxide (NaOH), sodium borohydride (NaBH_4), and potassium ferrate (K_2FeO_4), yielded >70% defluorination. These reagents together with another alkaline $\text{Ca}(\text{OH})_2$, a common oxidant KMnO_4 , and a common reductant Na_2SO_3 were also screened for their effectiveness in promoting hydrothermal defluorination of PFASs present in AFFF #1. **Figure 4.3.1** shows the order of decreasing reactivity of these reagents with respect to defluorination: NaOH ($108 \pm 9.83\%$), NaBH_4 ($88.5 \pm 5.77\%$), Na_2SO_3 ($82.9 \pm 1.29\%$), KMnO_4 ($18.0 \pm 0.83\%$), and $\text{Ca}(\text{OH})_2$ ($3.3 \pm 1.34\%$). Consistent with results observed during reactions of PFOS, NaOH was the most reactive amendment followed by NaBH_4 and Na_2SO_3 , and findings were consistent with the conclusion that individual reagents are effective through their effect on solution pH conditions. The greatest defluorination of AFFF #1 with NaOH amendment indicated the same OH^- catalyzed mechanism may apply to a broad range of PFASs beyond PFOS. Interestingly, lower reactivity of $\text{Ca}(\text{OH})_2$ compared to the control experiment (no amendment) was observed while $\text{Ca}(\text{OH})_2$ was able to greatly increase the system pH to >12. This was likely because the F^- released during reactions will readily react with Ca^{2+} to produce insoluble CaF_2 . Further study is needed in the future to confirm this. A similar result was observed in Hori et al. (Hori et al., 2014).

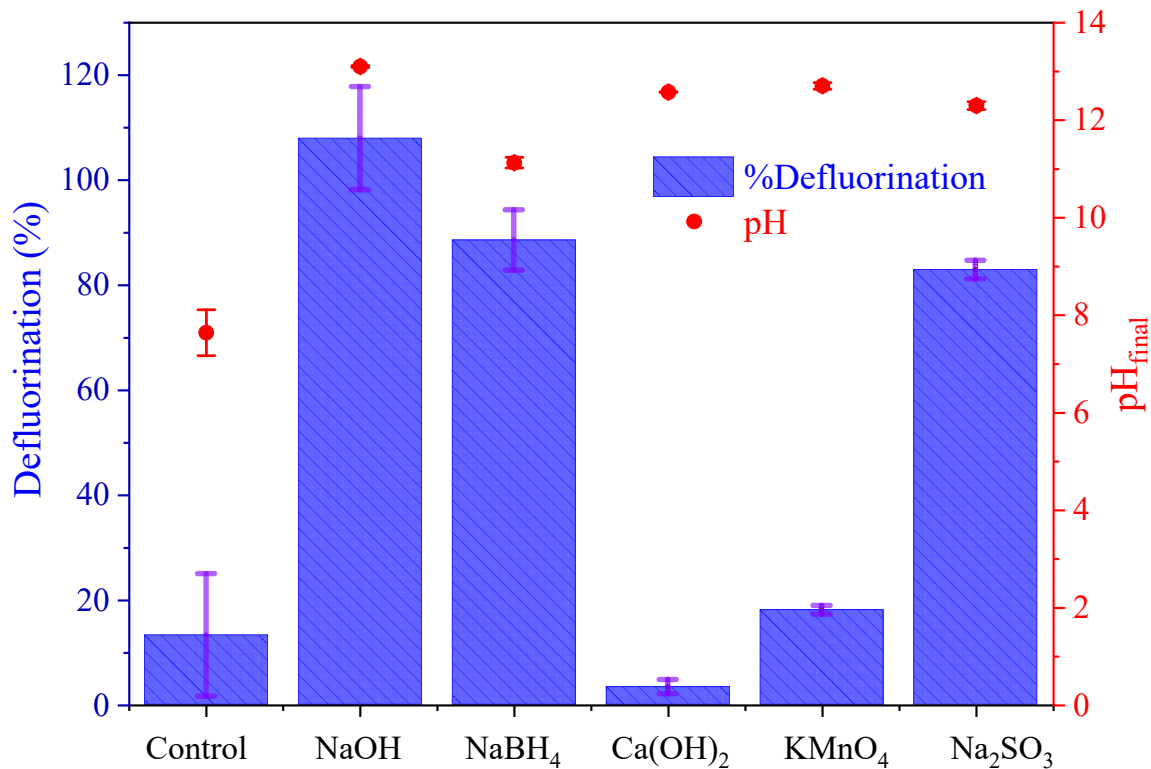


Figure 4.3.1 Sorting of effective amendments in the hydrothermal defluorination of PFASs present in AFFF #1. Symbols show the measured pH of the solution following reactions : AFFF diluted 1-to-1000, 1 mol/L amendment concentration, 350°C, 180 min reaction time. Control reaction was AFFF in unamended water at 350°C for 180 min.

Due to the highest reactivity and low cost, NaOH was selected as the amendment for the following hydrothermal experiments. Results of defluorination for hydrothermal reaction of a series of diluted AFFF #1 (up to 1-to-2 dilution) are provided in **Figure 4.3.2**. Near 100% defluorination for all reactions suggested the effectiveness of hydrothermal reaction on the defluorination of concentrated AFFF wastes (e.g., unused AFFF stockpiles). Hydrothermal treatment was also assessed for the fluorotelomer based AFFF (AFFF #2) under the optimized condition. Like AFFF #1, the observed defluorination was close to 100% for AFFF #2, indicating the potential for successful application of hydrothermal defluorination to a wide range of PFASs. To the best of our knowledge, this is the first treatment method, other than incineration, demonstrating ~100% defluorination of concentrated AFFF mixtures.

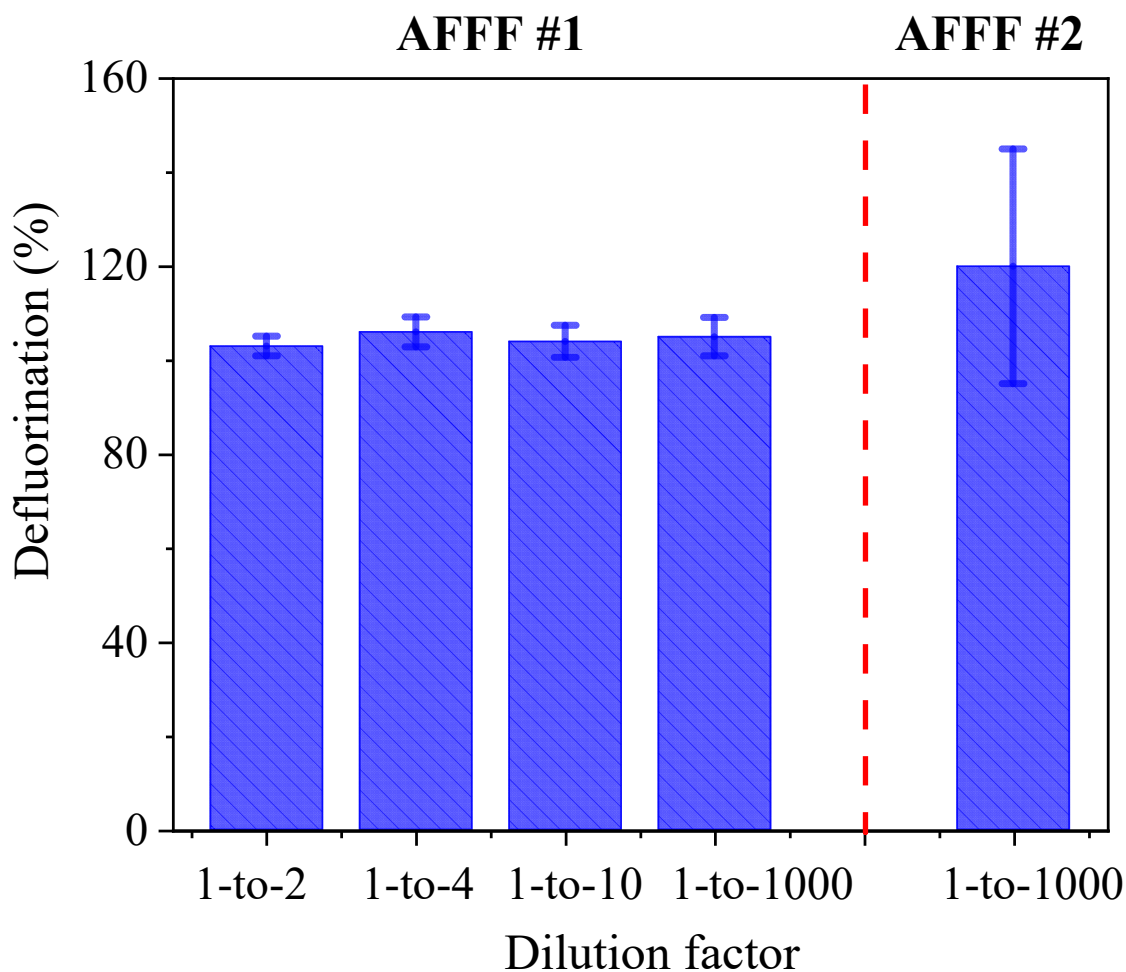


Figure 4.3.2 Extent of hydrothermal defluorination of AFFF #1 and #2 when the mixture was diluted to different extents prior to reaction. Reaction conditions: 5 mol/L NaOH, 350°C, 90 min reaction time.

Previous studies demonstrated that reaction temperature plays an important role in hydrothermal processing of biomass to yield solid, liquid, and gaseous products. Hydrothermal defluorination of AFFF #1 by varying reaction temperature over a range of 200-350 °C (5 M NaOH and reaction time 90 mins) was investigated and the result is shown in **Figure 4.3.3a**. As expected, higher reaction temperature promoted more rapid defluorination of AFFF. The extent of defluorination observed for AFFF #1 after reaction for 90 min increased from 11.2% at 200 °C to 98.6% at 350 °C. **Figure 4.3.3b** shows the effect of varying NaOH concentration on the kinetics of defluorination in diluted AFFF #1 solutions. Consistent with trends already noted for PFOS (Figure 4.2.1, eq 4.2.1), defluorination increases with increasing alkali concentration.

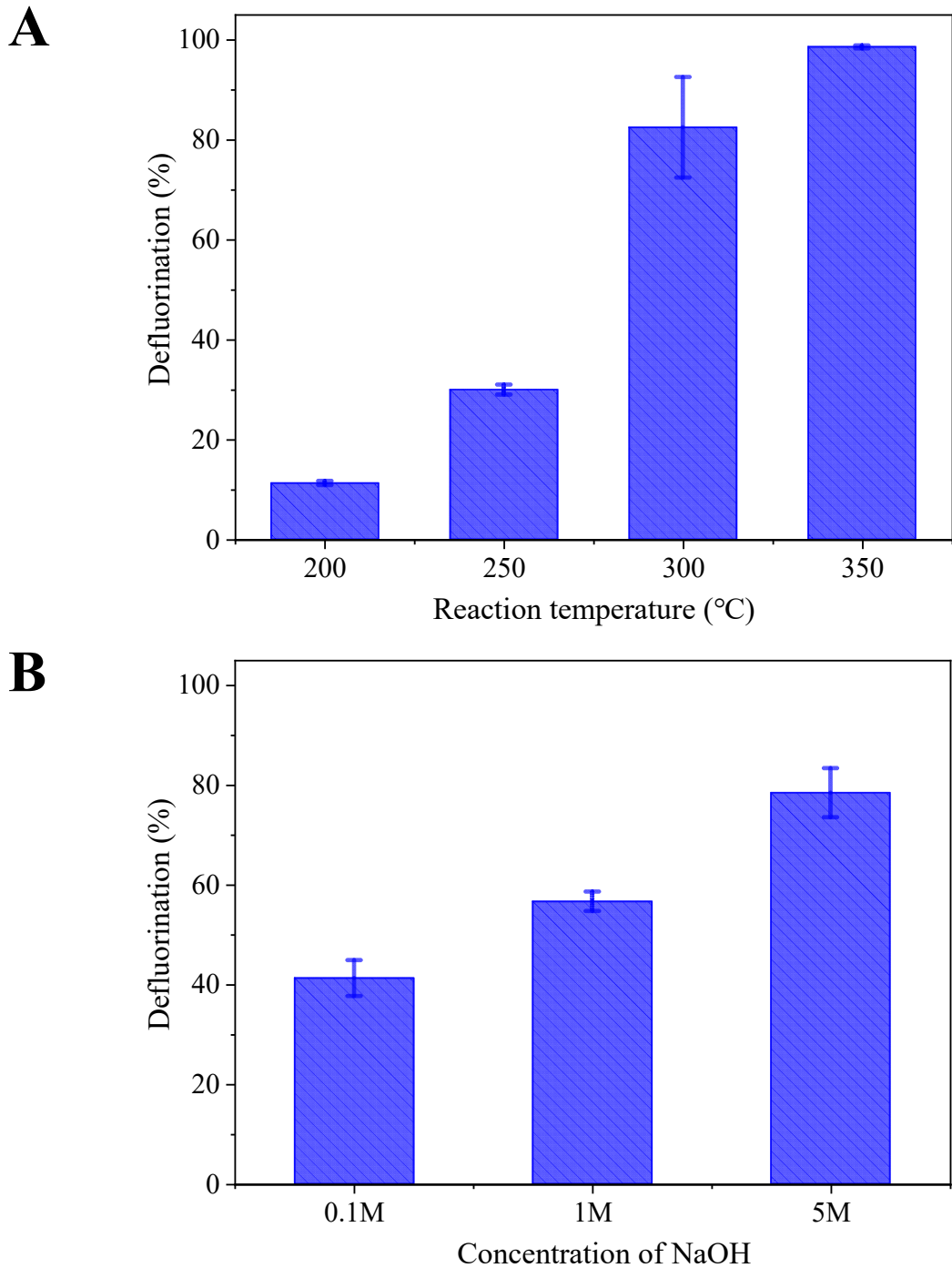


Figure 4.3.3 Defluorination observed during alkaline hydrothermal treatment of AFFF #1 solution with (a) different reaction temperatures, and (b) different concentrations of NaOH amendment. Reaction conditions: AFFF diluted 1-to-1000, 5 M NaOH reaction for 90 min in panel (a), AFFF diluted 1-to-1000, 0.1-5 M NaOH reaction for 15 min under 350°C in panel (b).

4.3.3 Targeted analysis of PFASs during alkaline hydrothermal treatment

Through LC-Q-ToF targeted analysis, the degradation of 14 PFASs identified in AFFF #1 during hydrothermal reaction over a range of reaction time is shown in **Figure 4.3.4a**. Fourteen of the identified PFASs degraded completely within 15 min. A series of PFASs (C3-C8) were more recalcitrant, but were also non-detectable after reaction for 30 min. These findings are consistent with data observed in experiments initiated with either PFOS or PFOA as the sole PFAS in the reaction. The longer required reaction time before PFSA concentrations were not detectable is also consistent with the more severe reaction conditions required for PFOS than PFOA; the former requires higher reaction temperatures/times and amendment with concentrated alkali, whereas the latter degrades readily at lower temperatures in the absence of alkali amendments. Targeted analysis of PFASs in AFFF #2 demonstrate that fluorotelomer acids are also effectively degraded under alkaline hydrothermal conditions (**Figure 4.3.4b**).

4.3.4 Suspect screening analysis of PFASs during alkaline hydrothermal treatment

To track degradation of a broader range of PFASs present in the AFFF mixtures, LC-QToF-MS suspect screening and associated semi-quantification analysis protocols were applied to track the estimated concentrations of suspected PFASs during hydrothermal reactions. **Figures 4.3.5** and **4.3.6** show “bubble plots” tracking the estimated concentrations of PFASs in the two AFFF mixtures before and after hydrothermal reaction. In these plots, individual bubbles represent different PFAS structures detected during targeted or QToF suspect screening analysis from screening list of >1500 PFAS structures. The individual analytes are arranged according to their chromatographic retention times (x-axis) and mass-to-charge ratio (m/z; y-axis), and the diameters of the individual bubbles are proportional to chromatographic peak area. Results presented in Figure 4.3.5 show collectively the rapidly shrinking mass of PFASs in AFFF #1 following hydrothermal treatment for 90 min. More than 99% of the PFASs identified through suspect screening analysis in AFFF #1 were degraded within 90 min. Tests also confirmed that all PFASs detected in the AFFF #2 were completely degraded in samples collected after reaction for 90 min (Figure 4.3.6).

4.3.5 ¹⁹F-NMR spectroscopy

Analysis of reaction solutions before and after reaction with ¹⁹F NMR confirmed the rapid and complete degradation and defluorination of PFASs present in the AFFF mixtures (**Figure 4.3.7**). The complex spectral features associated with variable molecular structures of organically bound fluorine in the unreacted AFFF #1 and AFFF #2 mixtures are lost after 30 min of reaction, being replaced by a single peak (-120 ppm) corresponding to inorganic fluoride ion. The rapid destruction observed in these experiments, where the concentrated AFFF were reacted with minimal dilution (diluted only 1-to-2 for AFFF #1 and 1-to-4 for AFFF #2) also highlights the effectiveness of this process for destruction of unused stockpiles of legacy AFFF formulations.

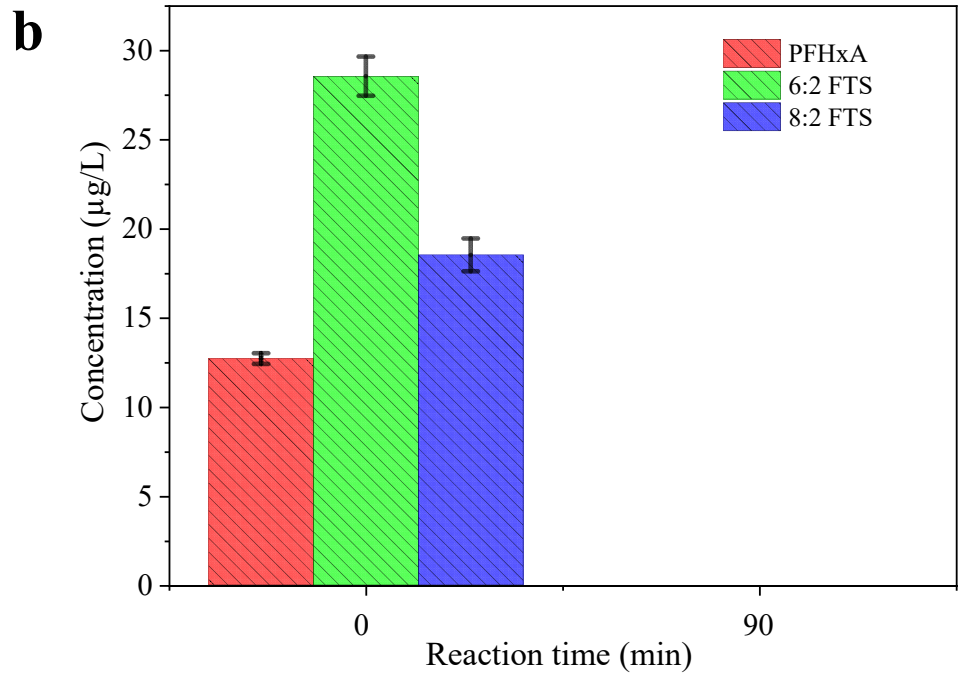
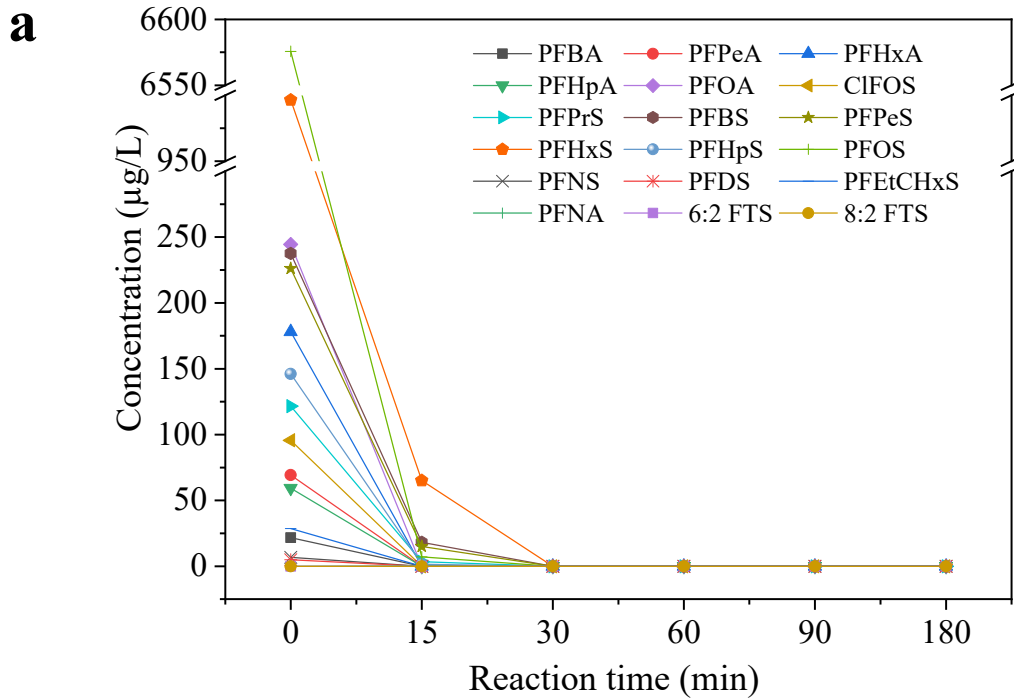


Figure 4.3.4 Removal of targeted PFASs observed following alkaline hydrothermal treatment of (a) AFFF #1 solution, and (b) AFFF #2 solution.

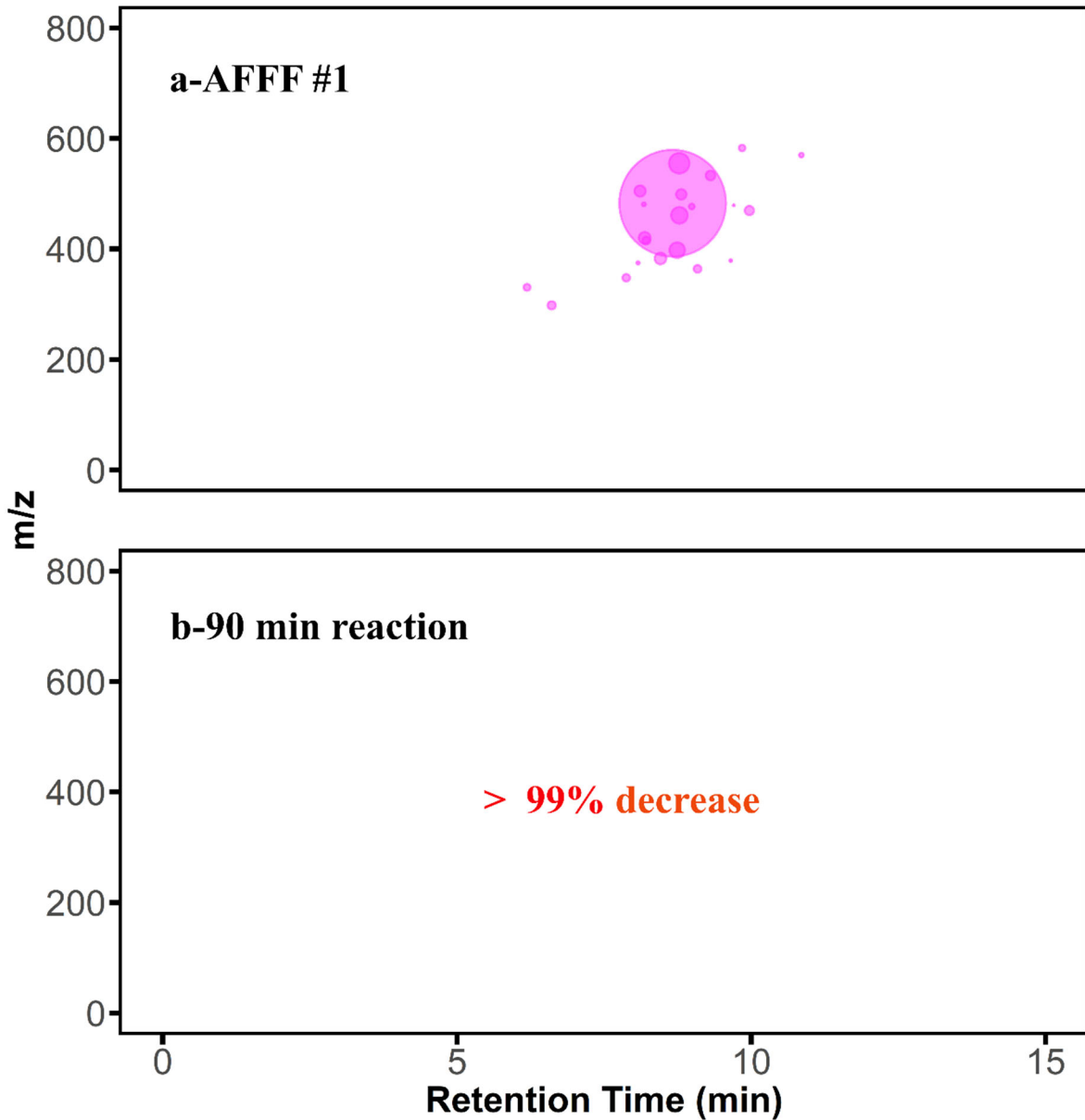


Figure 4.3.5 Bubble plots summarizing removal of PFASs identified in AFFF #1 identified by LC-QToF-MS suspect screening analysis. Total mass spec peak area removal of identified analytes listed in each plot. Individual bubbles represent individual PFAS, arranged by chromatographic retention time (RT) and mass-to-charge ratio (m/z). Diameter of individual bubbles represents the measured mass spec peak area response. Reaction conditions: AFFF diluted 1-to-1000, 350°C, 5 M NaOH.

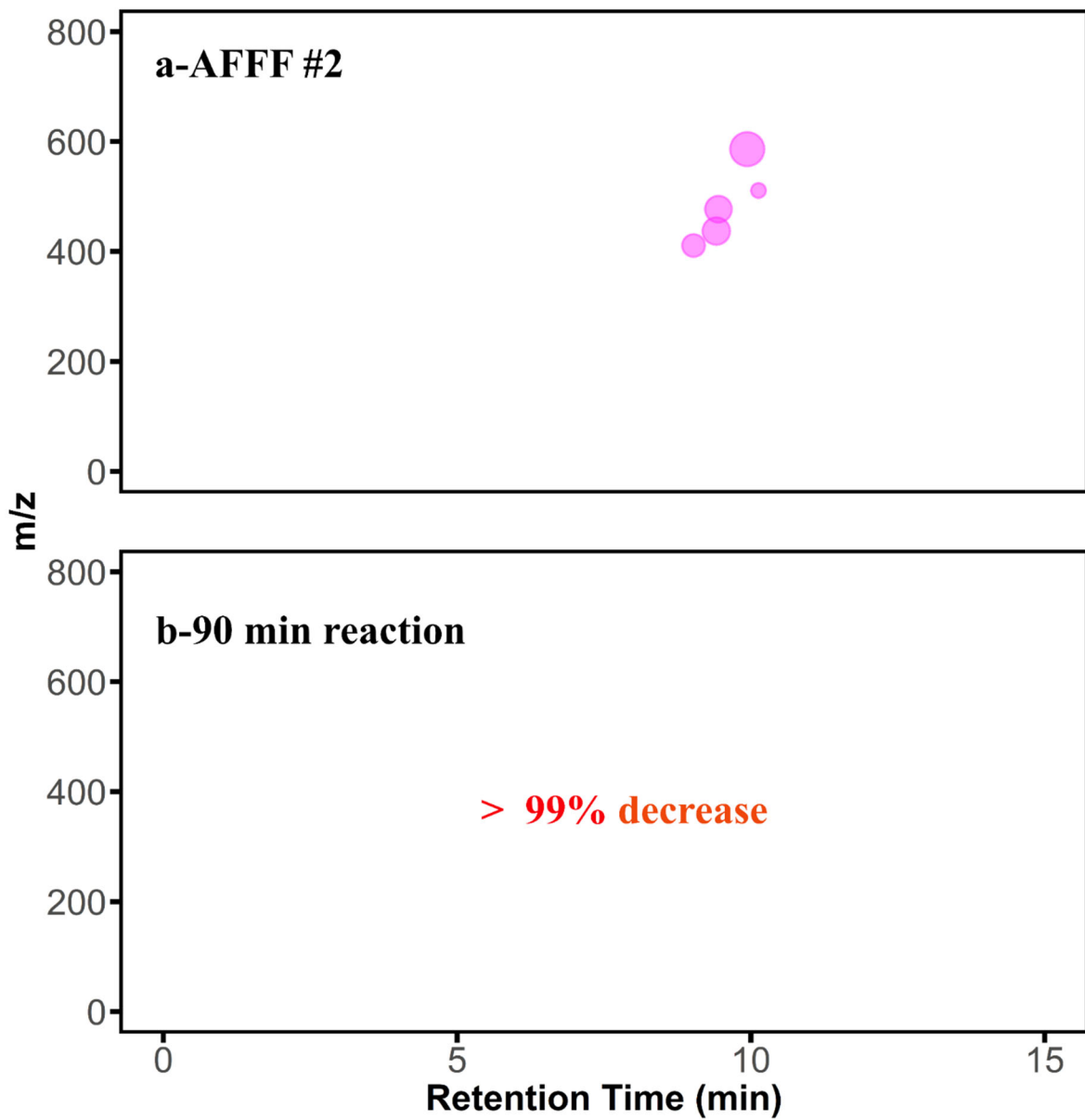


Figure 4.3.6 Bubble plots summarizing removal of PFASs identified in AFFF #2 identified by LC-QToF-MS suspect screening analysis. Reaction conditions: AFFF diluted 1-to-1000, 350°C, 5 M NaOH.

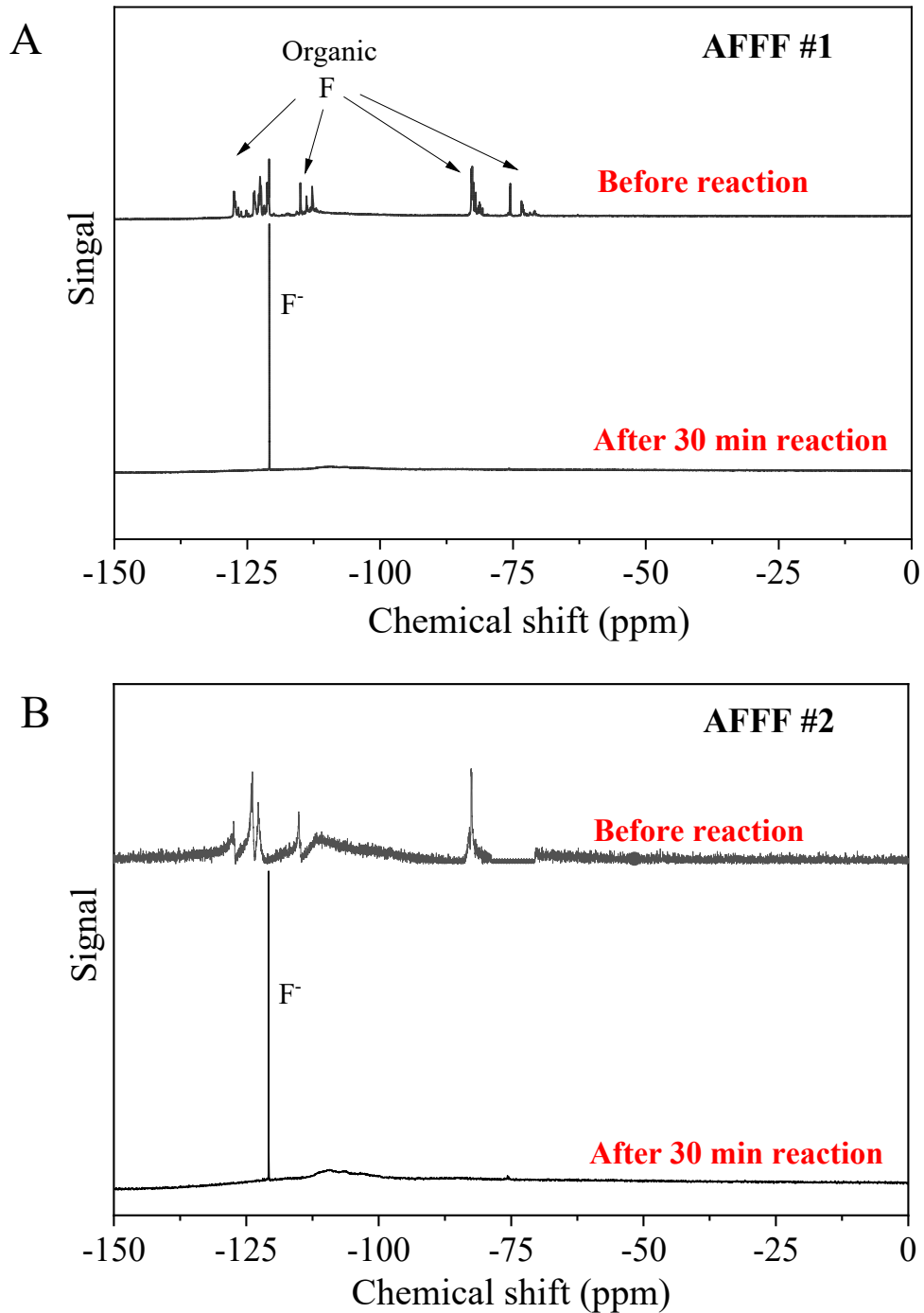


Figure 4.3.7 ^{19}F -NMR spectra of (a) diluted AFFF #1 (diluted 1-to-2) and (b) diluted AFFF #2 (diluted 1-to-4) before and after hydrothermal reaction for 30 min. Reaction conditions: 5 M NaOH amendment, 350°C.

4.3.6 Analysis of volatile reaction products

Preliminary tests were also conducted to identify any volatile reaction products from hydrothermal treatment of AFFF solutions. Selected reactions were performed in reactors outfitted with gas sampling ports. GC-TCD was applied to measure major reaction products. Results as shown in **Figure 4.3.8a** indicate that CO₂ is the major component in the product gas, consistent with mineralization of organic compounds in the AFFF, including PFASs. Measurements with GC-FID (**Figure 4.3.8b**) show that a series of isomers of butene, ethane, and n-butane were also detected, consistent with gasification reactions. 2-butene was also detected by GC-MS analysis (**Figure 4.3.9**). No volatile organofluorine compounds were detected, consistent with mineralization of PFASs to fluoride ion. However, current GC-MS libraries are lacking in volatile fluorine-containing species, and detailed quantification was not performed in this work, so future work is recommended to more specifically analyze and quantify gas product composition to ensure that there is negligible emissions of potentially hazardous volatile organic byproducts during alkaline hydrothermal treatment of PFAS-containing waste streams.

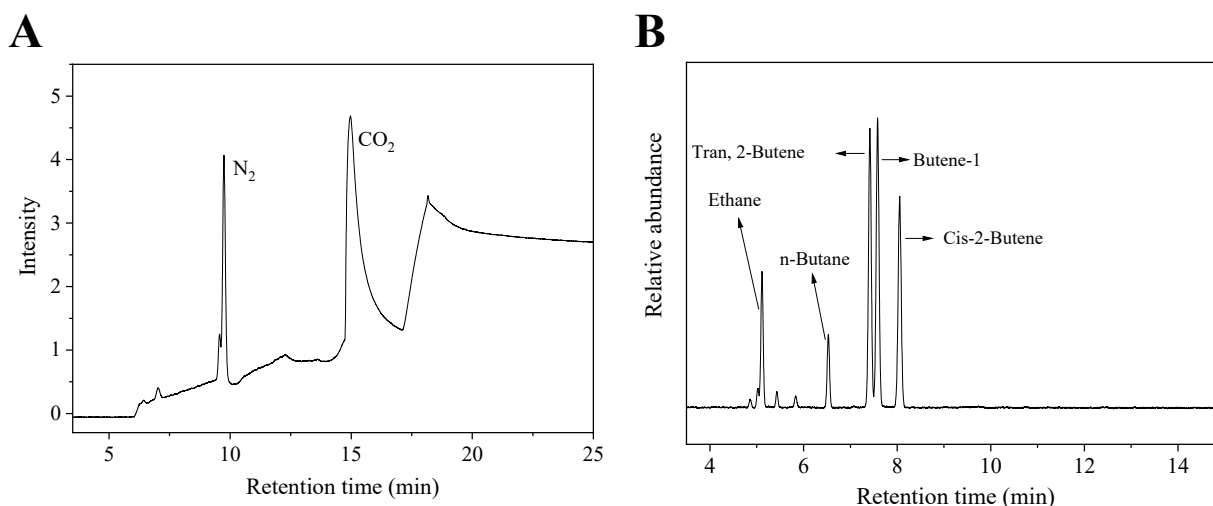


Figure 4.3.8 GC-TCD (a) and GC-FID (b) chromatograms of reactor headspace following alkaline hydrothermal treatment of AFFF #1. Reaction conditions: AFFF diluted 1-to-10, 5 M NaOH, 350°C, and 90 min reaction time.

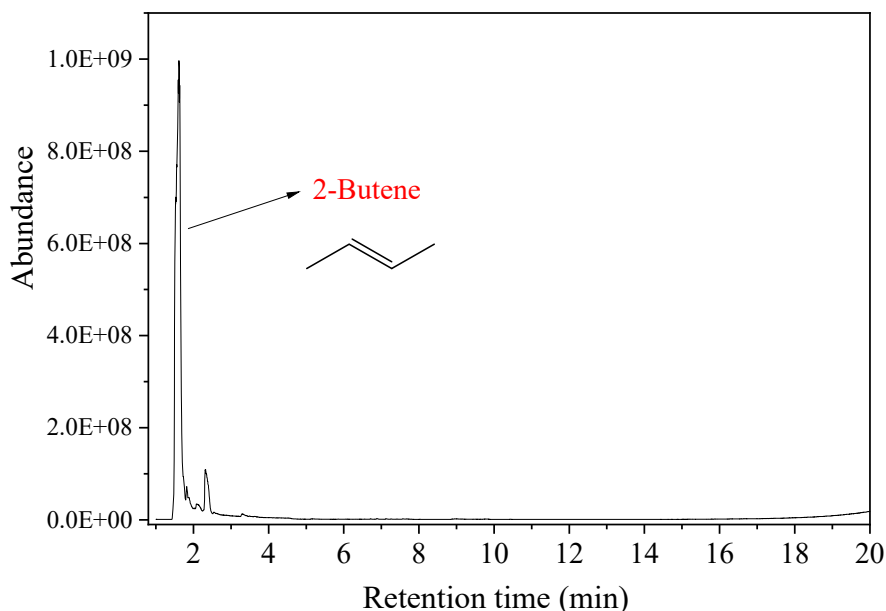
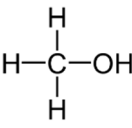
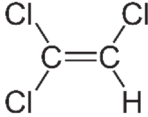
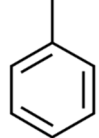
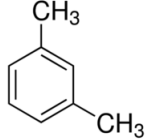
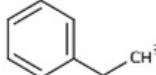


Figure 4.3.9 GC-MS chromatogram of reactor headspace after alkaline hydrothermal treatment of AFFF #1 (DGBE was the main chemical detected in the headspace before reaction). Reaction conditions: AFFF diluted 1-to-10, 5 M NaOH, 350°C, and 90 min reaction time.

4.4 Reactivity of AFFF Co-Solvents and Co-Contaminants

As part of this limited scope project, experiments were also conducted to assess the stability and/or degradation of co-solvents and co-contaminants often associated with AFFF-impacted sites. **Table 4.4.1** summarizes findings from these tests. The hydrothermal reactivities of these compounds were investigated individually under identical hydrothermal conditions (350°C, 1 mol/L NaOH, and 90 min reaction time). Collectively, these results indicate that the two co-solvents, DGBE and methanol, are minimally affected by exposure to alkaline hydrothermal conditions, whereas TCE (a model chlorinated solvent) and the aromatic hydrocarbon contaminants (benzene, toluene, ethylbenzene, and m-xylene) were completely degraded under the same conditions. Stability of methanol is consistent with past reports where methanol was included in hydrothermal experiments for degradation of PCBs to promote greater solubilization of the contaminants (Yamasaki et al., 1980). Degradation of TCE suggests a common nucleophilic attack mechanism that might be applicable to other halogenated organic contaminants. The mechanisms for degradation of the aromatic hydrocarbons is unclear, but it is possible that the same reactive nucleophiles responsible for PFAS decomposition attack the electron-rich aromatic bonds in these structures. Further detailed studies of alkaline hydrothermal reaction of PFAS co-contaminants are recommended to better understand applicability to addressing mixed contaminants often detected at AFFF-impacted sites like fire training areas. Nonetheless, findings suggest that this technology may be broadly applicable for many of the contaminants detected at these locations.

Table 4.4.1 Summary of results from screening experiments of hydrothermal reactivity of co-solvents and co-contaminants associated with AFFF and AFFF-impacted sites

Co-contaminant or co-solvent	Structure	Removal During Alkaline Hydrothermal Treatment (%) ^a
Diethylene glycol butyl ether (DGBE; butyl carbitol) – Cosolvent		17.6
Methanol – Cosolvent		11.2
Benzene – Co-contaminant		100
Trichloroethylene – Co-contaminant		100
Toluene - Co-contaminant		100
m-Xylene - Co-contaminant		100
Ethylbenzene – Co-contaminant		100

^a Reaction conditions: 350°C, 1 mol/L NaOH, and 90 min reaction time. Initial concentration of DGBE and methanol = 5000 mg/L. Initial concentration of co-contaminants = 50 mg/L.

4.5 Alkaline Hydrothermal Treatment of IDW and PFAS-Contaminated Soil

4.5.1 Characterization of investigation-derived waste samples

Two aqueous IDWs (MW-004 and MW-008) were characterized by targeted LC-QToF-MS analysis and were confirmed with PFASs contamination. Table 2 summarized the targeted PFASs concentrations in two IDWs. One of the two samples (MW-008) is much higher in concentration than the other, with PFOA and PFH_xS concentrations exceeding 1 mg/L. The other sample (MW-

004) is much lower in concentration, and the ratio of PFOS:PFOA is very different in the two samples, suggesting different sources of AFFF.

Table 4.5.1 Measured PFAS composition in aqueous IDW samples before and after alkaline hydrothermal treatment

PFAS compound	MW-004 (µg/L)		MW-008 (µg/L)	
	Before HTL	After HTL*	Before HTL	After HTL*
PFPeA	3.04 ± 3.2 ^a	< 0.22	4.52 ± 0.50	< 0.22
PFHxA	2.56 ± 0.06	< 0.01	36.2 ± 1.2	< 0.01
PFHpA	0.60 ± 0.02	< 0.22	4.39 ± 0.32	< 0.22
PFOA	3.28 ± 0.26	< 0.11	439 ± 39	< 0.11
PFBS	0.03 ± 0.00	< 0.01	8.18 ± 0.53	< 0.01
PFPeS	0.07 ± 0.00	< 0.01	13.5 ± 0.6	< 0.01
PFHxS	2.81 ± 0.04	< 0.01	252 ± 7	< 0.01
PFHpS	0.18 ± 0.00	< 0.01	3.79 ± 0.11	< 0.01
PFOS	10.96 ± 0.32	< 0.01	21.0 ± 2.1	< 0.01
FOSA	2.57 ± 0.04	< 0.01	< 0.01	< 0.01
6:2 FTS	2.36 ± 0.05	< 0.11	< 0.11	< 0.11
8:2 FTS	1.18 ± 0.03	< 0.01	< 0.01	< 0.01
Cl-PFOS	0.03 ± 0.01	< 0.01	< 0.01	< 0.01

* Concentrations lower than method detection limit values listed

^a Variability represents the full range of values measured in duplicate experiments

4.5.2 Characterization of PFAS-contaminated soil samples

Three PFAS-contaminated soils collected previously from different DoD sites throughout the U.S (Wurtsmith soil, JAX soil, and PAFB soil) were used instead for testing hydrothermal reaction of IDW soil samples. A table of soil properties is shown in **Table 4.5.2**. Soils were extracted with four rounds of basic methanol together with labeled surrogate standards before cleanup and analysis with LC-QToF-MS. **Tables 4.5.3, 4.5.4, 4.5.5** show results of the three soil analyses. Wurtsmith soil was most heavily contaminated with PFASs where the PFOS concentration was 46 times and 3 times higher than that in JAX soil, and PAFB soil, respectively. PFCAs (up to 340 ng/g, PFHxA), PFSAs (up to 22900 ng/g, PFOS), fluorotelomer acids (up to 215ng/g, 6:2 FTS), and sulfonamide precursors (up to 619 ng/g, MeFOSAA) were the dominant PFASs in Wurtsmith soil. JAX soil showed much lower PFASs concentration relative to Wurtsmith soil. The highest concentration of PFSAs in JAX soil was PFOS at 490 ng/g. PAFB soil was dominated by PFCAs (up to 115ng/g, PFHxA) and PFSAs (up to 7310 ng/g, PFOS). These three soils with different properties and PFASs contamination were used to test the stability of PFASs in soil with hydrothermal reaction.

Table 4.5.2 Soils properties of soils Wurtsmith and PAFB

Soil property	Wurtsmith	JAX	PAFB
% sand	97	na	79
% silt	0	na	6
% clay	3	na	15
CEC	3.3	na	9.5
AEC	-1.19	na	-0.04
%OC	4	na	1.1
pH	6.7	na	6.7

na. Data not available

Table 4.5.3 Measured PFAS composition in PFAS-contaminated soil from Wurtsmith AFB before and after alkaline hydrothermal treatment

PFAS compound	Wurtsmith soil (ng/g)		
	Before HTL	After HTL*	Removal (%)**
PFPeA	146 ± 31 ^a	< 0.01*	>99.99
PFHxA	340 ± 15	< 0.01	>99.99
PFHpA	35.3 ± 2.0	< 0.01	>99.97
PFOA	150 ± 17	< 0.01	>99.99
PFNA	1.73 ± 0.04	< 0.01	>99.42
PFDA	7.85 ± 0.86	< 0.02	>99.75
PFUdA	3.93 ± 0.54	< 0.01	>99.75
PFDoA	12.5 ± 3.2	< 0.02	>99.84
FOSA	223 ± 15	< 0.02	>99.99
MeFOSA	6.16 ± 1.42	< 0.02	>99.68
FOSAA	18.0 ± 4.0	< 0.02	>99.89
MeFOSAA	619 ± 170	4.10 ± 3.64	99.34
6:2 FTS	215 ± 37	< 0.01	>99.99
8:2 FTS	97.8 ± 32.0	< 0.01	>99.99
10:2 FTS	4.88 ± 2.02	< 0.02	>99.59
6:2 UFTCA	1.38 ± 0.55	< 0.12	>91.30
PFPPrS	16.2 ± 1.3	1.33 ± 0.18	91.80
PFBS	156 ± 24	7.82 ± 2.58	94.98
PFPeS	355 ± 78	19.1 ± 5.26	94.63
PFHxS	3960 ± 679	284 ± 83	92.83
PFHpS	62.8 ± 7.7	2.59 ± 0.92	95.88
PFOS	22900 ± 1470	1450 ± 466	93.67
PFNS	1900 ± 105	11.9 ± 4.7	99.37
PFDS	1390 ± 139	6.32 ± 2.01	99.54
PFDoS	683 ± 60	1.19 ± 0.33	99.83
Cl-O-PFNS	0.11 ± 0.00	< 0.02	>81.82

*Concentration lower than the method detection limit for each analyte indicated.

**Removal % is calculated using the detection limit in comparison to the initial concentration.

^a Variability represents the standard deviation measured in triplicate experiments

Table 4.5.4 Measured PFAS composition in PFAS-contaminated soil from Jacksonville NAS before and after alkaline hydrothermal treatment

PFAS compound	JAX soil (ng/g)		
	Before HTL	After HTL*	Removal (%)**
PFHxA	10.1 ± 3.2 ^a	1.89 ± 0.13	81.23
PFOA	12.6 ± 2.0	< 0.01*	>99.92
PFDA	0.79 ± 0.29	< 0.02	>97.47
FOSA	29.1 ± 6.3	< 0.02	>99.93
6:2 FTS	139 ± 101	< 0.01	>99.99
8:2 FTS	23.6 ± 19.6	< 0.01	>99.96
PFBS	5.37 ± 1.95	0.10 ± 0.03	98.16
PFPeS	2.46 ± 0.84	< 0.02	>99.19
PFHxS	76.5 ± 9.6	< 0.60	>99.22
PFHpS	0.06 ± 0.02	< 0.02	>66.67
PFOS	490 ± 60	23.1 ± 17.0	95.29

*Concentration lower than the method detection limit for each analyte indicated.

**Removal % is calculated using the detection limit in comparison to the initial concentration.

^a Variability represents the standard deviation measured in triplicate experiments

Table 4.5.5 Measured PFAS composition in PFAS-contaminated soil from Peterson AFB before and after alkaline hydrothermal treatment

PFAS compound	PAFB soil (ng/g)		
	Before HTL	After HTL*	Removal (%)**
PFPeA	122 ± 44 ^a	< 0.01*	>99.99
PFHxA	115 ± 17	0.38 ± 0.24	99.67
PFOA	16.8 ± 1.2	0.93 ± 0.12	94.46
PFDA	0.18 ± 0.03	0.52 ± 0.31	-189.92***
FOSA	30.0 ± 1.5	< 0.02	>99.93
6:2 FTS	47.5 ± 10.7	< 0.01	>99.98
8:2 FTS	34.1 ± 2.8	< 0.01	>99.97
PFPPrS	9.00 ± 0.35	< 0.06	>99.33
PFBS	47.2 ± 1.9	0.27 ± 0.11	99.43
PFPeS	35.0 ± 1.7	< 0.02	>99.94
PFHxS	194 ± 30	< 0.60	>99.69
PFHpS	4.68 ± 1.03	< 0.02	>99.57
PFOS	7310 ± 415	20.6 ± 7.5	99.72
PFNS	51.4 ± 2.5	< 0.01	>99.98
PFDS	1.27 ± 0.02	< 0.02	>98.43
Cl-PFOS	36.8 ± 4.24	< 0.01	>99.97

*Concentration lower than the method detection limit for each analyte indicated.

**Removal % is calculated using the detection limit in comparison to the initial concentration.

***In increase in PFDA concentration is attributed to an artifact in the chemical analysis procedure.

^a Variability represents the standard deviation measured in triplicate experiments

4.5.3 Destruction of PFASs in aqueous IDW samples

Hydrothermal conversion experiments were conducted with two aqueous IDW samples and results showed near complete decomposition of PFASs except MW-004 showed PFOS at a concentration

of 0.003 $\mu\text{g/L}$ after reaction which is still under HAL (0.07 $\mu\text{g/L}$). Although we don't have geochemical data of two IDWs, ~100% removal of PFASs demonstrated the effectiveness and robustness of hydrothermal destruction of PFASs present in aqueous IDW samples. Future work will include examination of the influence of common cations (e.g., Ca^{2+}), anions (e.g., HCO_3^-), and DOM present in groundwater on the hydrothermal reaction of PFASs.

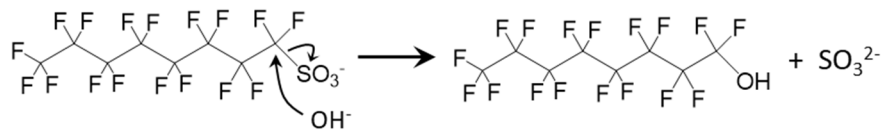
4.5.4 Destruction of PFASs in contaminated soils

The soil experiment results show a similar finding as aqueous IDWs where most of PFASs in all three soils achieved 95-100% removal after hydrothermal reaction. This further indicates the difference of matrix among three soils did not significantly influence the reactivity of PFASs during hydrothermal reaction. A future investigation of the technology's use for site remediation of PFAS-contaminated water and soil will be possible.

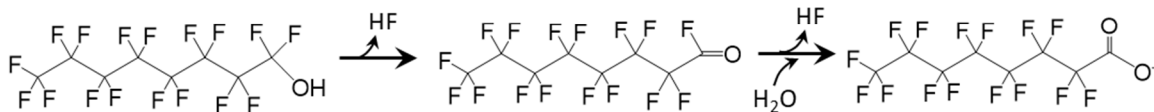
4.6 Tentative Mechanism for Hydrothermal Transformation and Mineralization of PFASs

Results obtained in this limited scope project are consistent with a tentative mechanism for PFAS transformation wherein OH^- catalyzes a series of nucleophilic substitution and decarboxylation reactions that defluorinate PFOS/PFOA and perfluorocarboxylate intermediates (**Figures 4.6.1 and 4.6.2**). The initial OH^- substitution reaction with the sulfonate head group forms an unstable perfluorinated alcohol (*Step 1*), which undergoes rapid HF elimination (to produce a ketone), and then hydration to release a second F^- and form PFOA (*Step 2*). Further decarboxylation then converts PFOA sequentially to increasingly short-chain perfluorocarboxylates, releasing 2F^- ions with each reaction (*Step 3*). Reactions initiated with PFOA show that the compound is much more reactive than PFOS, indicating that the initial cleavage of the sulfonate group is rate limiting, with further decarboxylation steps occurring much more rapidly.

Step 1: Nucleophilic attack of OH^- and release of polar headgroup



Step 2: HF elimination and hydration reactions to produce PFOA



Step 3: Sequential decarboxylation leading to chain shortening and mineralization

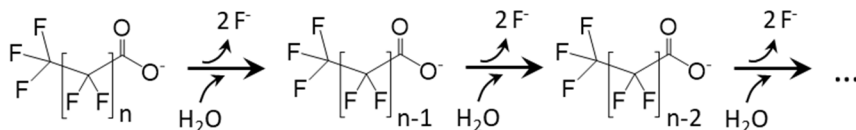


Figure 4.6.1 Proposed mechanism for OH^- mediated decomposition of PFOS under hydrothermal conditions.

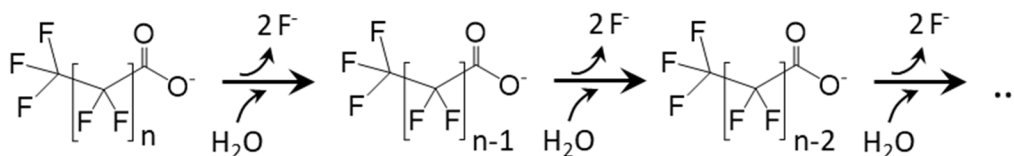


Figure 4.6.2 Proposed mechanism for decomposition of PFOA under hydrothermal conditions.

While application of strong alkalis like NaOH to promote decomposition of persistent organic contaminants in near-critical water has not been commonly reported, a small number of studies have reported on dehalogenation of PCBs and chlorinated solvents (Yamasaki et al., 1980, 2000). Furthermore, literature on biomass conversion contains numerous reports of strong alkalis catalyzing decomposition and gasification reactions in near-critical and supercritical water (Guo et al., 2010, 2010). Addition of strong bases also catalyze decarboxylation of both short- and long-chain carboxylic acids (Belsky et al., 1999; Fu et al., 2010). Interestingly, findings from the present study indicate that the fully perfluorinated PFOA and shorter-chain carboxylate intermediates (i.e., PFHxA and PFPeA) are less stable in hydrothermal water than un-fluorinated alkyl carboxylic acids reported previously (Belsky et al., 1999; Watanabe et al., 2006). Octanoic acid, the un-fluorinated analogue of PFOA was found to be unreactive, with a residual concentration of 45.8 ± 0.3 mg/L from the starting concentration of 50.8 ± 1.0 mg/L under conditions where >99% PFOA degradation was observed within 30 min (250°C , no solution amendments). The electron-withdrawing character of fluorine substituents may act to stabilize the penta-coordinate intermediate formed by the initial nucleophilic attack of $\text{OH}^-/\text{H}_2\text{O}$ on the carbon adjacent to the carboxylate and sulfonate head groups.

The lag between PFOS degradation and F^- release observed at lower temperatures is suggestive of kinetic limitations on intermediate transformations that release F^- under these conditions. While LC-MS/MS revealed only minimal formation of shorter chain carboxylates (**Figure 4.2.2**), the perfluorinated alcohol and ketone intermediates are not readily observed by the methods used here. Further analysis of intermediates and products derived from wider range of PFASs is needed to confirm the active mechanisms.

4.7 Assessment of Energy Requirements for Alkaline Hydrothermal PFAS Treatment

Experimental results demonstrate that the full suite of PFASs identified in AFFF and AFFF-impacted waters and sediments can be effectively degraded and mineralized by hydrothermal reaction in water at $\geq 300^\circ\text{C}$ amended with NaOH. It is anticipated that energy input requirements for this process will be significantly lower than those required for incineration of the same liquid waste streams based upon the assumption that (a) the required temperatures are lower than those required for hazardous waste incineration ($\geq 650^\circ\text{C}$) and (b) hydrothermal reaction in condensed phase water avoids parasitic energy losses associated with vaporizing water from liquid to gaseous states. The following calculations, although only meant to roughly compare input heat requirements, confirm this finding (**Table 4.7.1**). More detailed analysis of energy and chemical

inputs using results from continuous-flow hydrothermal reactor tests is recommended for future research.

Table 4.7.1 Estimated heat input requirements for alkaline hydrothermal treatment and incineration of PFAS-contaminated water

	Input Heat Requirement (kWh/m ³)
Alkaline hydrothermal treatment	
Reaction at 300°C (no heat recovery)	274
Reaction at 300°C (60% heat recovery)	110
Reaction at 350°C (no heat recovery)	317
Reaction at 350°C (60% heat recovery)	127
Incineration	
Rotary kiln at 650-850°C with 1,100°C afterburner	1,336
Rotary kiln at 650-850°C with 1,400°C afterburner	1,556
Circulating bed combustion chamber at 750°C (no heat recovery)	1,099
Circulating bed combustion chamber at 750°C (60% heat recovery)	440
Circulating bed combustion chamber at 1,100°C (no heat recovery)	1,336
Circulating bed combustion chamber at 1,100°C (60% heat recovery)	534

Figure 4.7.1 shows a simplified depiction of a hydrothermal reactor for the treatment of PFAS-contaminated water. PFAS-contaminated water is mixed with alkali (e.g., NaOH) and water flows through a pre-heating zone where water temperature is increased from ambient using heat exchangers fed by treated water exiting the main reaction zone. The pre-heated water then flows into the main reaction chamber where it is heated to the target temperature of 350°C for the desired reactor residence time. The treated water is cooled by heat exchanger connected to the pre-heat zone of the reactor. The final effluent will require neutralization and other treatment depending on the final use of the water.

We assume that the major energy input requirements are those associated with raising the temperature of the feed water from ambient temperature (assumed to be 20°C) to the target reaction temperature (assumed to be 300 - 350°C). This can be estimated using isochoric specific heat values of water (i.e., condensed phase water at constant volume), C_v [kJ/(kg K)], integrated over the expected temperature change:

$$\text{Required Heat (kWh/m}^3\text{)} = \left(\sum_i C_{v,i} \Delta t_i \right) \left(\frac{1000 \text{ kg}}{\text{m}^3} \right) \left(\frac{1 \text{ kWh}}{3600 \text{ kJ}} \right) \quad (4.7.1)$$

where $C_{v,i}$ is the average temperature-variant isochoric specific heat value, and Δt_i is the incremental temperature change over which $C_{v,i}$ is valid (**Table 4.7.2**). The 1000 kg/m³ and the 1

kWh/3600 kJ are conversion factors to yield the desired units of energy input per unit volume of water treated.

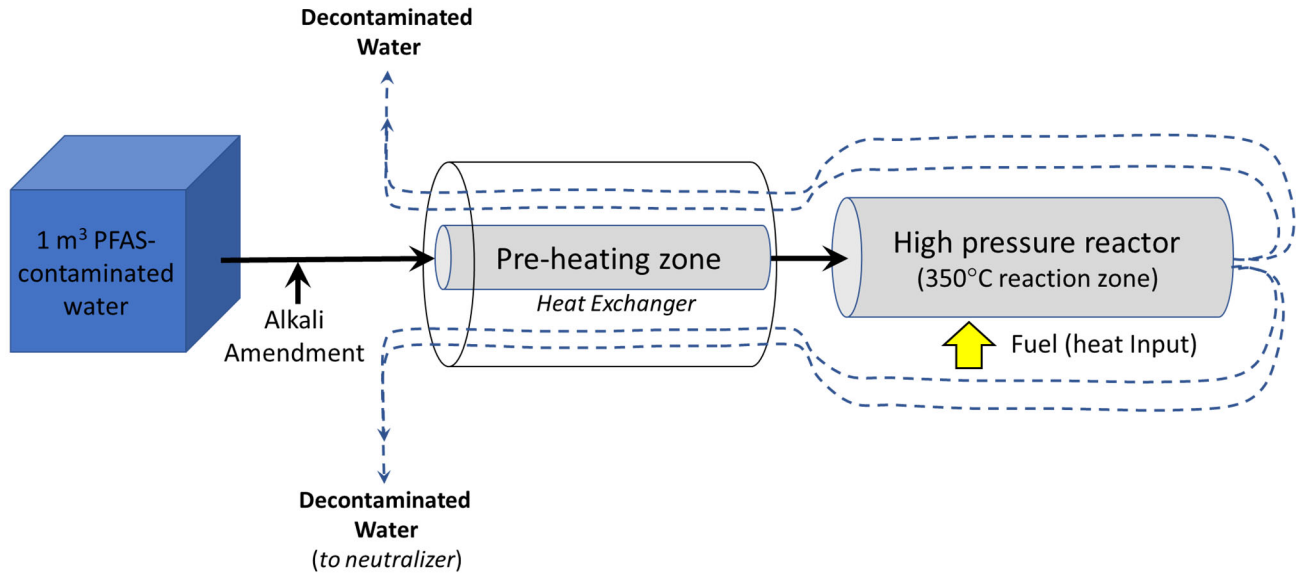


Figure 4.7.1 Schematic of a continuous-flow hydrothermal reactor with integrated heat recovery.

Application of equation 4.7.1 yields required heat inputs of 274 and 317 kWh/m³ for treatment of PFAS-contaminated water at 300°C and 350°C, respectively, if no efforts are made for heat recovery. If heat exchangers are integrated into the system and are able to recover 60% of the heat from the treated water (e.g., to pre-heat influent water), inputs can be reduced to 110 kWh/m³ and 127 kWh/m³, respectively, for hydrothermal processing at 300°C and 350°C. Input heat requirements for wet suspensions of sediment are expected to vary slightly due to differences in C_v of the solid phases compared to water.

Similar calculations can be performed for incineration processes that take place in either a cement kiln system (**Figure 4.7.2**; 650 – 850°C primary chamber with 1100 – 1400°C afterburner) or a circulating fluidized bed combustion chamber (**Figure 4.7.3**; 750 – 1100°C). The latter option often includes integrated heat recovery to improve energy efficiencies. Here, calculations are modified to include the heat required to first vaporize the condensed water ($\Delta_{vap}H_T$), then raising the temperature of the resulting water vapor to the target reaction temperatures:

$$\text{Required Heat (kWh/m}^3\text{)} = \left(\Delta_{vap}H_T + \sum_i C_{p,i} \Delta t_i \right) \left(\frac{1000 \text{ kg}}{\text{m}^3} \right) \left(\frac{1 \text{ kWh}}{3600 \text{ kJ}} \right) \quad (4.7.2)$$

where $C_{p,i}$ is now the temperature-variant isobaric specific heat value (specific heat at constant pressure), and Δt_i is the incremental temperature change over which $C_{p,i}$ is valid (**Table 4.7.3**). The 1000 kg/m³ is a conversion from the mass to volume of PFAS-contaminated water.

Table 4.7.2 Isochoric specific heat values of liquid water ($C_{v,i}$) at different temperatures

Temperature Range (°C)	$C_{v,i}$ kJ/(kg K)
20-25	20.73725
25-30	20.6385
30-40	40.956
40-50	40.5005
50-60	40.0155
60-70	39.5095
70-80	38.9905
80-90	38.4665
90-100	37.943
100-110	37.4245
110-120	36.9145
120-140	72.356
140-160	70.482
160-180	68.737
180-200	67.128
200-220	65.658
220-240	64.329
240-260	63.151
260-280	62.15
280-300	61.379
300-320	60.958
320-340	61.209
340-350	63.753

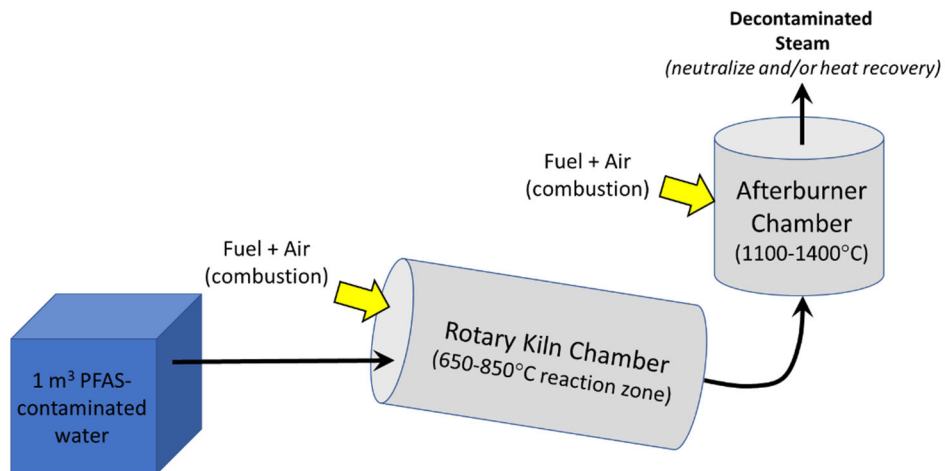


Figure 4.7.2 Schematic of a rotary kiln incinerator with afterburner.

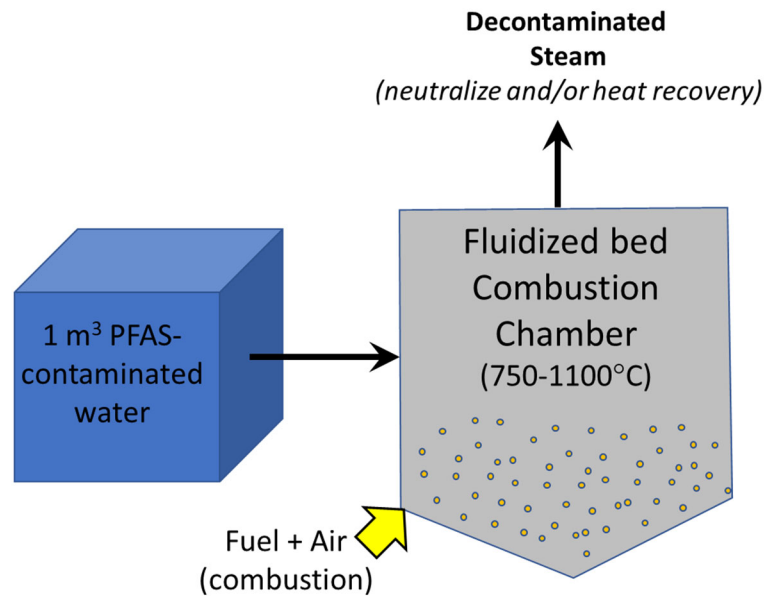


Figure 4.7.3 Schematic of an incinerator with circulating fluidized bed combustion chamber

For incineration in a cement kiln, application of equation 4.7.2 yields required heat inputs of 1,336 and 1,556 kWh/m³ for incineration of PFAS-contaminated water with afterburner set to 1,100°C and 1,400°C, respectively. Generally, heat recovery is not integrated into cement kiln systems.

For incineration in a circulating fluidized bed combustion chamber, application of equation 4.7.2 yields required heat inputs of 1,099 and 1,336 kWh/m³ for incineration of PFAS-contaminated water with afterburner set to 750°C and 1,100°C, respectively. If heat exchangers are integrated into the system and are able to recover 60% of the heat from the treated water (e.g., to pre-heat influent water), inputs can be reduced to 440 kWh/m³ and 534 kWh/m³, respectively, for the two ends of the temperature range. In the initial wet sediments have no fuel value themselves, expected heat requirements will be higher due to the need to heat the solid phases to the same reaction temperatures.

While the calculated energy inputs are simplistic, they nonetheless illustrate the potential energy savings of hydrothermal processes for destruction of PFASs in liquid waste streams compared to incineration at much higher temperatures. At the same time, it is apparent that energy requirements are much higher than most water treatment technologies, including high pressure membrane processes used for seawater desalination. Thus, hydrothermal destruction technologies are not appropriate for treating dilute groundwater plumes, and would be reserved for treatment of small volume waste streams, including IDW and concentrates generated from other treatment processes (e.g., ion exchange regenerant waste, membrane concentrates, sludge solid residuals). In these scenarios, only a very small fraction of the total treated water volume is subjected to hydrothermal treatment, justifying the high energy per unit volume inputs. The same conclusion applies to most all destructive technologies currently being investigated.

Table 4.7.3 Isobaric specific heat values of water vapor ($C_{p,i}$) at different temperatures

Temperature (°C)	$C_{p,i}$ kJ/(kg K)
2	1.859
27	1.864
52	1.871
77	1.88
102	1.89
127	1.901
177	1.926
227	1.954
277	1.984
327	2.015
377	2.047
427	2.08
477	2.113
527	2.147
577	2.182
627	2.217
650	2.2345
677	2.252
727	2.288
750	2.3055
777	2.323
827	2.358
850	2.375
877	2.392
927	2.425
977	2.458
1027	2.49
1077	2.521
1100	2.5365
1127	2.552
1227	2.609
1327	2.662
1400	2.6865
1427	2.711
1527	2.756
1627	2.798
1727	2.836

5.0 Conclusions and Implications for Future Research/Implementation

5.1 Summary and Conclusions of Present Study

Findings from this limited scope project demonstrate a promising new strategy for achieving complete destruction and defluorination of PFASs present in IDW as well as other concentrate streams. To our knowledge, this is the first effort demonstrating that subcritical hydrothermal reaction conditions can be combined with low-cost alkali amendments to achieve complete degradation and defluorination of PFASs, both individual solutes and complex mixtures of PFASs (e.g., AFFF). The following is a summary of major conclusions derived from this study:

- Screening experiments conducted with a wide range of solution amendments, including acids, bases, oxidants, reductants, salts, and metallic nanoparticles, demonstrate that amendment with reagents that increase solution pH promotes degradation and defluorination of PFOS and other PFASs detected in AFFF.
- Rates of hydrothermal PFAS degradation and defluorination increase with increasing solution temperature and alkali amendment concentration. Conditions that lead to complete defluorination are identified.
- Whereas hydrothermal decomposition of PFOS and related perfluoroalkyl sulfonic acids require higher temperatures and alkali amendments, decomposition of PFOA and related perfluoroalkyl carboxylic acids occurs at lower temperatures and without need for alkali amendments.
- Kinetics experiments show that rates of PFOS destruction follow a generalized second-order model, where rates of PFOS degradation are linearly dependent upon molar concentrations of both PFOS and OH⁻.
- LC-QToF-MS analysis of PFASs within AFFF mixtures shows that the full diversity of PFASs detected through both targeted and suspect screening analyses are degraded during alkaline hydrothermal treatment.
- PFASs detected in AFFF mixtures derived principally from electrochemical fluorination processes (AFFF #1) and fluorotelomerization processes (AFFF #2) are both subject to alkaline hydrothermal destruction.
- NMR spectroscopy measurements confirm rapid conversion of organically bonded fluorine structures in AFFF to inorganic fluoride ion.
- No volatile organo-fluorine compounds were detected as reaction byproducts. Carbon dioxide was the major gas product observed, together with lesser amounts of short-chain organic hydrocarbons.
- Preliminary tests with AFFF co-solvents suggest that the solvents are stable during alkaline hydrothermal treatment. These structures are expected to be readily biodegradable.
- Preliminary tests with organic co-contaminants associated with AFFF sites (e.g., FTAs), including TCE (halogenated solvent) and aromatic hydrocarbons (associated with fuel

contamination) show that these chemicals will also degrade along with PFASs during alkaline hydrothermal treatment.

- Tests conducted with PFAS-contaminated aqueous IDW samples and PFAS-contaminated soil samples collected from DoD sites demonstrate that PFASs are rapidly degraded in these matrices, supporting further investigation of the technology's use for managing PFAS contamination.
- Analysis determined that heat requirements for optimal alkaline hydrothermal treatment of PFAS-contaminated aqueous solutions are significantly lower than heat requirements for incineration of the same contaminated matrices.

5.2 Implications for Technology Development and Implementation

The findings summarized indicate a very promising technology pathway for treatment of PFAS-contamination that can achieve complete destruction of the PFASs, thereby eliminating future liabilities associated with contamination at DoD facilities. The broad efficacy and lower heat requirements compared to conventional hazardous waste incineration is suggestive of an alternative technology for managing a variety of high moisture content PFAS wastes and concentrates (**Figure 5.2.1**), including:

- Aqueous and soil investigation-derived wastes
- Unused stockpiles of AFFF containing legacy PFASs requiring disposal
- PFAS-contaminated source zone soils, sediments, and concentrated solutions
- Waste ion exchange concentrate management, including PFAS-contaminated still bottoms and aqueous/co-solvent mixtures
- High pressure membrane reject streams with elevated PFAS concentrations
- Accident site wastes collected following application of AFFF
- PFAS-contaminated wastewater sludge and biosolids
- Rinse solutions from AFFF spray equipment
- Manufacturing wastewater with elevated PFAS concentrations where adsorption/membranes are not practical for direct treatment

While the alkaline hydrothermal treatment process appears to be more energy efficient than incineration, the process still requires considerable energy inputs per unit volume of contamination treated. Thus, the process would not be recommended as an application for direct treatment or remediation of dilute groundwater plumes. Instead, it is recommended that alkaline hydrothermal treatment be combined into hybrid treatment systems where physical separation processes (e.g., ion exchange, nanofiltration) are applied to remove PFASs from the contaminated water, concentrating the PFASs in a low-volume secondary stream (e.g., waste ion exchange regenerant brine) that would then be subjected to hydrothermal treatment and destruction (**Figure 5.2.2**)



Figure 5.2.1 Illustration of potential applications of the alkaline hydrothermal treatment technology for management of PFASs.

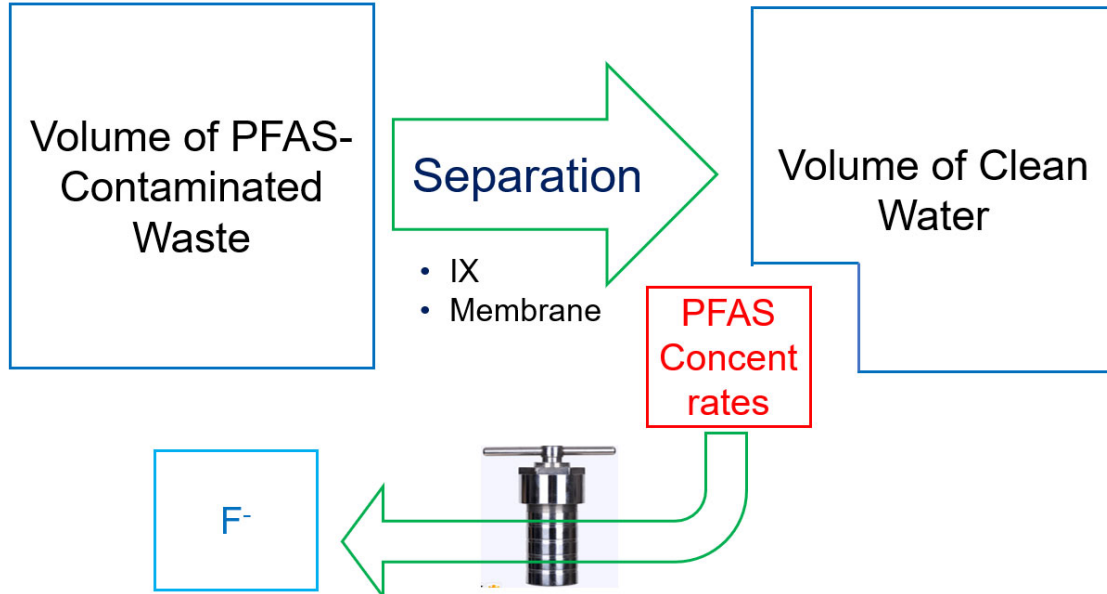


Figure 5.2.2 Illustration of hybrid treatment approach that combines hydrothermal treatment with physical separation processes to concentrate PFAS contamination into smaller volume solutions before hydrothermal treatment.

While incineration is a mature technology, public acceptance of incineration of PFAS-containing wastes is low, and some incinerators are reluctant to accept PFAS-containing wastes due to concerns about generation of corrosive hydrofluoric acid (HF) and impending regulations on PFAS-associated emissions. Transportation of PFAS-contaminated wastes off site to centralized incineration facilities also raises serious concerns about inadvertent releases. Hydrothermal destruction technologies are conducive to application of mobile treatment units for small scale treatment needs (e.g., treatment of IDW samples generated on site).

5.3 Potential Next Steps and Proposed Follow-On Research

The promising findings from this limited scope project are highly supportive of an alternative treatment technology for PFAS-containing wastes that can achieve both removal and destruction of the PFASs. Still, a number of fundamental and applied research questions need to be answered to advance this technology and translate application to the field. We would like to propose a follow-on SERDP research project that would address a number of important questions and provide a path forward for development and application of this technology for management of DOD sites. The following is a summary of the major objectives of a proposed follow-on research effort:

Objective 1: Improve understanding of the reaction mechanisms and molecular constraints controlling transformation of individual PFASs. Findings from the limited scope project demonstrate a wide range of PFAS structures are subject to hydrothermal destruction, and are suggestive of an operative mechanism. However, a deeper understanding of the controlling mechanisms and structure-reactivity trends is needed to rationally design effective hydrothermal treatment systems. We propose to combine experiments with computational modeling (i.e., DFT - Density Functional Theory) to accomplish this in the follow on research.

Kinetics experiments will be conducted with representative PFASs to determine the temperature and OH⁻ dependence of rate constants. This will include long- and short chain perfluoroalkyl acids, fluorotelomer acids, and a range of precursor structures. Reaction rates will be evaluated systematically at a range of temperatures (200 – 350°C) with variable concentrations of NaOH (0.1 – 5 M). PFASs will be monitored by LC-QToF-MS, and fluoride ion release will be monitored by ISE + ion chromatography analysis. Additional experiments with short-chain PFASs (e.g., trifluoroacetate and trifluoromethane sulfonate) will be conducted using ¹⁹F- and ¹³C-NMR techniques to identify transient intermediates. The simpler nature of the short-chain structures will facilitate spectroscopic identification of intermediates.

Previous DFT calculations performed by a proposed collaborator investigating 1,2-F atom shift reactions and remediation via hydrated electron reduction were in excellent agreement with the experimental findings (Van Hoomissen and Vyas, 2019). Similar methods would be applied here to understand the molecular steps associated with base-catalyzed hydrolysis, decarboxylation, and desulfurization. Activation barriers will be calculated and compared to experimental findings to develop structure-reactivity relationships. Furthermore, calculations will also be performed using specialized basis sets to interpret ¹⁹F and ¹³C NMR experimental data.

Objective 2: Evaluate hydrothermal PFAS destruction within concentrate byproduct solutions.

We would also plan to build upon findings from the limited scope project to expand the application space to include hydrothermal treatment of PFAS in different concentrates obtained from physical separations processes, including:

1. Ion exchange regenerant waste brines
2. Regenerant streams from other adsorbents
3. NR and RO membrane reject streams
4. Foam fractionation treatment system concentrates

Destruction of PFASs within thermal soil treatment vapor condensate streams is also being separately evaluated as part of a recently funded ESTCP project (ER20-D1-5250) that PI Strathmann is involved in.

Individual concentrate streams will be fully characterized before treatment. PFAS composition will be assessed using both target and suspect screening LC-QToF-MS approaches. Halogenated organic and hydrocarbon co-contaminants will also be measured by GC-MS/MS and GC-FID analysis. Important water quality parameters (i.e., pH, alkalinity, conductivity) and non-target water constituents (dissolved organic carbon, common inorganic cations, anions) will also be determined. The kinetics for transformation of individual PFASs in the concentrates will be evaluated in batch reactions conducted over a range of temperatures with variable concentrations of NaOH and Ca(OH)₂. Concentrate streams containing alcohol co-solvents (e.g., methanol for IX regeneration) will be studied both with the co-solvent present and after separating the co-solvent (to mimic “still bottoms”). If PFAS mineralization can be accomplished without co-solvent destruction, this would enable re-use of the waste brine/co-solvent mixture without need for separate distillation and recovery steps for the co-solvent.

Objective 3: Explore the potential for in situ reactivation of PFAS-laden sorbents.

PFAS-laden GAC adsorbents are typically shipped off site for thermal reactivation, incineration, or landfilling. As an alternative, it may be possible to apply hydrothermal conditions to wet GAC beds to achieve in situ destruction of the adsorbed PFASs, re-activating the adsorbent in the process. The same approach will also be examined for reactivation of spent IX resins, and we will explore collaboration with other SERDP-supported researchers that are developing improved adsorbent materials for PFASs (e.g., ER18-1026 Damian Helbling PI; Rational Design and Implementation of Novel Polymer Adsorbents). Following reaction, the treated GAC mixture will then be diluted in excess water and supernatant would be collected and analyzed for F⁻ release and any desorbed PFAS byproducts. The measured F⁻ concentration will be compared with the total fluoride initially loaded (as PFOS and PFOA) to quantify extent of mineralization. The solid will be further extracted with basic methanol and analyzed for PFASs. The treated solid will then be dried and re-weighed to assess any loss of material mass during the treatment process.

It is also important that the hydrothermally treated adsorbents retain their effectiveness as adsorbents. To provide an initial assessment of the effects of treatment on adsorbent efficacy, we will propose to run small-scale PFOS column breakthrough experiments to compare virgin adsorbents and hydrothermally treated adsorbents.

Objective 4: Further evaluate influence of site specific soil properties and solution conditions on PFAS treatment. Experiments included in the limited scope project demonstrated the alkaline hydrothermal treatment can be applied to destroy PFASs present in contaminated soil matrices. However, only a limited number of experiments at a single reaction condition and time were conducted with three PFAS-contaminated soils collected from DoD facilities. Here, we would propose to expand on this work to examine reactions in a wider range of contaminated soils and sediments with variable soil and geochemical properties as well as soil moisture contents. This would enable us to identify any properties that may be expected to inhibit or enhance PFAS reactions under hydrothermal conditions. In addition, time-resolved experiments will be performed to assess rates of PFAS transformation under different treatment conditions to compare with treatment of aqueous solutions. This will ultimately be important when designing treatment operations.

Objective 5: Construct and apply a continuous-flow reactor for hydrothermal destruction of PFAS-contaminated water and soil/water mixtures. Results from batch experiments conducted as part of the limited scope project and the objectives described above will be used to inform the design of a continuous-flow reactor for hydrothermal treatment of PFASs. Continuous-flow reactors have several benefits over batch reactors, both as research tools and practical treatment systems. As a research tool, the flow-through operation allows for continuous tuning of process variables and eliminates errors associated with heating/cooling reaction fluid. In practical applications, the continuous process allows for higher throughput, better operational flexibility, real-time process monitoring and control, and more efficient operation.

Here, we will propose to construct a laboratory-scale reactor capable of continuously treating up to 5-20 mL/min of PFAS liquid streams concentrate solution. The reactor design will enable the collection of aqueous and gas samples at various residence times and temperatures to allow for analysis of both dissolved and potentially volatile products. The modular reactor design will also allow for inserting a bed of catalyst in the flow path to study heterogeneous catalysis (*see Objective 6*) or operate with NaOH-amended solutions. Corrosion mitigation, pressurization, heating methods, effluent quenching, and mixing must be considered in the design. (Pinkard et al., 2019) PFAS reaction rates will be measured from the analysis of the effluent over the range of operational conditions. Outcomes from this work will provide chemical kinetic rates of PFAS hydrolysis to inform design of continuous reactors of different scales, and establish the fate of intermediate species during hydrothermal processing of a variety of PFASs.

Objective 6: Assess the potential of heterogeneous catalysts for PFAS destruction. Substitution of homogeneous alkalis like NaOH with a heterogeneous catalyst could significantly reduce both chemical inputs and residuals from hydrothermal treatment. Past work shows that many organic compounds subject to base-catalyzed hydrolysis are also subject to hydrolytic decomposition catalyzed by metal-containing surfaces (e.g., halogenated phosphate esters). (Fang et al., 2018) This task will screen a wide range of potential materials that have been documented to catalyze either hydrolysis, decarboxylation, or organic chemical gasification reactions. Catalysts will initially be screened for PFOS destruction since sulfonic acid analogues have, so far, been shown to be the most recalcitrant PFASs. Materials that exhibit promising activity will then studied for their effectiveness in treating the same PFAS concentrate streams described in Objective 2 using a continuous-flow reactor constructed as part of Objective 4.

Objective 7: Use experimental data to inform a cost and energy analysis of hydrothermal treatment. Results from experiments conducted in continuous-flow reactors will be used to further refine estimates of the energy requirements and costs for hydrothermal treatment of different PFAS-contaminated concentrate streams. Data will also be used to estimate capital costs for construction of hydrothermal reactors scaled to treat different volumes of PFAS-contaminated waste each day (e.g., 500, 5,000, and 50,000 gallons per day of PFAS concentrate). This analysis will be critical to planning of subsequent field demonstrations through ESTCP or other funding mechanisms.

Further details, methodologies, and project team will be detailed in a full proposal submission when requested by the SERDP program office.

6.0 Literature Cited

- Appleman, T.D., Higgins, C.P., Quiñones, O., Vanderford, B.J., Kolstad, C., Zeigler-Holady, J.C., Dickenson, E.R.V., 2014. Treatment of poly- and perfluoroalkyl substances in U.S. full-scale water treatment systems. *Water Research* 51, 246–255. <https://doi.org/10.1016/j.watres.2013.10.067>
- Arvaniti, O.S., Stasinakis, A.S., 2015. Review on the occurrence, fate and removal of perfluorinated compounds during wastewater treatment. *Science of The Total Environment* 524–525, 81–92. <https://doi.org/10.1016/j.scitotenv.2015.04.023>
- Backe, W.J., Day, T.C., Field, J.A., 2013. Zwitterionic, Cationic, and Anionic Fluorinated Chemicals in Aqueous Film Forming Foam Formulations and Groundwater from U.S. Military Bases by Nonaqueous Large-Volume Injection HPLC-MS/MS. *Environ. Sci. Technol.* 47, 5226–5234. <https://doi.org/10.1021/es3034999>
- Barzen-Hanson, K.A., Field, J.A., 2015. Discovery and Implications of C2 and C3 Perfluoroalkyl Sulfonates in Aqueous Film-Forming Foams and Groundwater. *Environ. Sci. Technol. Lett.* 2, 95–99. <https://doi.org/10.1021/acs.estlett.5b00049>
- Barzen-Hanson, K.A., Roberts, S.C., Choyke, S., Oetjen, K., McAlees, A., Riddell, N., McCrindle, R., Ferguson, P.L., Higgins, C.P., Field, J.A., 2017. Discovery of 40 Classes of Per- and Polyfluoroalkyl Substances in Historical Aqueous Film-Forming Foams (AFFFs) and AFFF-Impacted Groundwater. *Environ. Sci. Technol.* 51, 2047–2057. <https://doi.org/10.1021/acs.est.6b05843>
- Belsky, A.J., Maiella, P.G., Brill, T.B., 1999. Spectroscopy of Hydrothermal Reactions 13. Kinetics and Mechanisms of Decarboxylation of Acetic Acid Derivatives at 100–260 °C under 275 bar. *J. Phys. Chem. A* 103, 4253–4260. <https://doi.org/10.1021/jp984122d>
- Biller, P., Sharma, B.K., Kunwar, B., Ross, A.B., 2015. Hydroprocessing of bio-crude from continuous hydrothermal liquefaction of microalgae. *Fuel* 159, 197–205. <https://doi.org/10.1016/j.fuel.2015.06.077>
- Brendel, S., Fetter, E., Staude, C., Vierke, L., Biegel-Engler, A., 2018. Short-chain perfluoroalkyl acids: environmental concerns and a regulatory strategy under REACH. *Environmental Sciences Europe* 30, 9. <https://doi.org/10.1186/s12302-018-0134-4>
- Bruton, T.A., Sedlak, D.L., 2017. Treatment of Aqueous Film-Forming Foam by Heat-Activated Persulfate Under Conditions Representative of In Situ Chemical Oxidation. *Environ. Sci. Technol.* 51, 13878–13885. <https://doi.org/10.1021/acs.est.7b03969>
- Butt, C.M., Muir, D.C.G., Mabury, S.A., 2014. Biotransformation pathways of fluorotelomer-based polyfluoroalkyl substances: A review. *Environ Toxicol Chem* 33, 243–267. <https://doi.org/10.1002/etc.2407>
- Elliott, D.C., Baker, E.G., Beckman, D., Solantausta, Y., Tolenhiemo, V., Gevert, S.B., Hörnell, C., Östman, A., Kjellström, B., 1990. Technoeconomic assessment of direct biomass liquefaction to transportation fuels. *Biomass* 22, 251–269. [https://doi.org/10.1016/0144-4565\(90\)90021-B](https://doi.org/10.1016/0144-4565(90)90021-B)
- Elliott, D.C., Hart, T.R., Neuenschwander, G.G., Rotness, L.J., Roesijadi, G., Zacher, A.H., Magnuson, J.K., 2014. Hydrothermal Processing of Macroalgal Feedstocks in Continuous-Flow Reactors. *ACS Sustainable Chem. Eng.* 2, 207–215. <https://doi.org/10.1021/sc400251p>
- Fang, Y., Kim, E., Strathmann, T.J., 2018. Mineral- and Base-Catalyzed Hydrolysis of Organophosphate Flame Retardants: Potential Major Fate-Controlling Sink in Soil and

- Aquatic Environments. *Environ. Sci. Technol.* 52, 1997–2006. <https://doi.org/10.1021/acs.est.7b05911>
- Fu, J., Lu, X., Savage, P.E., 2010. Catalytic hydrothermal deoxygenation of palmitic acid. *Energy & Environmental Science* 3, 311. <https://doi.org/10.1039/b923198f>
- Genifuel - Welcome [WWW Document], n.d. URL <http://www.genifuel.com/> (accessed 10.9.17).
- González-Martínez, A., de Simón-Martín, M., López, R., Táboas-Fernández, R., Bernardo-Sánchez, A., 2019. Remediation of Potential Toxic Elements from Wastes and Soils: Analysis and Energy Prospects. *Sustainability* 11, 3307. <https://doi.org/10.3390/su11123307>
- Gu, Y., Dong, W., Luo, C., Liu, T., 2016. Efficient Reductive Decomposition of Perfluorooctanesulfonate in a High Photon Flux UV/Sulfite System. *Environ. Sci. Technol.* 50, 10554–10561. <https://doi.org/10.1021/acs.est.6b03261>
- Guo, Y., Wang, S.Z., Xu, D.H., Gong, Y.M., Ma, H.H., Tang, X.Y., 2010. Review of catalytic supercritical water gasification for hydrogen production from biomass. *Renewable and Sustainable Energy Reviews* 14, 334–343. <https://doi.org/10.1016/j.rser.2009.08.012>
- Hori, H., Nagaoka, Y., Tanaka, M., Tsuruho, K., Sano, T., Yamashita, N., Taniyasu, S., Kutsuna, S., 2006. Efficient Decomposition of Environmental Persistent Perfluorooctanesulfonate and Related Fluorochemicals Using Zerovalent Iron in Subcritical Water. *Environ. Sci. Technol.* 40, 1049–1054.
- Hori, H., Sakamoto, T., Ohmura, K., Yoshikawa, H., Seita, T., Fujita, T., Morizawa, Y., 2014. Efficient-Oxygen Induced Mineralization of Melt-Processable Fluoropolymers in Subcritical and Supercritical Water. *Ind. Eng. Chem. Res.* 53, 6934–6940. <https://doi.org/10.1021/ie500446s>
- Houde, M., Martin, J.W., Letcher, R.J., Solomon, K.R., Muir, D.C.G., 2006. Biological Monitoring of Polyfluoroalkyl Substances. *Environ. Sci. Technol.* 40, 3463–3473.
- Houtz, E.F., Higgins, C.P., Field, J.A., Sedlak, D.L., 2013. Persistence of Perfluoroalkyl Acid Precursors in AFFF-Impacted Groundwater and Soil. *Environ. Sci. Technol.* 47, 8187–8195. <https://doi.org/10.1021/es4018877>
- Hu, X.C., Andrews, D.Q., Lindstrom, A.B., Bruton, T.A., Schaidler, L.A., Grandjean, P., Lohmann, R., Carignan, C.C., Blum, A., Balan, S.A., Higgins, C.P., Sunderland, E.M., 2016. Detection of Poly- and Perfluoroalkyl Substances (PFASs) in U.S. Drinking Water Linked to Industrial Sites, Military Fire Training Areas, and Wastewater Treatment Plants. *Environ. Sci. Technol. Lett.* 3, 344–350. <https://doi.org/10.1021/acs.estlett.6b00260>
- Huang, S., Jaffé, P.R., 2019. Defluorination of Perfluorooctanoic Acid (PFOA) and Perfluorooctane Sulfonate (PFOS) by *Acidimicrobium* sp. Strain A6. *Environ. Sci. Technol.* 53, 11410–11419. <https://doi.org/10.1021/acs.est.9b04047>
- K. Barzen-Hanson, J. Field, S. Roberts, S. Choyke, P.L. Ferguson, C.P. Higgins, n.d. Closing the mass balance on per- and polyfluorinated alkyl substances in groundwater at aqueous film-forming foam (AFFF) impacted sites. Manuscript In Preparation.
- Le, T.X.H., Haflich, H., Shah, A.D., Chaplin, B.P., 2019. Energy-Efficient Electrochemical Oxidation of Perfluoroalkyl Substances Using a Ti4O7 Reactive Electrochemical Membrane Anode. *Environ. Sci. Technol. Lett.* 6, 504–510. <https://doi.org/10.1021/acs.estlett.9b00397>

- Lee, Y., Lo, S., Kuo, J., Hsieh, C., 2011. Decomposition of perfluorooctanoic acid by microwave-activated persulfate: Effects of temperature, pH, and chloride ions. *Front. Environ. Sci. Eng.* 6, 17–25. <https://doi.org/10.1007/s11783-011-0371-x>
- Lee, Y.-C., Lo, S.-L., Chiueh, P.-T., Chang, D.-G., 2009. Efficient Decomposition of Perfluorocarboxylic Acids in Aqueous Solution using Microwave-Induced Persulfate. *Wat. Res.* 43, 2811–2816.
- Lin, H., Niu, J., Ding, S., Zhang, L., 2012. Electrochemical degradation of perfluorooctanoic acid (PFOA) by Ti/SnO₂-Sb, Ti/SnO₂-Sb/PbO₂ and Ti/SnO₂-Sb/MnO₂ anodes. *Water Research* 46, 2281–2289. <https://doi.org/10.1016/j.watres.2012.01.053>
- Merino, N., Qu, Y., Deeb, R.A., Hawley, E.L., Hoffmann, M.R., Mahendra, S., 2016. Degradation and Removal Methods for Perfluoroalkyl and Polyfluoroalkyl Substances in Water. *Environmental Engineering Science* 33, 615–649. <https://doi.org/10.1089/ees.2016.0233>
- Miehr, R., Tratnyek, P.G., Bandstra, J.Z., Scherer, M.M., Alowitz, M.J., Bylaska, E.J., 2004. Diversity of contaminant reduction reactions by zerovalent iron: Role of the reductate. *Environ. Sci. Technol.* 38, 139–147. <https://doi.org/10.1021/es034237h>
- Moody, C.A., Field, J.A., 2000. Perfluorinated Surfactants and the Environmental Implications of Their Use in Fire-Fighting Foams. *Environ. Sci. Technol.* 34.
- Moody, C.A., Field, J.A., 1999. Determination of Perfluorocarboxylates in Groundwater Impacted by Fire-Fighting Activity. *Environ. Sci. Technol.* 33, 2800–2806.
- Nickerson, A., Maizel, A.C., Kulkarni, P.R., Adamson, D.T., Kornuc, J.J., Higgins, C.P., 2020. Enhanced extraction of AFFF-associated PFASs from source zone soils. *Environmental Science & Technology*. <https://doi.org/10.1021/acs.est.0c00792>
- Ochiai, T., Iizuka, Y., Nakata, K., Murakami, T., Tryk, D.A., Fujishima, A., Koide, Y., Morito, Y., 2011. Efficient electrochemical decomposition of perfluorocarboxylic acids by the use of a boron-doped diamond electrode. *Diamond and Related Materials* 20, 64–67. <https://doi.org/10.1016/j.diamond.2010.12.008>
- Ochoa-Herrera, V., Sierra-Alvarez, R., Somogyi, A., Jacobsen, N.E., Wysocki, V.H., Field, J.A., 2008. Reductive Defluorination of Perfluorooctane Sulfonate. *Environ. Sci. Technol.* 42, 3260–3264. <https://doi.org/10.1021/es702842q>
- Park, H., Vecitis, C.D., Cheng, J., Dalleska, N.F., Mader, B.T., Hoffmann, M.R., 2011. Reductive degradation of perfluoroalkyl compounds with aquated electrons generated from iodide photolysis at 254 nm. *Photochem. Photobiol. Sci.* 10, 1945–1953. <https://doi.org/10.1039/C1PP05270E>
- Parsons, J.R., Saez, M., Dolfing, J., Voogt, P., 2008a. Biodegradation of Perfluorinated Compounds. *Rev. Environ. Contam. Toxicol.* 196, 53–71.
- Parsons, J.R., Saez, M., Dolfing, J., Voogt, P., 2008b. Biodegradation of Perfluorinated Compounds. *Rev. Environ. Contam. Toxicol.* 196, 53–71.
- Peterson, A.A., Vogel, F., Lachance, R.P., Froeling, M., Antal, M.J., Tester, J.W., 2008. Thermochemical biofuel production in hydrothermal media: A review of sub- and supercritical water technologies. *Energy & Environmental Science* 1, 32–65. <https://doi.org/10.1039/b810100k>
- Pinkard, B.R., Gorman, D.J., Tiwari, K., Rasmussen, E.G., Kramlich, J.C., Reinhall, P.G., Novosselov, I.V., 2019. Supercritical water gasification: practical design strategies and operational challenges for lab-scale, continuous flow reactors. *Heliyon* 5, e01269. <https://doi.org/10.1016/j.heliyon.2019.e01269>

- Prevedouros, K., Cousins, I.T., Buck, R.C., Korzeniowski, H., 2006. Sources, Fate and Transport of Perfluorocarboxylates. *Environ. Sci. Technol.* 40, 32–44.
- Remde, A., Debus, R., 1996. Biodegradability of Fluorinated Surfactants under Aerobic and Anaerobic Conditions. *Chemosphere* 32, 1563–1574.
- Sahu, S.P., Qanbarzadeh, M., Ateia, M., Torkzadeh, H., Maroli, A.S., Cates, E.L., 2018. Rapid Degradation and Mineralization of Perfluorooctanoic Acid by a New Petitjeanite $\text{Bi}_3\text{O}(\text{OH})(\text{PO}_4)_2$ Microparticle Ultraviolet Photocatalyst. *Environ. Sci. Technol. Lett.* <https://doi.org/10.1021/acs.estlett.8b00395>
- Savage, P.E., 2012. Algae Under Pressure and in Hot Water. *Science* 338, 1039–1040. <https://doi.org/10.1126/science.1224310>
- Savage, P.E., 2009. A perspective on catalysis in sub- and supercritical water. *J. Supercritical Fluids* 47, 407–414.
- Schaefer, C.E., Andaya, C., Urriaga, A., McKenzie, E.R., Higgins, C.P., 2015. Electrochemical treatment of perfluorooctanoic acid (PFOA) and perfluorooctane sulfonic acid (PFOS) in groundwater impacted by aqueous film forming foams (AFFFs). *Journal of Hazardous Materials* 295, 170–175. <https://doi.org/10.1016/j.jhazmat.2015.04.024>
- Schultz, C.A., Gundl, T.J., 2000. pH Dependence on Reduction Rate of 4-Cl-Nitrobenzene by Fe(II)/Montmorillonite Systems. *Environ. Sci. Technol.* 34, 3641–3648.
- Schultz, M.M., Barofsky, D.F., Field, J.A., 2003. Fluorinated Alkyl Surfactants. *Environ. Engr. Sci.* 20.
- Schymanski, E.L., Jeon, J., Gulde, R., Fenner, K., Ruff, M., Singer, H.P., Hollender, J., 2014. Identifying Small Molecules via High Resolution Mass Spectrometry: Communicating Confidence. *Environmental Science & Technology* 48, 2097–2098. <https://doi.org/10.1021/es5002105>
- Sharma, V.K., 2002. Potassium Ferrate(VI): An Environmentally Friendly Oxidant. *Adv. Environ. Res.* 6, 143–156.
- Stratton, G.R., Dai, F., Bellona, C.L., Holsen, T.M., Dickenson, E.R.V., Mededovic Thagard, S., 2017. Plasma-Based Water Treatment: Efficient Transformation of Perfluoroalkyl Substances in Prepared Solutions and Contaminated Groundwater. *Environ. Sci. Technol.* 51, 1643–1648. <https://doi.org/10.1021/acs.est.6b04215>
- Su, C.M., Puls, R.W., 1999. Kinetics of trichloroethene reduction by zerovalent iron and tin: Pretreatment effect, apparent activation energy, and intermediate products. *Environ. Sci. Technol.* 33, 163–168. <https://doi.org/10.1021/es980481a>
- Tsitonaki, A., Petri, B., Crimi, M., Mosbaek, H., Siegest, R., Bjerg, P.L., 2010. In Situ Chemical Oxidation of Contaminated Soil and Groundwater using Persulfate: A Review. *Rev. Environ. Sci. Technol.* 40, 55–91.
- Van Hoomissen, D.J., Vyas, S., 2019. Early Events in the Reductive Dehalogenation of Linear Perfluoroalkyl Substances. *Environ. Sci. Technol. Lett.* 6, 365–371. <https://doi.org/10.1021/acs.estlett.9b00116>
- Vardon, D.R., Scott, J., Sharma, B.K., Yu, G., Wang, Z., Schideman, L., Zhang, Y., Strathmann, T.J., 2011. Characterization of Hydrothermal Liquefaction Biocrude Oils Produced from Primary Sludge, Swine Manure and Algal Feedstocks.
- Vecitis, C.D., Wang, Y., Cheng, J., Park, H., Mader, B.T., Hoffmann, M.R., 2010. Sonochemical Degradation of Perfluorooctanesulfonate in Aqueous Film-Forming Foams. *Environ. Sci. Technol.* 44, 432–438.

- Wang, F., Shih, K., Lu, X., Liu, C., 2013. Mineralization Behavior of Fluorine in Perfluorooctanesulfonate (PFOS) during Thermal Treatment of Lime-Conditioned Sludge. *Environ. Sci. Technol.* 47, 2621–2627. <https://doi.org/10.1021/es305352p>
- Wang, Z., DeWitt, J.C., Higgins, C.P., Cousins, I.T., 2017. A Never-Ending Story of Per- and Polyfluoroalkyl Substances (PFASs)? *Environ. Sci. Technol.* <https://doi.org/10.1021/acs.est.6b04806>
- Watanabe, M., Iida, T., Inomata, H., 2006. Decomposition of a long chain saturated fatty acid with some additives in hot compressed water. *Energy Conversion and Management* 47, 3344–3350. <https://doi.org/10.1016/j.enconman.2006.01.009>
- Watanabe, N., Takata, M., Takemine, S., Yamamoto, K., 2018. Thermal mineralization behavior of PFOA, PFHxA, and PFOS during reactivation of granular activated carbon (GAC) in nitrogen atmosphere. *Environ Sci Pollut Res Int* 25, 7200–7205. <https://doi.org/10.1007/s11356-015-5353-2>
- Wu, B., Hao, S., Choi, Y., Higgins, C.P., Deeb, R., Strathmann, T.J., 2019. Rapid Destruction and Defluorination of Perfluorooctanesulfonate by Alkaline Hydrothermal Reaction. *Environmental Science & Technology Letters* [acs.estlett.9b00506](https://doi.org/10.1021/acs.estlett.9b00506)
- Yamasaki, Nakamichi., Yasui, Takaji., Matsuoka, Kiyoshi., 1980. Hydrothermal decomposition of polychlorinated biphenyls. *Environ. Sci. Technol.* 14, 550–552. <https://doi.org/10.1021/es60165a011>
- Yamasaki, Y., Enomoto, H., Yamasaki, N., Nakahara, M., 2000. NMR Study of Hydrothermal Reactions of Dichloromethane with and without Alkali. *BCSJ* 73, 2687–2693. <https://doi.org/10.1246/bcsj.73.2687>
- Yang, S., Cheng, J., Sun, J., Hu, Y., Liang, X., 2013. Defluorination of Aqueous Perfluorooctanesulfonate by Activated Persulfate Oxidation. *PLOS ONE* 8, e74877. <https://doi.org/10.1371/journal.pone.0074877>
- Zhang, K., Huang, J., Yu, G., Zhang, Q., Deng, S., Wang, B., 2013. Destruction of Perfluorooctane Sulfonate (PFOS) and Perfluorooctanoic Acid (PFOA) by Ball Milling. *Environ. Sci. Technol.* 47, 6471–6477. <https://doi.org/10.1021/es400346n>
- Zhuo, Q., Luo, M., Guo, Q., Yu, G., Deng, S., Xu, Z., Yang, B., Liang, X., 2016. Electrochemical Oxidation of Environmentally Persistent Perfluorooctane Sulfonate by a Novel Lead Dioxide Anode. *Electrochimica Acta* 213, 358–367. <https://doi.org/10.1016/j.electacta.2016.07.005>

APPENDIX A: Supporting Data

Table A1 Semiquantitative analysis of PFASs compounds with corresponding calibrant and internal standard.				
Compound	Class	Chain length	Calibrant	Internal standard
1OH-5:2 FTS	1OH-X:2 FTS	5	PFPeS	¹³ C2-PFOS
AmPr-FOAd	AmPr-FAAd	7	MeFOSA	d3-MeFOSA
AmPr-FNAd	AmPr-FAAd	8	MeFOSA	d3-MeFOSA
AmPr-FEtSA	AmPr-FASA	2	MeFOSA	d3-MeFOSA
AmPr-FPrSA	AmPr-FASA	3	MeFOSA	d3-MeFOSA
AmPr-FBSA	AmPr-FASA	4	MeFOSA	d3-MeFOSA
AmPr-FPeSA	AmPr-FASA	5	MeFOSA	d3-MeFOSA
AmPr-FHxSA	AmPr-FASA	6	MeFOSA	d3-MeFOSA
AmPr-FHpSA	AmPr-FASA	7	MeFOSA	d3-MeFOSA
AmPr-FOSA	AmPr-FASA	8	MeFOSA	d3-MeFOSA
AmPr-FBSA-PrA	AmPr-FASA-PrA	4	FOSAA	d3-MeFOSAA
AmPr-FPeSA-PrA	AmPr-FASA-PrA	5	FOSAA	d3-MeFOSAA
AmPr-FHxSA-PrA	AmPr-FASA-PrA	6	FOSAA	d3-MeFOSAA
CEtAmPr-FPrSA	CEtAmPr-FASA	3	FOSAA	d3-MeFOSAA
CMeAmPr-FPrSA	CMeAmPr-FASA	3	FOSAA	d3-MeFOSAA
CMeAmPr-FBSA	CMeAmPr-FASA	4	FOSAA	d3-MeFOSAA
CMeAmPr-FPeSA	CMeAmPr-FASA	5	FOSAA	d3-MeFOSAA
CMeAmPr-FHxSA	CMeAmPr-FASA	6	FOSAA	d3-MeFOSAA
CMeAmPr-FOSA	CMeAmPr-FASA	8	FOSAA	d3-MeFOSAA
DiMeA-MeOHPr-FHxSAPrS	DiMeA-MeOHPr-FASAPrS	6	PFHxS	¹⁸ O2-PFHxS
diOHBAmPr-FHxSA	diOHBAmPr-FASA	6	PFHpA	¹³ C4-PFHpA
diOHPrAm-MeOHPr-FBSA	diOHPrAm-MeOHPr-FASA	4	PFPeA	¹³ C5-PFPeA
diOHPrAm-MeOHPr-FPeSA	diOHPrAm-MeOHPr-FASA	5	PFHxA	¹³ C2-PFHxA
diOHPrAm-MeOHPr-FHxSA	diOHPrAm-MeOHPr-FASA	6	PFHpA	¹³ C4-PFHpA
diOHPrAm-MeOHPr-FOSA	diOHPrAm-MeOHPr-FASA	8	PFNA	¹³ C5-PFNA
diOHPrAm-MeOHPr-FHxSAPrS	diOHPrAm-MeOHPr-FASAPrS	6	PFHxS	¹⁸ O2-PFHxS
diOHPrAm-MeOHPr-FHpSAPrS	diOHPrAm-MeOHPr-FASAPrS	7	PFHpS	¹⁸ O2-PFHxS
diOHPrAm-MeOHPr-FOSAPrS	diOHPrAm-MeOHPr-FASAPrS	8	PFOS	¹³ C4-PFOS
EtFPrSAA	EtFASAA	3	FOSAA	d3-MeFOSAA

EtFBSAA	EtFASAA	4	FOSAA	d3-MeFOSAA
EtFPeSAA	EtFASAA	5	FOSAA	d3-MeFOSAA
EtFHxSAA	EtFASAA	6	FOSAA	d3-MeFOSAA
EtFHpSAA	EtFASAA	7	FOSAA	d3-MeFOSAA
F5S-PFPrA	F5S-PFAA	2	PFPeA	¹³ C5-PFPeA
F5S-PFOA	F5S-PFAA	7	PFDA	¹³ C2-PFDA
F5S-PFMeS	F5S-PFAS	1	PFPrS	¹³ C3-PFBS
F5S-PFHxS	F5S-PFAS	6	PFOS	¹³ C4-PFOS
F5S-PFHpS	F5S-PFAS	7	PFNS	¹³ C4-PFOS
F5S-PFOS	F5S-PFAS	8	PFDS	¹³ C4-PFOS
F5S-PFNS	F5S-PFAS	9	PFDoS	¹³ C4-PFOS
FEtSA	FASA	2	MeFOSA	d3-MeFOSA
FPrSA	FASA	3	MeFOSA	d3-MeFOSA
FBSA	FASA	4	MeFOSA	d3-MeFOSA
FPeSA	FASA	5	MeFOSA	d3-MeFOSA
FHxSA	FASA	6	MeFOSA	d3-MeFOSA
FHpSA	FASA	7	MeFOSA	d3-MeFOSA
FPrSAA	FASAA	3	FOSAA	d3-MeFOSAA
FBSAA	FASAA	4	FOSAA	d3-MeFOSAA
FPeSAA	FASAA	5	FOSAA	d3-MeFOSAA
FHxSAA	FASAA	6	FOSAA	d3-MeFOSAA
H-PFPeA	H-PFAA	3	PFPeA	¹³ C5-PFPeA
H-PFNA	H-PFAA	7	PFNA	¹³ C5-PFNA
H-PFBS	H-PFAS	2	PFBS	¹³ C3-PFBS
H-PFHxS	H-PFAS	4	PFHxS	¹⁸ O2-PFHxS
H-PFHpS	H-PFAS	5	PFHpS	¹⁸ O2-PFHxS
H-PFOS	H-PFAS	6	PFOS	¹³ C4-PFOS
H-PFNS	H-PFAS	7	PFNS	¹³ C4-PFOS
H-PFDS	H-PFAS	8	PFDS	¹³ C4-PFOS
H-PFUdS	H-PFAS	9	PFDoS	¹³ C4-PFOS
H-PFDoS	H-PFAS	10	PFDoS	¹³ C4-PFOS
H-UPFHp-O/OH	H-UPFA-O/OH	7	PFHpA	¹³ C4-PFHpA
H-UPFOS	H-UPFAS	4	PFHpS	¹⁸ O2-PFHxS
H-UPFDS	H-UPFAS	6	PFNS	¹³ C4-PFOS
K-PFPeS	K-PFAS	3	PFBS	¹³ C3-PFBS
K-PFHxS	K-PFAS	4	PFPeS	¹³ C2-PFOS
K-PFOS	K-PFAS	6	PFHpS	¹⁸ O2-PFHxS
K-PFNS	K-PFAS	7	PFOS	¹³ C4-PFOS
K-PFDS	K-PFAS	8	PFNS	¹³ C4-PFOS
K-PFUdS	K-PFAS	9	PFDS	¹³ C4-PFOS

K-PFDoS	K-PFAS	10	PFDoS	¹³ C4-PFOS
K-PFTrDS	K-PFAS	11	PFDoS	¹³ C4-PFOS
K-PFTeDS	K-PFAS	12	PFDoS	¹³ C4-PFOS
MeFPrSA	MeFASA	3	MeFOSA	d3-MeFOSA
MeFBSA	MeFASA	4	MeFOSA	d3-MeFOSA
MeFPeSA	MeFASA	5	MeFOSA	d3-MeFOSA
MeFHxSA	MeFASA	6	MeFOSA	d3-MeFOSA
MeFHpSA	MeFASA	7	MeFOSA	d3-MeFOSA
MeFPrAA	MeFASAA	3	FOSAA	d3-MeFOSAA
MeFBAA	MeFASAA	4	FOSAA	d3-MeFOSAA
MeFPeSAA	MeFASAA	5	FOSAA	d3-MeFOSAA
MeFHxSAA	MeFASAA	6	FOSAA	d3-MeFOSAA
MeFHpSAA	MeFASAA	7	FOSAA	d3-MeFOSAA
OAmPr-FPrSA	OAmPr-FASA	3	MeFOSA	d3-MeFOSA
OAmPr-FBSA	OAmPr-FASA	4	MeFOSA	d3-MeFOSA
OAmPr-FPeSA	OAmPr-FASA	5	MeFOSA	d3-MeFOSA
OAmPr-FHxSA	OAmPr-FASA	6	MeFOSA	d3-MeFOSA
O-PFOS	O-PFAS	6	PFHpS	¹⁸ O2-PFHxS
O-PFNS	O-PFAS	7	PFOS	¹³ C4-PFOS
O-PFDS	O-PFAS	8	PFNS	¹³ C4-PFOS
O-PFDoS	O-PFAS	10	PFDoS	¹³ C4-PFOS
O-PFTeDS	O-PFAS	12	PFDoS	¹³ C4-PFOS
PFDo-OS	PFA-OS	10	PFDS	¹³ C4-PFOS
PFDo-OS	PFA-OS	12	PFDoS	¹³ C4-PFOS
PFTrDS	PFAS	13	PFDoS	¹³ C4-PFOS
PFTeDS	PFAS	14	PFDoS	¹³ C4-PFOS
PFPeDS	PFAS	15	PFDoS	¹³ C4-PFOS
PFHxDS	PFAS	16	PFDoS	¹³ C4-PFOS
PFPrSi	PFASi	3	PFPrS	¹³ C3-PFBS
PFBSi	PFASi	4	PFBS	¹³ C3-PFBS
PFPeSi	PFASi	5	PFPeS	¹³ C2-PFOS
PFHxSi	PFASi	6	PFHxS	¹⁸ O2-PFHxS
PFHpSi	PFASi	7	PFHpS	¹⁸ O2-PFHxS
PFOSi	PFASi	8	PFOS	¹³ C4-PFOS
S-OHPrAmPr-FPeSA	SOHPrAmPr-FASA	5	PFHxA	¹³ C2-PFHxA
SPrAmPr-FHxSA	SPrAmPr-FASA	6	MeFOSA	d3-MeFOSA
SPrAmPr-FHpSA	SPrAmPr-FASA	7	MeFOSA	d3-MeFOSA
SPrAmPr-FOSA	SPrAmPr-FASA	8	MeFOSA	d3-MeFOSA
SPr-FOSA	SPr-FASA	8	MeFOSA	d3-MeFOSA
UPFHxS	UPFAS	3	PFPeS	¹³ C2-PFOS

UPFHpS	UPFAS	4	PFHxS	¹⁸ O ₂ -PFHxS
UPFOS	UPFAS	5	PFHpS	¹⁸ O ₂ -PFHxS
UPFNS	UPFAS	6	PFOS	¹³ C ₄ -PFOS
UPFDS	UPFAS	7	PFNS	¹³ C ₄ -PFOS
UPFUdS	UPFAS	8	PFDS	¹³ C ₄ -PFOS
UPFDoS	UPFAS	9	PFDoS	¹³ C ₄ -PFOS
UPFTrDS	UPFAS	10	PFDoS	¹³ C ₄ -PFOS
UPFTeDS	UPFAS	11	PFDoS	¹³ C ₄ -PFOS
UPFPeDS	UPFAS	12	PFDoS	¹³ C ₄ -PFOS
11:1 PFDoS	X:1 PFAS	11	PFDoS	¹³ C ₄ -PFOS
12:2 FTS	X:2 FTS	12	PFDoS	¹³ C ₄ -PFOS
6:2 FTSA	X:2 FTSA	6	MeFOSA	d ₃ -MeFOSA
8:2 FTSO2PrAd-DiMeEtS	X:2 FTSO2PrAd-DiMeEtS	8	PFOS	¹³ C ₄ -PFOS
6:2 FTSO-PrAd-DiMePrS	X:2 FTSO-PrAd-DiMePrS	6	PFHxS	¹⁸ O ₂ -PFHxS
6:2 FTThPrA	X:2 FTThPrA	6	PFHpA	¹³ C ₄ -PFHpA
4:2 FTTh-PrAd-DiMeEtS	X:2 FTTh-PrAd-DiMeEtS	4	PFBS	¹³ C ₃ -PFBS
6:2 FTTh-PrAd-DiMeEtS	X:2 FTTh-PrAd-DiMeEtS	6	PFHxS	¹⁸ O ₂ -PFHxS
8:2 FTTh-PrAd-DiMeEtS	X:2 FTTh-PrAd-DiMeEtS	8	PFOS	¹³ C ₄ -PFOS
10:2 FTTh-PrAd-DiMeEtS	X:2 FTTh-PrAd-DiMeEtS	10	PFDS	¹³ C ₄ -PFOS
6:2 OH-MeOH-FTTh-PrA	X:2 OH-MeOH-FTTh-PrA	6	PFHpA	¹³ C ₄ -PFHpA
7:3 K-FTTh-K-OH-PrA	X:3 K-FTTh-K-OH-PrA	7	PFOA	¹³ C ₄ -PFOA

APPENDIX B: LIST OF PUBLICATIONS

Articles in peer-reviewed journals

B. Wu, S. Hao, Y. Choi, C.P. Higgins, R. Deeb, and T.J. Strathmann. (2019). Rapid Destruction and Defluorination of Perfluorooctanesulfonate by Alkaline Hydrothermal Reaction. *Environmental Science & Technology Letters*. 6, 630-636. DOI: [10.1021/acs.estlett.9b00506](https://doi.org/10.1021/acs.estlett.9b00506)

J. Yu, A. Nickerson, Y. Li, Y. Fang, and T.J. Strathmann (2020). Fate of Per- and Polyfluoroalkyl Substances (PFASs) during Hydrothermal Liquefaction of Municipal Wastewater Treatment Sludge. *Environmental Science: Water Research & Technology* 6, 1388-1399. DOI: [10.1039/c9ew01139k](https://doi.org/10.1039/c9ew01139k)

S. Hao, Y. Choi, B. Wu, C.P. Higgins, R. Deeb, and T.J. Strathmann. Alkaline hydrothermal destruction and defluorination of per- and polyfluoroalkyl substances (PFASs) in aqueous film-forming foam (AFFF). Manuscript in prep.

S. Hao, Y. Choi, C.P. Higgins, R. Deeb, and T.J. Strathmann. Application of Alkaline hydrothermal treatment for destruction of per- and polyfluoroalkyl substances (PFASs) in contaminated soil and water. Manuscript in prep.

Intellectual Property

T.J. Strathmann, C.P. Higgins, B. Wu, S. Hao (2019). Hydrothermal Technology for Decontamination and Mineralization of Perfluoro- and Polyfluoroalkyl Substances (PFAS) in Wastes, Concentrate Solutions, and Chemical Stockpiles. Full patent application submitted November 2019.

Conference Presentations, Lectures, Webinars

Timothy J. Strathmann, Boran Wu, Shilai Hao, Christopher P. Higgins, Rula Deeb. (2018). Hydrothermal Destruction of Per- and Polyfluoroalkyl Substances (PFASs) in Site Investigation-Derived Wastes (IDW). Poster presented at the 2018 SERDP-ESTCP Partners Meeting, Washington, DC, November 2018.

Boran Wu, Shilai Hao, Rula Deeb, Timothy J. Strathmann. (2019). *Development of Hydrothermal Technologies for the Effective Destruction of Refractory Perfluoroalkyl Substances (PFASs)*. Poster presented at the 2019 Remediation Technology (RemTec) Conference, Westminster, CO, February 2019.

Shilai Hao, Boran Wu, Youn-Jeong Choi, Christopher Higgins, Rula Deeb, Elisabeth Hawley, Timothy Strathmann (2019). Hydrothermal Technologies for Destruction of Site Investigation Wastes Contaminated with PFAS (ER18-1501). Poster presented at the SERDP-ESTCP PFAS Workshop, San Diego, CA, July 2019.

Shilai Hao, Boran Wu, Youn-Jeong Choi, Christopher Higgins, Timothy Strathmann (2019). Hydrothermal Treatment: A Novel Method for Destruction and Defluorination of Per- and Polyfluoroalkyl Substances (PFASs) in Aqueous Film-Forming Foam (AFFF). Oral presentation at the American Chemical Society National Meeting, San Diego, CA, August 2019.

Timothy Strathmann, Christopher Bellona, Christopher Higgins, Charles Schaefer, Trevor Boyer, Harold Wright, Garrett McKay, Charlie Liu, Raul Tenorio, Yida Fang, Anderson Ellis. (2019) Laboratory and Pilot-Scale Studies on Innovative Pathways for Removal and Destruction of Perfluoroalkyl Substances (PFAS). Special invited keynote presentation at the 2019 International Water Association (IWA) Micropol Conference, Seoul, South Korea, October 2019.

Timothy Strathmann (2019) Accomplishing Removal and Destruction of Per- and Polyfluoroalkyl Substances (PFASs) in Contaminated Groundwater. Special invited lecture at the Seoul National University, October 2019.

Timothy Strathmann (2019) Accomplishing Removal and Destruction of Per- and Polyfluoroalkyl Substances (PFASs) in Contaminated Groundwater. Special invited lecture at the 6th International Workshop on Frontiers in Environmental Chemical Research, Pohang University of Science and Technology (POSTECH), Pohang, South Korea, October 2019.

Timothy J. Strathmann, Boran Wu, Shilai Hao, Younjeong Choi, Christopher P. Higgins, Rula Deeb. (2019) Rapid and Complete Destruction of Per- and Polyfluoroalkyl Substances (PFASs) in Aqueous and Soil Samples by Application of an Innovative Hydrothermal Processing Technology. Poster presented at the 2019 SERDP-ESTCP Partners Meeting, Washington, DC, November 2019.

Timothy J. Strathmann, Shilai Hao, Boran Wu, Christopher P. Higgins, Rula Deeb. (2020). An Innovative Hydrothermal Destruction Technology that Achieves Rapid and Complete Defluorination of PFASs. Special keynote presentation at the 2020 Emerging Contaminants Summit. Westminster, CO, March 2020.

Shilai Hao, Boran Wu, Youn-Jeong Choi, Rula Deeb, Christopher P. Higgins, Timothy J. Strathmann. (2020) Destruction and Defluorination of Per- and Polyfluoroalkyl Substances (PFASs) in Aqueous Film-Forming Foam (AFFF) by Hydrothermal Treatment. Poster presented at the 2020 Emerging Contaminants Summit. Westminster, CO, March 2020.

Timothy J. Strathmann, Shilai Hao, Boran Wu, Christopher Higgins, and Rula Deeb. Hydrothermal ALkaline Treatment (HALT): An Innovative Technology for Complete Destruction of PFAS in Contaminated Water and Soil. SERDP-ESTCP Webinar, June 2020.